

Mechanisms for Inactivation in Piezo Ion Channels

by

Jason Wu

Department of Neurobiology  
Duke University

Date: \_\_\_\_\_

Approved:

\_\_\_\_\_  
Jörg Grandl, Supervisor

\_\_\_\_\_  
Donald Lo, Chair

\_\_\_\_\_  
Hiroaki Matsunami

\_\_\_\_\_  
Stefan Zauscher

Dissertation submitted in partial fulfillment of  
the requirements for the degree of Doctor  
of Philosophy in the Department of  
Neurobiology in the Graduate School  
of Duke University

2017

ABSTRACT

Mechanisms for Inactivation in Piezo Ion Channels

by

Jason Wu

Department of Neurobiology  
Duke University

Date: \_\_\_\_\_

Approved:

\_\_\_\_\_  
Jörg Grandl, Supervisor

\_\_\_\_\_  
Donald Lo, Chair

\_\_\_\_\_  
Hiroaki Matsunami

\_\_\_\_\_  
Stefan Zauscher

An abstract of a dissertation submitted in partial  
fulfillment of the requirements for the degree  
of Doctor of Philosophy in the Department of  
Neurobiology in the Graduate School of  
Duke University

2017

Copyright by  
Jason Wu  
2017

## **Abstract**

An organism's ability to sense mechanical forces is critical for the detection of environmental stimuli as well as the regulation of internal processes necessary for survival. In vertebrates, the molecular mechanisms of somatosensation has remained an important and unresolved neurobiological question. In the past decade, Piezo ion channels have emerged as the first vertebrate ion channels identified responsible for transforming somatosensory stimuli into excitatory signals in the nervous system, generating our sense of touch. However, little still is known about the precise mechanisms for how Piezo channels activate and inactivate in the presence of stimuli and how they could potentially be modulated.

By using a combination of engineered and biomolecular methods combined with electrophysiology, I identify distinct structural domains within Piezo ion channels that are necessary for specific aspects of channel inactivation. First, I engineered a method by which magnetic nanoparticles were used to mechanically pull on individual domains of the Piezo channel to screen for mechanically sensitive structures. This experiment revealed a particularly striking effect for one domain, manifested as a profound slowing of channel inactivation kinetics. Next, I generated chimeric constructs to exchange this domain with a homologous structure and demonstrated its sufficiency for mediating the kinetics for inactivation. Finally, I introduced point mutations at key residues within the

immediately adjacent pore domain and identified a structural correlate for the modulation of inactivation by voltage. These findings together provide a foundation for understanding the mechanism for inactivation in Piezo channels, and more broadly, for further studying the complexities in transducing mechanical force that create our sense of touch.

## **Dedication**

To my grandparents.

# Contents

Abstract .....	iv
List of Tables .....	xi
List of Figures .....	xii
Acknowledgements .....	xv
1. Introduction .....	1
1.1 Overview .....	1
1.2 Mechanotransduction in cell biology .....	3
1.2.1 Sensing force through the cytoskeleton .....	4
1.2.2 Sensing force through ion channels .....	5
1.3 The roles of Piezo throughout the body .....	8
1.3.1 Piezos in the peripheral nervous system .....	8
1.3.2 Piezos in non-sensory tissue .....	13
1.4 The activation and inactivation of Piezos .....	16
1.5 The architecture of Piezo .....	23
1.6 Activation mechanisms and modulation of Piezos .....	25
1.6.1 Mechanisms of mechanical activation .....	25
1.6.2 Modulation of Piezos .....	30
1.7 Insights into Piezo function through disease .....	31
1.8 The puzzle of Piezo inactivation .....	32
1.8.1 Case study: Inactivation of voltage gated sodium channels .....	33

1.9.2 Case study: Inactivation of voltage gated potassium channels .....	34
1.9.3 The challenge: Inactivation of Piezo ion channels .....	36
1.9 Open questions and aims .....	37
2. Localized force application reveals mechanically sensitive domains of Piezo1 .....	39
2.1 Introduction.....	39
2.2 Experimental Methods.....	40
2.2.1 Cloning and characterization.....	40
2.2.2 Cell culture .....	41
2.2.3 Nanoparticle labeling.....	42
2.2.4 Immunostaining .....	42
2.2.5 Double labeling.....	43
2.2.6 Myc-tag labeling .....	44
2.2.7 Electromagnetic needle.....	44
2.2.8 Magnetic force calibration.....	45
2.2.9 Electrophysiology .....	47
2.2.10 Electrophysiology analysis.....	48
2.2.11 NP <sub>o</sub> and single channel analysis .....	50
2.2.12 Statistical analysis.....	50
2.3 Localized force application by magnetic nanoparticles .....	51
2.4 Magnetic force induces domain-specific loss of inactivation.....	59
2.5 Magnetic force acts directly on channel domains .....	64
2.6 Magnetic force specifically perturbs mechanical gating .....	70

2.7 Discussion.....	75
3. Inactivation of mechanically-activated Piezo1 ion channels is determined by the C-terminal extracellular domain and the inner pore helix.....	80
3.1 Introduction.....	80
3.2 Experimental Methods.....	82
3.2.1 Construct subcloning and characterization .....	82
3.2.2 Cell culture .....	84
3.2.3 Electrophysiology .....	84
3.2.4 Fluorescence imaging .....	86
3.2.5 Protein purification and NativePAGE gel .....	87
3.2.6 Data analysis .....	88
3.2.7 Statistical analysis.....	89
3.3 Voltage modulates Piezo1 and Piezo2 inactivation kinetics in a continuous manner .....	89
3.4 The C-terminal extracellular domain is sufficient to confer inactivation kinetics	93
3.5 A single lysine residue in the inner pore helix confers voltage dependence of inactivation to Piezo1 .....	99
3.6 MTSET accessibility to inner pore-helix residue V2467 is voltage dependent ....	103
3.7 Discussion.....	107
4. Concluding Remarks and Future Directions .....	112
4.1 Major results and interpretations.....	112
4.1.1 Identification of mechanosensitive domains .....	113
4.1.2 Structure-function relationships of the CED and inner pore helix.....	114

4.1.3 Hypotheses for the mechanism of Piezo inactivation .....	117
4.2 Potentials for Piezo in tool development .....	119
4.2.1 The advent of magnetogenetics.....	119
4.2.2 Directions for Piezo and ion channels in magnetogenetics.....	121
4.3 The question of Piezo activation .....	125
4.3.1 Activation through the tether model.....	125
4.3.2 Activation through the bilayer model.....	126
4.3.3 Transduction of tension sensing to pore opening.....	129
4.4 Solving the mechanism of inactivation .....	131
Appendix: Supporting data.....	135
References .....	142
Biography.....	155

## List of Tables

Table 1: Magnetic pulling does not affect voltage sensitivity of Kv1.2-BBS constructs....	74
Table 2: List of mutations in Piezo1 and Piezo2 associated with human diseases .....	135
Table 3: Primer list. Complementary primer sets used to insert bungarotoxin binding sequence or myc tag. ....	137
Table 4: Candidate ion channels for magnetogenetics.. ....	140

## List of Figures

Figure 1: Somatosensory pathways.....	10
Figure 2: Expression and physiological roles of Piezos.....	14
Figure 3: Piezos are mechanically activated ion channels.....	18
Figure 4: Current and future methods of stimulating Piezos.....	19
Figure 5: Adapting versus inactivating currents.....	22
Figure 6: The architecture of Piezo1.....	24
Figure 7: Potential mechanisms of mechanical sensing and activation.....	27
Figure 8: Nanoparticle labeling strategy.....	52
Figure 9: Scale diagram of BBS-Piezo1 binding complex.....	53
Figure 10: Specificity of nanoparticle labeling.....	54
Figure 11: Efficiency of nanoparticle labeling.....	56
Figure 12: Stability of nanoparticle labeling.....	57
Figure 13: Piezo1-BBS construct functionality.....	58
Figure 14: Electromagnetic needle setup.....	59
Figure 15: Effect of magnetic pulling force on Piezo1 inactivation.....	61
Figure 16: Effect of magnetic pulling on BBS-constructs.....	62
Figure 17: Effect of magnetic field on Piezo1-BBS constructs at resting tension.....	63
Figure 18: Point mutations in the CED and pore domain.....	64
Figure 19: Calibration of magnetic force.....	65
Figure 20: Effect of magnetic field and nanoparticle labeling separately.....	66

Figure 21: Steric hindrance effects on CED. ....	67
Figure 22: Effect of membrane tethering on Piezo1. ....	68
Figure 23: Non-reversibility of magnetic pulling. ....	69
Figure 24: Effect of magnetic pulling on single channel conductance. ....	70
Figure 25: Kv1.2-BBS nanoparticle labeling. ....	71
Figure 26: Testing effects of magnetic pulling effect on Kv1.2-BBS.....	72
Figure 27: Magnetic force affects mechanical activation. ....	75
Figure 28: Inactivation kinetics of Piezo1 and Piezo2.....	90
Figure 29: Effect of ion permeation on inactivation. ....	92
Figure 30: Effect of membrane tension on inactivation. ....	93
Figure 31: The CED confers kinetics of inactivation. ....	95
Figure 32: Inactivation kinetics of chimeric constructs.....	96
Figure 33: Effects of MTSET modification in the CED.....	97
Figure 34: Characterization of CED deletion. ....	98
Figure 35: Schematic of open state modulation of inactivation.....	99
Figure 36: Charged residues in the pore helices. ....	100
Figure 37: Charge neutralization effects on inactivation.....	101
Figure 38: Effects of charge reversal on inactivation. ....	102
Figure 39: Experimental setup for MTSET modification of inner pore helix. ....	104
Figure 40: Effect of MTSET modification on inner pore helix. ....	105
Figure 41: Testing the voltage dependency of MTSET modification.....	106
Figure 42: MTSET modification of inactivation is voltage dependent. ....	107

Figure 43: Sequence alignment between Piezo1 and Piezo2 C-termini.....	116
Figure 44: Design of electromagnetic needle. ....	136
Figure 45: Labeling specificity of tagged constructs. ....	137
Figure 46: Confirmation of MTSET functionality.....	140

## Acknowledgements

My thanks go first and foremost to my advisor Jörg Grandl for his generous guidance, responsiveness, inspiration, and support throughout my graduate career. He has made my time here move as smoothly as possible, working closely with me to constantly improve experiments and drive our research forward, and always looking for new opportunities for my professional development as a scientist. There isn't a day that I've been in this lab and haven't learned something new. Thank you to all current and past lab members who have built a comfortable and fun environment to do research in while constantly providing scientific feedback. Particular thanks go to Amanda Lewis, Mike Young, and Raman Goyal for their valuable collaboration, without whom I would not have been able to reach the same level of scientific success. Thanks also to all members of my committee for their support and feedback.

A special thanks goes to my previous mentor Anne Taylor, who took a risk and opened the door to science for me during a major transition in my career.

Thanks to both longtime friends and new friends I've made at Duke for the comic relief and support outside of my academic life. Finally, thank you to my parents, brother, and other family members for their constant unconditional love and encouragement.

# 1. Introduction

## 1.1 Overview

Mechanosensation is the physiological response to the mechanical forces we encounter in our environment, whether it is a touch to the skin or the vibrations of sound through air. The sense of touch and pain in particular are critical for us to learn about the environment, avoid harmful stimuli, and form bonds with others. Of our five primary senses, molecular receptors have long been identified and studied for taste, olfaction, and vision, yet a first receptor for touch has only recently been discovered, and the precise mechanosensing molecules for hearing are still debated (Chaudhari & Roper, 2010; Fleischer, 2009; Lamb, Collin, & Pugh, 2007; Pan & Holt, 2015). Therefore, understanding the molecular mechanisms of mechanosensation has remained a pressing goal in sensory neurobiology. However, the concept of mechanosensation extends beyond our nervous system and into functions of non-sensory organs and cells, as well as processes in organisms without a nervous system at all such as bacteria and plants (Wu, Lewis, & Grandl, 2017). While diverse in biological function, it has since been discovered that many of these processes share a common dependency on a single family of ion channel known as Piezos.

Piezo ion channels were discovered in 2010 in the laboratory of Ardem Patapoutian through an extensive siRNA screen as the first bona fide mechanically activated excitatory ion channels found in mammals (Coste et al., 2010). This indicates

that Piezos fulfill certain widely accepted requirements to be considered as mechanically activated ion channels: 1. They are located in mechanosensory organs, 2. They are required for the direct response to mechanical stimuli, 3. Alterations in properties of the channel directly affect its mechanical response, and 4. Mechanical gating can be achieved when the channel is expressed in heterologous systems (Árnadóttir & Chalfie, 2010; Coste et al., 2010). It was initially shown that eukaryotes possess two channel homologs, Piezo1 and Piezo2, and both are pore forming subunits that when assembled, allow for the non-selective conductance of cations across the cell membrane when stimulated by physical force. In sensory tissues, this mediates the excitatory signals that initiate action potentials propagating to the central nervous system which are ultimately perceived as the sensations of touch, pain, and balance. An understanding of how Piezo channels function is therefore an important step in studying methods in which to modulate these senses in various pathological conditions. However, Piezos reveal little if any similarity to other known proteins both by sequence homology and structure, and thus a mechanistic understanding of how the channel functions on a structural level is still in its most early stages.

The aim of this dissertation is to investigate the mechanisms by which Piezo channels function on a biophysical scale. Specifically, I set out to identify structural domains within Piezo that confer channel activation and inactivation, akin to structure-function relationships that mediate specific properties of other well-studied channels

such as voltage sensors in voltage-gated ion channels (Long, Campbell, & Mackinnon, 2005). Using a combination of patch clamp electrophysiology and biomolecular engineering, I identified distinct structural domains that are necessary for conferring the kinetics and voltage dependency of Piezo channel inactivation. These findings provide the first identification of structural correlates for channel inactivation in Piezos, as well as insights into understanding the biophysical mechanisms of Piezo function.

## ***1.2 Mechanotransduction in cell biology***

Cells convert mechanical forces in their environment into downstream biochemical processes through the mechanism of mechanotransduction. The forces that cells may undergo in a biological context may manifest in the forms of membrane stretch, shear stress, osmotic pressure, or matrix stiffness and texture.

Mechanotransduction, however, is not a passive process, as cells are also able to generate force by means of ATP-dependent dynamic cytoskeletal organizations (Nourse & Pathak, 2017; Paluch et al., 2015). Transduction of forces results in processes including cell differentiation, migration, apoptosis, development, transcription, and change in membrane potential, to name only a few (Guillot & Lecuit, 2013; Pathak et al., 2014; Vogel & Sheetz, 2006). The molecules that mediate the processes of mechanotransduction fall into two broad categories: cytoskeletal adhesion complexes and ion channels.

### 1.2.1 Sensing force through the cytoskeleton

A cell's ability to exert and sense forces from neighboring cells and substrates is made possible by the cytoskeleton, and the mechanical interface between the cytoskeleton and the extracellular environment is largely mediated by focal adhesions. Focal adhesions are molecular contacts between the cell and the extracellular matrix (ECM) made up of a dynamic macromolecular complex of proteins including integrins, the actomyosin cytoskeleton, and adaptor proteins such as paxillin, talin, and vinculin (Elosegui-Artola et al., 2016; Goldmann, 2012). Through this complex, focal adhesions sense friction between the cell and its substrate. Force sensing through this mechanism induces nuclear translocation of the Yes-associated protein (YAP) and transcriptional coactivator with PDZ-binding motif (TAZ) transcription factors, regulates further adhesion growth, and remodels the cytoskeleton in dynamic processes such as cell migration (Dupont et al., 2011; Goldmann, 2012).

Focal adhesions enable the sensing of traction force through a dynamic "clutch" mechanism by which the integrin-ECM bond creates friction between the cell and substrate, leading to mechanical stress on connected adaptor proteins. This interaction in turn regulates actin polymerization and generates cytoskeletal tension (Elosegui-Artola et al., 2016; Goldmann, 2012). Specifically, the extracellular domain of the transmembrane protein integrin is bound to the ECM, and the intracellular domain of integrin is coupled to the actin cytoskeleton through the linker proteins talin and

vinculin. When the substrate deforms or when the cell moves, traction force is generated and the “clutch” is loaded. At low rigidities, force loading is slow and the integrin-ECM bond dissociates (“clutch” unloading) to regulate force transmission. As substrate rigidity increases however, force loading becomes faster than the lifetime of the integrin-ECM bond, and force is thus transferred to talin which unfolds under stress. The unfolding of talin induces vinculin binding for stabilization, downstream actin remodeling, and translocation of the YAP transcription factor through a still unclear mechanism (Elosegui-Artola et al., 2016). Thus, focal adhesions allow a cell to sense force between itself and the substrate and transduce this force into downstream processes, resulting in cytoskeleton-mediated mechanotransduction.

### **1.2.2 Sensing force through ion channels**

Prior to the discovery of Piezos, a number of other mechanosensitive ion channels have been identified in lower organisms such as bacteria and *C. elegans*. Mechanosensitive ion channels allow the passage of ions across cell membranes in response to mechanical force. The latency of this form of transduction can be less than a millisecond, which is a distinct advantage over cytoskeleton mediated mechanotransduction which can occur on the order of minutes.

Of the mechanosensitive channels identified so far, the bacterial Mechanosensitive channel of Large conductance (MscL) and the Mechanosensitive channel of Small conductance (MscS) are perhaps the most well studied. MscL and MscS

are pore forming subunits that as ion channels, open in response to lateral membrane tension and allow bacteria to respond to hypoosmotic shock (Árnadóttir & Chalfie, 2010; Iscla & Blount, 2012). MscL and MscS fulfill all four previously described requirements to be a mechanically activated ion channel, and until the discovery of Piezos, few eukaryotic channels have met these same requirements.

In eukaryotes, the family of *C. elegans* degenerins (DEG) and mammalian Epithelial Na<sup>+</sup> Channels (ENaC), together termed DEG/ENaC, have been identified as candidate mechanosensitive channels. In *C. elegans*, the DEG/ENaC proteins MEC-4 and MEC-10 are pore-forming subunits of a mechanosensory ion channel, identified in genetic screens for deficiencies in tactile detection (Arnadóttir, O'Hagan, Chen, Goodman, & Chalfie, 2011). It is proposed that attachments to the ECM and cytoskeleton allow force to directly open the MEC-4/MEC-10 channel, resulting in Na<sup>+</sup> influx and depolarization of sensory neurons (Sukharev & Corey, 2004). In *D. melanogaster*, the DEG/ENaC genes *pickpocket* and *balboa* have also been proposed to form mechanosensitive ion channels and are required for nociceptive response (Mauthner et al., 2014). In mammals, the DEG/ENaC family of acid sensing ion channels (ASICs) have also been demonstrated to be involved in, but not required for, mechanosensation in mammals (Árnadóttir & Chalfie, 2010).

Two-pore domain K<sup>+</sup> channels (K2Ps) such as TREK-1, TREK-2, and TRAAK, have been demonstrated to be directly activated by mechanical force to conduct K<sup>+</sup> ions

and serve as an inhibitory signal in mammalian sensory neurons. It has been proposed that TREK-1 channels may be gated by a tight linkage between the C-terminal domain and the inner leaflet of the lipid bilayer, and while the precise role of K2P channels in mechanosensation is still unclear, it has been proposed that they may serve a role in controlling the excitability of sensory neurons (Honoré, 2007).

A number of Transient receptor potential (TRP) channels have also been proposed as candidates for mechanosensitive ion channels. Notably the TRPN channel NompC was discovered in *Drosophila* in a screen for mechanically insensitive mutants (Kernan, Cowan, & Zuker, 1994). Mutations in NompC eliminate the peak mechanosensory current from hair bristles, but heterologous expression has yet to yield mechanically induced current (Árnadóttir & Chalfie, 2010). In mammals, TRPV4 has been demonstrated to be activated in heterologous expression by osmotic pressure, and it has been proposed to act as a mechanosensing channel in both neuronal and non-neuronal tissue. It is expressed widely in osmoregulating organs such as the kidney and the skin, and genetic knockout of TRPV4 in mice has been shown to affect nociceptive, but not gentle touch stimuli (Suzuki et al., 2003).

New classes of mechanosensitive channels remain to be discovered. Recently, a volume-regulated anion channel (VRAC) component called SWELL1 was identified to be important in regulating cell volume through sensing of ionic strength (Qiu et al., 2014). However, SWELL1 has not shown to be itself mechanically activated outside the

context of the VRAC, though point mutations in SWELL1 alter ion selectivity of VRAC, suggesting a key role in the pore forming complex.

Thus far, Piezo ion channels remain as the only mechanically activated excitatory ion channels in mammals. They are undeniably pore-forming subunits and inherently mechanosensitive. Additionally, they are widely expressed in a variety of pressure sensing organs, including the nervous system, and knockout models as well as mutations have resulted in clear physiological defects (J. Wu et al., 2017).

### ***1.3 The roles of Piezo throughout the body***

The role of mechanosensation is crucial to the function and development of many tissues throughout the human body. Piezo1 is largely expressed in non-sensory tissue such as the cardiovascular and renal systems, and Piezo2 is more commonly found in sensory tissue such as the dorsal root ganglia (DRG) and skin. Given the diversity in cellular environments and types of force encountered in these different organs, it is a wonder that only the two homologs of Piezo ion channels have been shown to be key mediators of mechanosensing in each of these systems.

#### **1.3.1 Piezos in the peripheral nervous system**

Of our five primary senses, touch and hearing, both of which depend on mechanosensation, are the last to be resolved on a molecular mechanistic level. Proprioception, our sense of our body's and limbs' relative positions in space is also dependent on mechanosensation and a molecular understanding of this sense is also in

its early stages. Piezo2 has been shown to be found in mechanosensory hair cells of the auditory system, but they are not required for these cells' mechanosensitive response (Z. Wu et al., 2017). In contrast Piezo2 has also been identified in DRGs innervating the skin and muscle spindles where it has been demonstrated to be necessary for the sense of light touch and proprioception. Piezo2 has also been shown to be expressed in the trigeminal ganglia (TG), which innervates the sensory regions of the face, in waterfowl as well as the star-nosed mole - the star nose is a highly specialized mechanosensor and the most densely innervated mammalian skin surface (Gerhold et al., 2013; Schneider et al., 2014).

DRGs are clusters of neuronal cell bodies in the peripheral nervous system that reside along the spinal nerve and send afferent axonal projections to the sensory endings in the skin and muscle as well to the dorsal horn of the spinal cord (Figure 1). The peripheral nerve endings in the skin are multimodal, meaning that they detect a variety of somatosensory stimuli including temperature, chemical contact, and mechanical force. Mechanical and proprioceptive stimuli are detected by sensory receptors that express Piezo2 and likely other mechanosensitive ion channels. This stimulation induces channel opening, membrane depolarization, and action potential propagation along the DRG to the spinal cord where it synapses onto interneurons, motorneurons, and second order neurons that ultimately form the spinothalamic tract projecting to the thalamus and somatosensory cortex of the central nervous system. DRG fibers are characterized

by their diameter, conduction velocity, and myelination, dividing them into classifications, the most commonly studied of which are termed A $\beta$ , which detects innocuous touch, and A $\delta$  and C fibers, which detect painful stimuli. The fibers are further categorized based on their adaptation kinetics, divided into fast adapting, intermediate adapting, and slow adapting fibers, which allows us to discriminate significant stimuli such as pain and initial contacts from constant stimuli such as the long term contact of clothing.

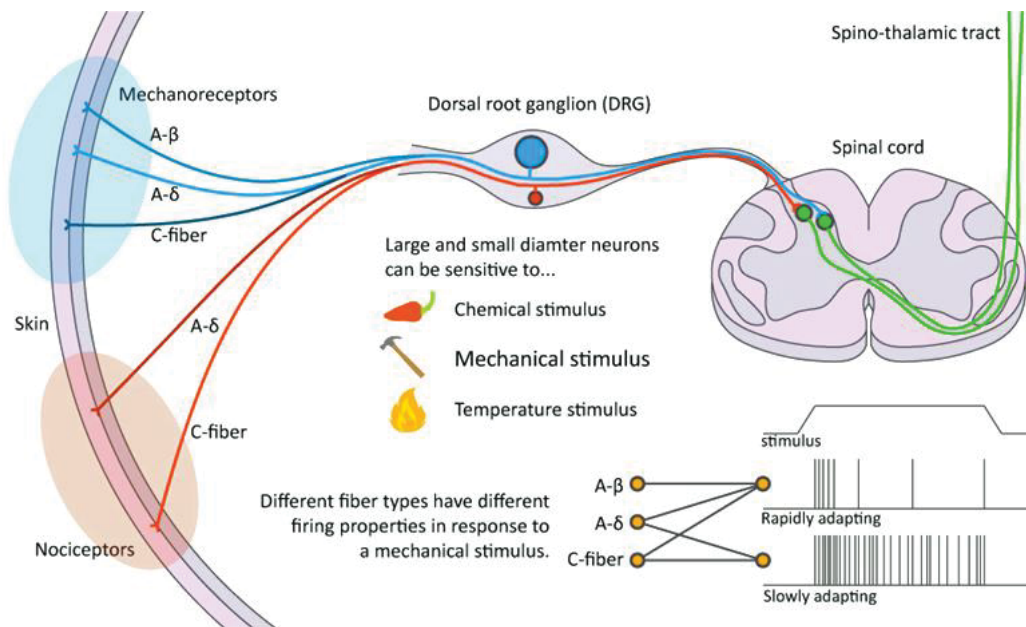


**Figure 1: Somatosensory pathways. Large (blue) and small (red) diameter dorsal root ganglion neurons project to the skin for sensing somatosensory stimuli and to the dorsal horn of the spinal cord to project to the central nervous system. Different fiber subtypes adapt to stimulus at different rates, measured by the frequency of sustained action potential firing in the presence of a stimulus.**

The first direct evidence for Piezo2's role in tactile sensation was its identification in Merkel cells, a specialized mechanosensory receptor in the skin that is in complex

with the nerve terminals of slowly adapting A $\beta$  fibers (Woo et al., 2014). In complementary studies, two different groups demonstrated that Piezo2 mediated mechanically activated currents in Merkel cells, and with knockout models they showed that it was also necessary for inducing slowly adapting action potentials in Merkel cells (Ikeda et al., 2014; Woo et al., 2014). Furthermore, tissue specific knockout models resulted in deficiencies in sensing light tactile stimuli, demonstrating its role in mammalian mechanosensation (Ikeda et al., 2014; Woo et al., 2014). Around the same time, Piezo2 was also identified in DRG sensory fibers that innervate Merkel cells and other mechanoreceptive organs of the skin (S. Ranade et al., 2014). When Piezo2 is knocked down in sensory fibers, the population of rapidly adapting DRGs is reduced, touch-induced action potentials are also reduced, and animals exhibit a behavioral loss of response to light touch (S. S. Ranade et al., 2014). In analogous experiments, Piezo2 was demonstrated to be the primary mechanosensor for proprioception (Woo et al., 2015). Piezo2 localizes to proprioceptive neurons that innervate golgi tendon organs as well as muscle spindles, specialized proprioceptive receptors that sense muscle stretch and movement. Akin to the described studies, knockout of Piezo2 in these neurons also caused a reduction of rapidly adapting DRG cells, a reduction in action potentials, and behavioral defects in posture and gait (Woo et al., 2015).

While the role of Piezo2 appears to be mostly involved in mediating non-noxious stimuli, some evidence has also been presented supporting the role of Piezos in

nociception, the sensory response of pain. In *Drosophila*, the single Piezo ortholog DmPiezo was shown to contribute to nociceptive response in larvae, and when knocked down in combination with *pickpocket* in sensory neurons, nociceptive response was entirely abolished (Kim et al., 2012). Piezo2 has also been implicated in hyperalgesia, a state of nociceptive sensitization, as it is potentiated by an inflammatory mediator bradykinin which induces hyperalgesia, and knockdown of Piezo2 reduces hyperalgesia (Dubin et al., 2012; Ferrari et al., 2015). Additionally, Piezo2 is potentiated by EPAC1, a cyclic amp sensor induced in neuropathic pain (Eijkelkamp et al., 2013).

Finally, recent studies have presented direct evidence that Piezos play an active role in human mechanosensation. Genetic studies and whole-exome sequencing identified human patients with a dominant mutation in Piezo2, thought to result in a non-functional channel. These patients are diagnosed with the disorder distal arthrogryposis, which is characterized by contractures of distal joints, gross motor impairment, and notably, deficits in proprioception and touch, tested by asking patients to detect the movement of distal digits (Mahmud et al., 2017; McMillin et al., 2014). Another study identified a patient also with distal arthrogryposis caused by a recessive Piezo2 stop mutation who exhibited defects in sensing joint position (Haliloglu et al., 2016). In a separate study, two undiagnosed patients with inactivating variants of Piezo2, identified with whole-exome sequencing, also exhibited proprioceptive deficits characterized by ataxia, dysmetria, and loss of balance (Chesler et al., 2016). The

perception of light touch was also impaired in glabrous skin, while broad somatosensory stimuli were still discernable for hairy skin. These studies, along with several others, highlight the effects of loss-of-function mutations in Piezo2 and their significant impact on human proprioception. While somatosensory defects are observed in some cases, the relatively mild phenotype suggest that other yet unidentified mechanoreceptors are at play.

### **1.3.2 Piezos in non-sensory tissue**

Outside the sensory nervous system, Piezos can be found in numerous different non-sensory organ systems throughout the body. Piezo1 is more commonly found in non-sensory tissue, though Piezo2 is present in some systems as well, and it has been shown to play specific roles in sensing the forces that determine the development and regulation of these tissues (Figure 2).

Perhaps the most notable of these roles can be observed in the cardiovascular system. In a mouse model, both global and endothelial-specific knockout of Piezo1 led to prenatal death, which attributed largely to a disrupted development of the vasculature system (Li et al., 2014; S. S. Ranade et al., 2014). Piezo1 is expressed in the endothelial cells that line the walls of blood vessels where it is believed to sense the shear stress of blood flow. Indeed, it has been shown that the sensing of shear stress via Piezo1 is necessary for proper vascular development as well as proper alignment of endothelial cell orientation (Li et al., 2014; S. S. Ranade et al., 2014).

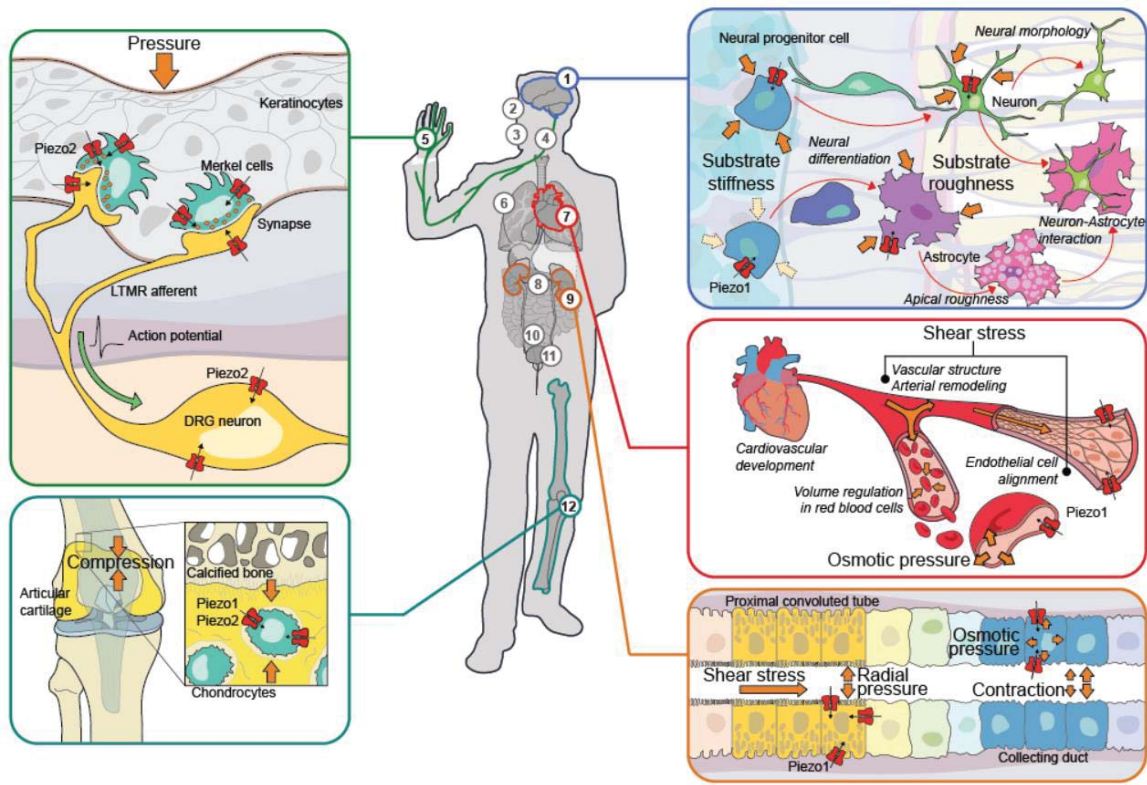


Figure 2: Expression and physiological roles of Piezos. Piezo1 and Piezo2 are expressed in a diverse set of organs and tissues within the human body, contributing to an equally diverse set of physiological roles. Numbered tissues are as follows: 1, brain; 2, optic nerve head; 3, periodontal ligament; 4, trigeminal ganglion; 5, dorsal root ganglion and skin; 6, lungs; 7, cardiovascular system and red blood cells; 8, gastrointestinal system; 9, kidney; 10, colon; 11, bladder; and 12, articular cartilage. Tissues in which Piezo function has been extensively studied are expanded to show detail. Top left inset illustrates Piezo2 expressed in Merkel cells of the skin, where mechanical activation of Piezo mediates depolarization and activation of dorsal root ganglion cell afferents, which also express Piezo2. Together, these cells are involved in sensing light touch and proprioception (DRG, dorsal root ganglion; LTMR, Low-threshold mechanoreceptor). Bottom left inset highlights the expression of both Piezo1 and Piezo2 in chondrocytes of articular cartilage, where they activate under compressive force. Top right inset illustrates the role of Piezo1 in sensing mechanical properties of the environment of neural progenitor cells, thereby initiating signaling pathways that lead to neuronal differentiation and subsequent development of neurite morphology, neuron–glia interactions, and nanoroughness of glial membranes. Middle right inset depicts the role of Piezo1 in regulating volume of red blood cells as well as sensing shear stress to regulate vascular branching and

**alignment of endothelial cells. Bottom right inset shows the role of Piezo1 in sensing fluid flow throughout the nephron of the kidney. Deficits in Piezo1 function in the kidney may lead to downstream effects on urinary osmolarity and renal pathologies.**

**Illustration from Wu, Lewis and Grandl, 2017.**

Piezo1 is also highly expressed in myocytes, smooth muscle cells of the heart, and mediates mechanosensitive current; smooth muscle-dependent knockdown of Piezo1 revealed that it mediates arterial remodeling, particularly in hypertension (Retailleau et al., 2015). Interestingly, in the adult endothelium, Piezo1 regulates blood pressure through vasoconstriction during whole body exercise, but not at rest (Rode et al, 2017). Piezo1 is also expressed on the surface of red blood cells, where it has been demonstrated to sense both shear stress and osmotic pressure, ultimately leading to ATP release and volume homeostasis (Cahalan et al., 2015; Cinar et al., 2015).

Of course, mechanical stress occurs in a number of other organ systems as well, and Piezo1 has been implicated in virtually all of those that have been studied. Both Piezo1 and Piezo2 are expressed in chondrocytes of articular cartilage, where they activate and regulate apoptosis under compression (Lee et al., 2014). In the renal epithelia, Piezo1 plays a role in sensing fluid flow and circumferential pressure as well as regulating urinary osmolarity (Martins et al., 2016; Peyronnet et al., 2013). In the gastrointestinal tract, Piezo2 is responsible for the mechanosensitivity of enterochromaffin cells, which detect static pressure (Alcaino, Farrugia, & Beyder, 2016). Other systems that have been shown to depend on the mechanosensitivity of Piezo channels include the lungs, optic nerves, periodontal ligaments, and colon, further

highlighting its importance and prevalence in animal biology (Choi, Sun, & Jakobs, 2015; Coste et al., 2010; Jin et al., 2015).

Apart from its roles in mechanosensing at the level of organ systems, Piezos have also been introduced as mediators and modulators of many basic cellular functions. When studied in vitro, Piezo1 was shown to influence epithelial cell division and extrusion as a consequence of sensing mechanical stretch or crowding (Gudipaty et al., 2017). A related study found that Piezo1, in network with myosin II, allowed cells to sense confinement as a possible mechanism for regulating cell motility and adapting to extracellular environments (Hung et al., 2016). The connection between Piezo1 and cell migration could provide insights into mechanisms of cancer cell metastasis, as Piezo1 was seen to be upregulated in the MCF-7 breast cancer cell line (Li et al., 2015). In the central nervous system, Piezo1 expression in neurons and neural progenitor cells allows for the sensing of the extracellular nanotopography and stiffness to determine pathways for neurogenesis or astrogenesis (Blumenthal et al., 2014; Pathak et al., 2014). These mechanisms in neurons also mediate the development of neurite morphology as well as cell-cell interactions. Together these studies demonstrate the wide significance of Piezo channels outside of sensory biology.

#### ***1.4 The activation and inactivation of Piezos***

To observe the electrophysiological properties of Piezo in vitro, Piezo ion channels are most commonly studied with two stimulation methods: pressure clamp

and force probe stimulation (Figure 3). For pressure clamp electrophysiology, a cell-attached seal is made on a Piezo expressing cell, and negative pressure is applied directly through the patch pipette to induce tension in the patch dome. This elicits channel opening, and current amplitude can be measured as a function of pressure to derive a gauge of pressure sensitivity, typically quantified as the pressure of half maximal activation ( $P_{50}$ ). However, this measurement is highly impacted by the precise geometries of the patch pipette as well as the physical integrity of the patch. To stimulate a cell with a force probe, a whole-cell patch is made onto a Piezo expressing cell, and a blunt glass pipette is controlled to indent the cell at varying depths. This method stimulates a large proportion of expressed channels, although due to the heterogeneity of cell structures and membrane compositions, it can be difficult to precisely measure the exact amount of force a single stimulation imposes upon the cell. Applying a force stimulation at varying voltages and under different buffer compositions reveals that Piezos are nonselective cation channels. Interestingly, Piezo2 is not reliably activated with pressure clamp stimulation, suggesting a difference between the precise force modality of the two methods, and perhaps that the activating mechanism between Piezo1 and Piezo2 are distinct as well.

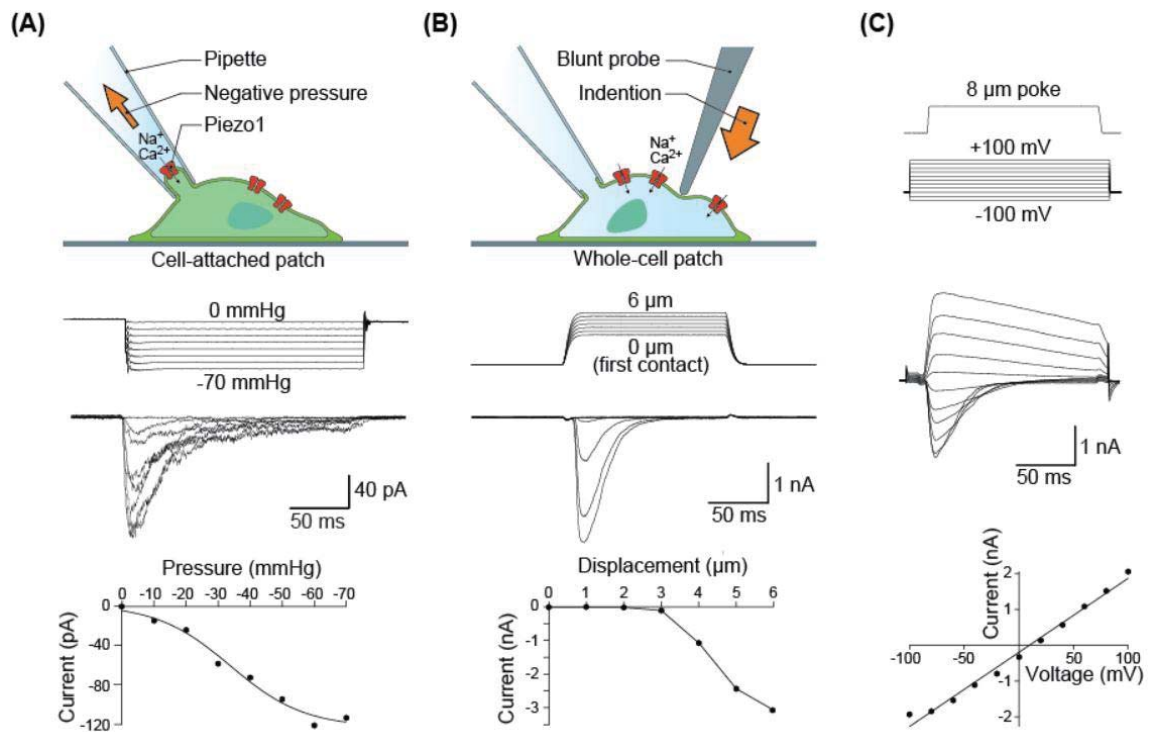


**Figure 3: Piezos are mechanically activated ion channels. (A) Schematic of pressure clamp setup, in which negative suction is applied to a cell-attached patch with a high-speed pressure clamp through the patch pipette, stimulating only those channels contained within the patch dome (above). Piezo1 peak current amplitudes initially rise with increasing magnitudes of pressure before reaching saturation (middle). The pressure–response relationship can be fit with a sigmoidal function to measure pressure sensitivity (below). (B) Schematic of force probe setup depicting cell deformation by a blunt probe (typically a fire-polished glass pipette) during a whole-cell recording, which activates a larger population of channels throughout the cell (above). Piezo1 current amplitudes increase with increasing steps of displacement beginning a few micrometers beyond first contact of the probe with the cell membrane. From these experiments, a current–displacement curve can be generated. Typically, currents do not plateau before cell rupture (below). (C) Voltage step protocol with a single force probe displacement during each step (top). A family of currents from a single cell illustrates the voltage dependence of channel inactivation, with severely slowed decay times at positive voltages (middle). An I–V curve plotted from peak current amplitudes reveals a reversal potential near 0 mV, demonstrating cationic nonselectivity (bottom). Adapted from Wu, Lewis, and Grandl, 2017.**

Both of these stimulation methods come with shortcomings, and thus a number of other methods have both been presented and are being developed to stimulate Piezo and other mechanically activated channels more precisely (Figure 4).

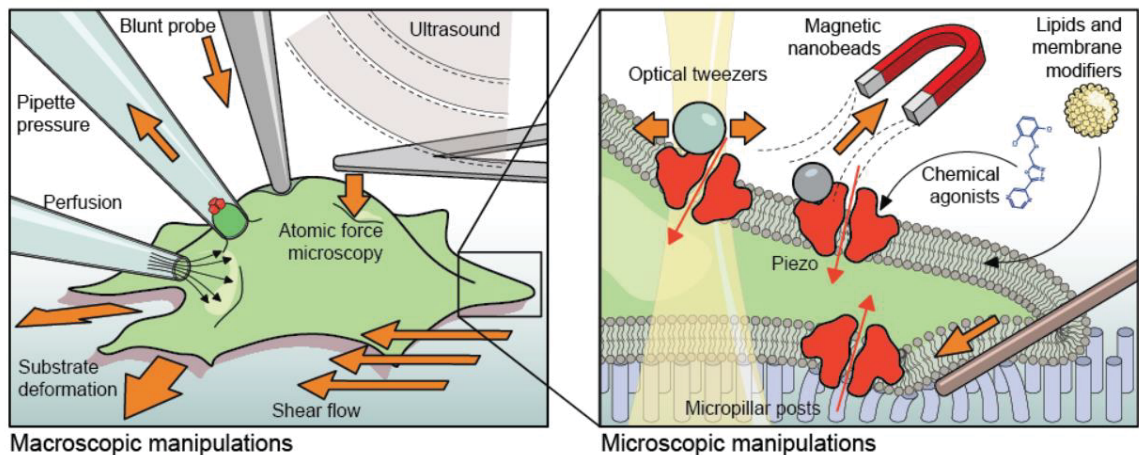


**Figure 4: Current and future methods of stimulating Piezos. Orange arrows represent direction of force in relation to cell or channel, and Piezo ion channels are illustrated in red. Left: Macroscopic methods for stimulating large populations of Piezo channels, whose activity can be measured with electrophysiology or through calcium imaging. These include directly deforming the cell with a force probe or with atomic force microscopy. High-pressure perfusion is an alternative method to deform the cell without physically contacting the membrane, while by contrast, shear flow achieved through microfluidic channels applies a parallel stress to the substrate surface. Both positive and negative pressures through a pipette can stimulate single or many Piezo channels. Substrate deformation with flexible membranes and remote vibration of the cell and surrounding milieu through ultrasound are yet untested methods for directly stimulating Piezo channels. Right: Microscopic modes of Piezo stimulation are shown magnified in the context of the plasma membrane. Deflection of micropillars stimulates single or small populations of Piezo channels through membrane deformation. The agonist Yoda1 directly activates Piezo1, though the mechanism is unknown. Lipids such as cholesterol modulate Piezo function, but have not yet been shown to directly induce activation. In theory, direct activation of the channel could be achieved through magnetic or optical control of nanoparticles bound to specific channel domains; application of force through magnetic nanobeads has been shown to perturb channel function, but neither technique has been shown to directly activate Piezo. Adapted from Wu, Lewis, and Grandl, 2017.**

For example, growing cells on micropillar arrays allows for fine stimulation of small subcellular regions by deflecting a single micropillar (Poole et al., 2014). Atomic force microscopy can stimulate cells with a direct measurement of the applied force, and shear stress can be applied to cells in microfluidic chambers (Lee et al., 2014; Li et al., 2014). The development of different manipulations to activate Piezo channels provides a toolbox of techniques that will be highly beneficial to answering specific future questions in mechanosensation.

Channel activation, the opening of the channel and passage of ions, occurs rapidly for both Piezo1 and Piezo2, reaching a peak amplitude within 10 ms of the onset of stimulus with either stimulation method (Coste et al., 2010). Evidence so far suggests that Piezo1 at least is activated directly by membrane tension. In one study, membrane tension was calculated by measuring the radius of a patch dome within a patch pipette during pressure clamp stimulation in relation to the amount of pressure applied (Lewis & Grandl, 2015). By analyzing current amplitude as a function of tension, the authors deduced that the mechanical sensitivity of Piezo was directly tuned by tension. In two other studies, Piezo activation was measured in lipid environments devoid of other possible contributing factors such as cytoskeleton and ECM, one in membrane blebs and another in artificial lipid bilayers, to also demonstrate that Piezo1 channels are inherently sensitive to membrane tension (Cox et al., 2016; Syeda et al., 2016).

The closing of ion channels can occur through certain distinct mechanisms, and it is important to distinguish between these. When presented with an activating stimulus, it becomes more energetically favorable for an ion channel to adopt an open state conformation. When that stimulus is removed, the channel returns to its closed state and the channel no longer conducts ions; this is called deactivation. However, in Piezos and many other ion channels, current begins to decay in the presence of the stimulus, and this can be attributed to one or both of two mechanisms: adaptation or inactivation (Figure 5). In the case of adaptation, a channel becomes desensitized to a stimulus allowing current to decay, but an additional stronger stimulus can once again activate the channel directly from the desensitized state. One study has demonstrated that this does not occur in Piezo1, and it has not yet been tested for Piezo2 (Gottlieb, Bae, & Sachs, 2012). In the case of inactivation however, current decays in the presence of a stimulus and cannot be induced again unless the stimulus is removed and the channel is given time to recover. This is observed for both Piezo1 and Piezo2, which exhibit a time-dependent recovery from inactivation after deactivation (Coste et al., 2013; Coste et al., 2012).

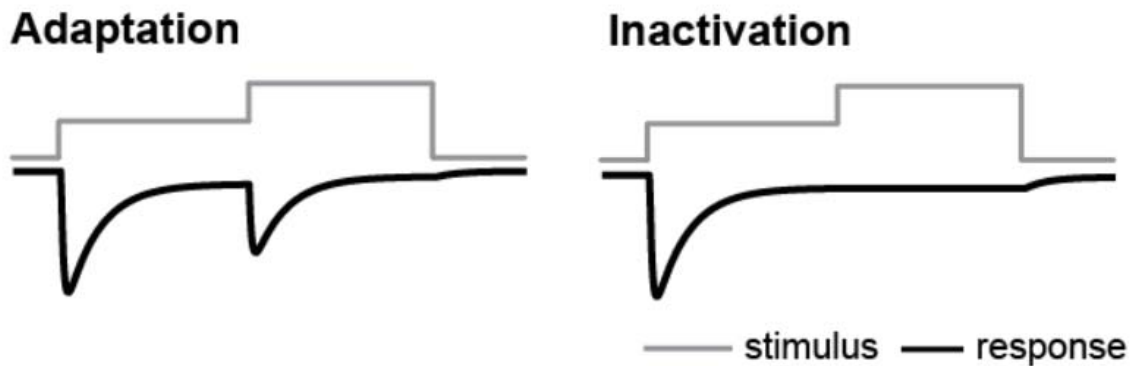


**Figure 5: Adapting versus inactivating currents. Idealized currents (black) in response to a two-pulse stimulus protocol (gray), demonstrating the presence of additional current upon an increase in stimulus intensity for an adapting, but not for an inactivating current. Figure by A. Lewis, from Wu, Lewis, and Grandl, 2017.**

The inactivation kinetics of Piezos can be measured by fitting a single exponential curve to the decaying current. With force probe stimulation, the time constant of inactivation differs between Piezo1 and Piezo2, ~10 ms and ~1 ms, respectively, at -100 mV, and inactivation slows as the holding potential becomes more positive, with time constants lengthening by an order of magnitude at +100 mV. While the role of inactivation in Piezos is still relatively unknown, one study has provided evidence that inactivation may enable sensory cells to filter the frequencies of repetitive mechanical stimuli, and it is becoming more evident that inactivation plays a critical role in disease as well (Bagriantsev, Gracheva, & Gallagher, 2014; Lewis et al., 2017). The mechanism of how inactivation occurs is also still relatively unclear, so further studies, including those presented in this dissertation, are necessary to closely examine the functions of structural domains and their mechanistic roles in inactivation.

## **1.5 The architecture of Piezo**

Piezo channels are one of the largest ion channel structures ever identified, with hydrophathy profiles predicting up to 30 transmembrane domains per subunit and little if any sequence similarity to other channels (Alper, 2017). A medium-resolution (4.8 Å) cryo-electron microscopy (cryo-EM) structural model of mouse Piezo1 reveals a trimeric structure, approximately 200 Å in diameter, with each monomer having at least 14 transmembrane domains (Figure 6) (Ge et al., 2015). The N-terminal ends of each trimer form the periphery of the channel and are arranged in a propeller-like formation, which have been termed 'blades'. The C-terminal end of each subunit interfaces to form the pore and a distinct cap structure which has been termed the 'C-terminal extracellular domain' (CED). The pore domain itself is composed of the last two transmembrane domains, an 'inner pore helix' (IH) and 'outer pore helix' (OH) from each subunit, and directly below is a formation of short helices forming a conserved structure that is referred to as the 'anchor' domain. Finally the intracellular face of the channel displays an intriguing 'beam' structure that spans the entire length of the blades and seemingly connects the pore domain to the periphery. However due to the course resolution of the model, the primary sequence cannot be assigned to most of the peripheral structures including the blades and beam (Ge et al., 2015).

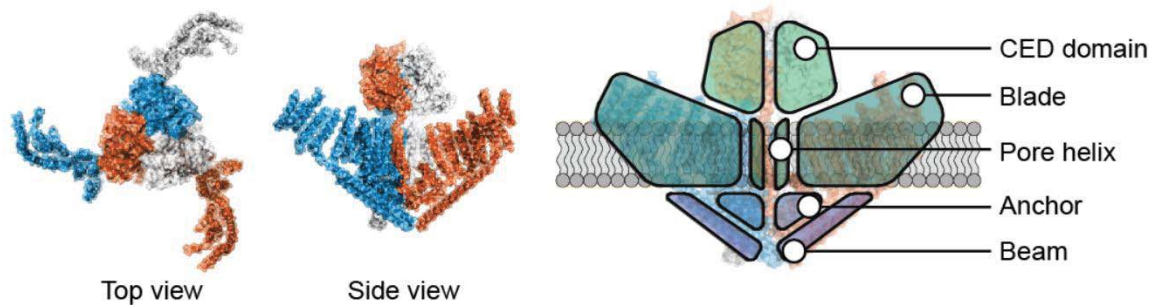


**Figure 6: The architecture of Piezo1. The cryo-EM structure (PDB 3JAC) of Piezo1 (left) reveals possible structural domains (right) that may play a role in mechanosensing and channel activation. Adapted from Wu, Lewis, and Grandl, 2017.**

The structural details surrounding the pore have been resolved and studied in greater detail. Initially, engineered chimeric channels between Piezo1 and DmPiezo revealed that the C-terminal region confers ion-permeation properties (Coste et al., 2015). Specifically, a glutamate residue (E2133) within the anchor domain was identified to influence, if not directly mediate, unitary conductance and ion selectivity as well as pore block, suggesting that this may be the site of the selectivity filter (Coste et al., 2015). Analysis of sequence homology for Piezo across species also revealed a highly conserved PF(X<sub>2</sub>)E(X<sub>6</sub>)W motif in the anchor, further supporting the notion that this domain plays an important role in channel function (Prole & Taylor, 2013). The CED was first crystallized from of *C. elegans* Piezo and revealed a unique  $\beta$ -sandwich fold that was unlike any previously characterized protein fold (Kamajaya et al., 2014). The CED of mouse Piezo1 was separately crystallized at an atomic resolution of 1.7 Å and revealed a similar structure as well a central cavity between the three subunits along its central axis, which may be a potential pathway for ion permeation (Ge et al., 2015). In sequence,

the CED is located in between the inner and outer pore helices, and together the IH-CED-OH sequence forms the central axis of the ion channel. The precise roles and mechanisms involving this domain are investigated in this dissertation.

## **1.6 Activation mechanisms and modulation of Piezos**

Activation mechanisms have been described for several mechanically activated ion channels (Nilius & Honoré, 2012; Sukharev & Corey, 2004). However, Piezos share very little sequence homology and structural similarity with other mechanically activated ion channels, so despite the emerging detail of structural data, uncovering the precise mechanism for mechanical activation of Piezos has been difficult. Nonetheless existing models of mechanical activation are instrumental in solving this question and hypothesizing about possible mechanisms in Piezo.

### **1.6.1 Mechanisms of mechanical activation**

Two commonly referenced models of mechano-gating in ion channels are the 'tether model' and the 'bilayer model' (Nilius & Honoré, 2012). The tether model describes a mechanism by which extracellular or intracellular components mechanically couple to an ion channel and pull on ion channel structures to induce channel opening. For example, DEG/ENaC channels have been shown to make connections to the ECM, and it is believed that a tether gating model is at play (O'Hagan, Chalfie, & Goodman, 2005). In auditory hair cells, although the identity of the actual ion channel involved is still debated, it has been established that an extracellular tether called the tip-link likely

gates a mechanically coupled ion channel upon deflection of stereocilia (Pan & Holt, 2015). The bilayer model on the other hand, describes the process by which tension within the lipid membrane directly gates an ion channel. When a membrane is stretched and thinned, hydrophobic residues normally buried within the lipid bilayer are exposed to solvent, causing an energetically unfavorable hydrophobic mismatch. As the helices shift to counteract this mismatch, the conformational structure of the ion channel changes and induces opening, as is the case for MscL (Nilius & Honoré, 2012). Another mechanism of gating through membrane stretch has been proposed for K2P channels, proposing that membrane stretch can displace alkyl chains of lipids that occupy a pore blocking cavity, though this has not yet been confirmed (Nilius & Honoré, 2012). When observing the structural features identified in the Piezo channel architecture, it is easy to suppose that either of these gating models may be at play, and from these models we can imagine various possible mechanisms of channel opening for Piezos (Figure 7).

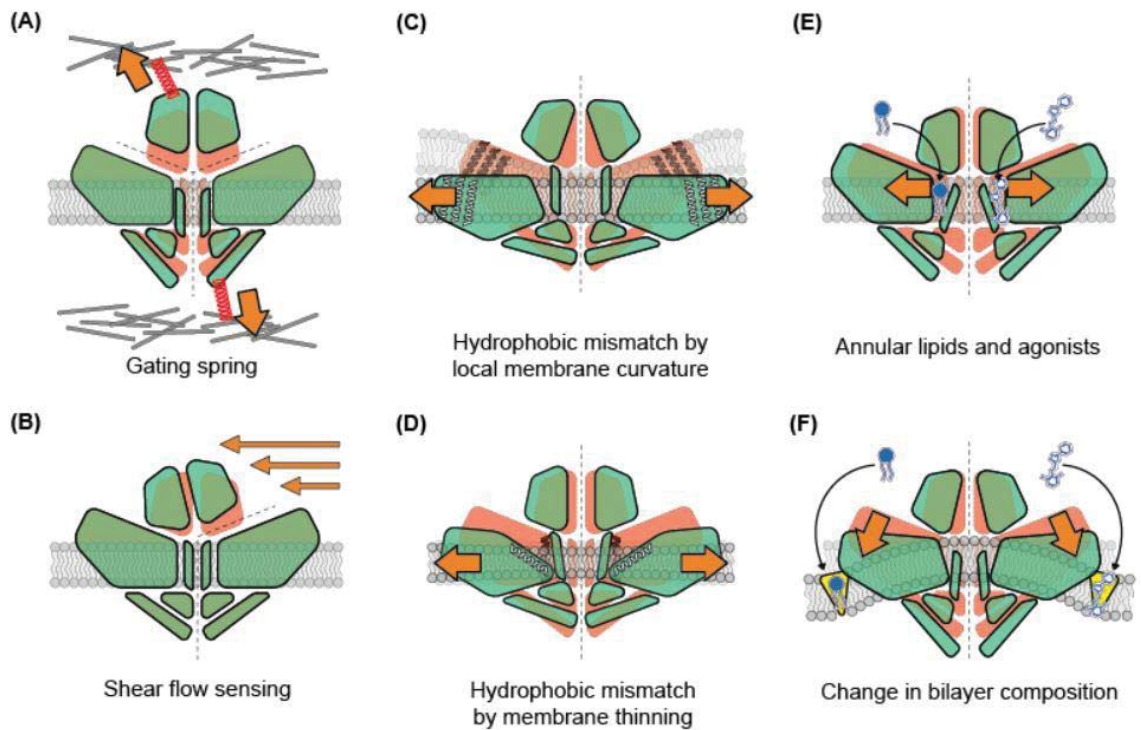


**Figure 7: Potential mechanisms of mechanical sensing and activation. Possible sensing mechanisms and conformational changes by which Piezo channels may activate in response to external forces. Potential ion-permeation pathways are indicated with broken lines; orange represents the closed channel conformation and green represents the open conformation upon applied force. (A) Tethering of either the CED domain to the extracellular matrix or the ‘beams’ to cytoskeletal elements may contribute to a gating spring mechanism of activation. (B) Similarly, local shear flow may displace the CED and expose an ion-permeation pathway. (C) The curved architecture of the cryo-EM Piezo1 structure supports the possibility that Piezo rests in a locally curved lipid bilayer environment. With rising membrane tension, the curvature is reduced, potentially causing hydrophobic mismatch of the ‘blades’ and conformational changes in the ‘beam’ and ‘anchor’ domains to open the pore. (D) Hydrophobic mismatch may also occur due to changes in plasma membrane thickness by in-plane membrane stretch, by which a tilt in the pore helices might lead to pore opening. (E) Annular lipids, agonists, and inhibitors may insert directly within the channel structure to initiate changes in channel conformation. (F) Lipids and chemical modifiers may also insert directly into the membrane causing changes in membrane stiffness, tension, or curvature, leading to channel activation. Adapted from Wu, Lewis, and Grandl, 2017.**

While Piezo1 does not need the cytoskeleton or ECM to activate, nor has it been shown to strongly interact with structural matrices, it remains possible that Piezo activation can be modulated through the tether model (Coste et al., 2012; Syeda et al., 2016). The large and protruding extracellular CED and blade domains are prime candidates for ECM interactions, and the intracellular beam domains could be sites for cytoskeletal connections. These hypothesis have not been tested in Piezo2, which responds differently to pressure clamp and force probe stimulation, nor has it been tested in a wide variety of cell lines with different cytoskeletal compositions, so a tether model gating mechanisms cannot yet be definitively ruled out.

Piezo1 is directly gated by tension, though the precise structural mechanism is still unclear (Syeda et al., 2016). In a bilayer model, the cross sectional area of MscL changes in plane with the bilayer under membrane stretch by  $\sim 20 \text{ nm}^2$ , which corresponds to the difference between a closed and open channel (Sukharev & Sachs, 2012). Similarly, in Piezos this change in area due to membrane stretch and therefore thinning, is estimated to be  $\sim 6\text{-}20 \text{ nm}^2$  under tension, suggesting that a similar activation mechanism is plausible (Bae et al., 2013). Apart from possible hydrophobic mismatch in Piezos through membrane thinning or global membrane curvature, the curved geometry of the blade raises the possibility that the channel induces a local membrane curvature itself. Perhaps then Piezo may be gated by the maintenance of stability within the bilayer through hydrophobic mismatch as this local curvature is released upon stretch.

Perhaps separate from either the tether or bilayer model, changes in lipid composition due to mechanical perturbation of the membrane could also mediate the gating of Piezos. For example, annular lipids, which form strong lipid-protein interactions, may gain accessibility to binding sites in the Piezo structure that induce activation. Alternatively, the change of local curvature of the membrane by asymmetric lipid incorporation into the surrounding of Piezo may also activate the channel. In one study, authors induce a fully active MscL channel by introducing the conically shaped phospholipid derivative LPC to one leaflet of the bilayer to alter intrinsic membrane curvature (Perozo et al., 2002). While Piezo1 is not sensitive to the direction of global membrane curvature, it is possible that it may be sensitive to changes in local curvature surrounding individual channels (Lewis et al., 2017).

Ultimately, the activation of Piezo channels remains an unsolved and remarkably complex question. Following the channel's ability to sense force must be a transduction to the process of pore opening, which itself could occur through a variety of different mechanisms and merits the attention of future studies. Nevertheless, the first step to activating a mechanically gated channel is the sensing of force, and this mechanism could occur through any individual or combination of the proposed mechanisms, or others that have not yet been described.

## 1.6.2 Modulation of Piezos

The potential for multiple gating mechanisms becomes more apparent when considering the diverse set of modulators that have been discovered to affect Piezo activation and inactivation. Piezo channels are blocked by the polycationic pore blocker ruthenium red and the spider toxin, GsMTx4 (Coste et al., 2012; Gottlieb et al., 2012). Thus far, only one chemical agonist, Yoda1, has been identified to activate Piezo1 in calcium imaging assays and induce a slowing or loss of inactivation by electrophysiology (Cahalan et al., 2015; Syeda et al., 2015). Both Yoda1 and GsMTx4 could in theory act on Piezo through direct interactions with the channel or indirectly through alterations in membrane properties. The phospholipid PIP<sub>2</sub> has also been shown to inhibit Piezo activity, which again could be attributed to modulations of the membrane or binding of the channel itself (Borbiro, Badheka, & Rohacs, 2015).

As a tension sensing molecules, Piezos are inescapably modulated by factors influencing membrane tension such as cytoskeletal structure and lipid bilayer composition. For example, cytoskeletal disruption by the application of cytochalasin-D, an actin polymerization inhibitor, decreases the pressure threshold for activation (Cox et al., 2016). Additionally, Piezos are sensitized by the integral membrane protein STOML3 due to its function in recruiting cholesterol to the membrane and increasing membrane stiffness (Poole et al., 2014). A number of factors are likely to act directly on channel structure as well; membrane voltage, divalent ions, and pH all affect the inactivation

kinetics of Piezo (Bae, Sachs, & Gottlieb, 2015; Coste et al., 2010; Gottlieb et al., 2012).

Notably, the only molecule shown to directly interact with Piezo1 by

coimmunoprecipitation is Polycystin-2 (PC2), a TRP family protein associated with polycystic kidney disease, which attenuates Piezo1 when in complex (Peyronnet et al., 2013). Together these studies highlight the polymodality of Piezo channels.

### ***1.7 Insights into Piezo function through disease***

Channelopathies caused by mutations in Piezo channels may be regarded as perhaps one of the most interesting modulators of channel function. Over 25 mutations in Piezo1 have been linked to various human disorders, though only a few have been characterized in detail (Alper, 2017). Loss-of-function mutations can lead to distal arthrogryposis as well as congenital lymphatic dysplasia, characterized by a swelling of the body due to failure in reuptake of lymph into the blood (Fotiou et al., 2015). Gain-of-function mutations, however, can also cause a variant of distal arthrogryposis as well as dehydrated hereditary xerocytosis, which is associated with dehydrated red blood cells and anemia (Alper, 2017; Bae et al., 2013). Single point mutations in human Piezo1 associated with xerocytosis caused a pronounced slowing of inactivation that varied depending on the site of the mutation (Bae et al., 2013). This leads to an increase in calcium influx and subsequent potassium channel activation, ultimately leading to cell dehydration (Cahalan et al., 2015). Interestingly, gain-of-function mutations in Piezo2 are also associated with variants of distal arthrogryposis even though other variants of

this disease are caused by loss-of-function mutations (Coste et al., 2013; McMillin et al., 2014). Electrophysiological characterization of these mutations reveal that channels inactivate at a similar rate to wild-type but are faster to recover from inactivation, thus again leading to a greater overall amount of calcium influx and hyperexcitability.

It is still unclear how single point mutations result in these effects on inactivation in Piezo channels, but the emergence of new structural models will be instrumental in answering this question. The precise locations of the point mutations in both Piezo1 and Piezo2 are found predominantly on the C-terminal half of the protein, with a notable concentration towards the distal end. Mutations that impact inactivation have been identified in the anchor, CED, inner pore helix, and the intracellular C-terminal tail, strongly implicating the C-terminal domains in inactivation (Wu, Goyal, & Grandl, 2016). However, a handful of mutations have also been identified closer to the N-terminal that also have similar effects on inactivation, raising the possibility that inactivation may be mediated by several different structures.

### ***1.8 The puzzle of Piezo inactivation***

It is now apparent that a wide array of seemingly unrelated stimuli and modulations in Piezo channels all share a common effect on the kinetics of channel inactivation. Additionally, inactivation has been shown to be necessary in regulating a variety of equally disparate biological functions. This raises the obvious question: How and why can so many different conditions affect the same specific channel function? In

order to answer this question it is useful to draw upon the vast body of established knowledge regarding ion channel inactivation.

Ever since the first seminal studies by Hodgkin and Huxley on the theory of the action potential in the squid giant axon, inactivation has been established as key property of ion channel function (Hodgkin & Huxley, 1952). Action potentials are made possible by the change in permeation of Na<sup>+</sup> and K<sup>+</sup> ions through ion channels in an axon, and this change in permeation depends on the properties of channel activation and inactivation. Since this discovery, multiple forms and mechanisms of ion channel inactivation have been studied in depth, and some key examples are reviewed here to aid in forming hypotheses for how and why Piezos inactivate.

### **1.8.1 Case study: Inactivation of voltage gated sodium channels**

Voltage gated sodium channels (Navs), as the name would suggest, are ion channels that conduct Na<sup>+</sup> in response to membrane depolarization. Navs activate during the rise phase of an action potential and inactivate upon repolarization. In an inactivated state, Navs cannot be reopened by depolarization until they return to a deactivated state, thus inducing a refractory period that allows for the forward propagation and frequency of action potential firing. Navs are made up of an  $\alpha$ -subunit which contains four domains (DI-DIV) of 6-transmembrane helices (S1-6S) that assemble as a pore-forming tetrameric structure, and one or more accessory  $\beta$ -subunit. Two general types of inactivation have been observed for Navs- fast inactivation and slow

inactivation (Goldin, 2003). Fast inactivation occurs through a mechanism by which a blocking particle formed by the DIII-DIV linker binds to a proximal docking site and blocks the pore, commonly referred to as a 'hinged lid' or 'ball and chain' mechanism (Raman & Bean, 2001). Fast inactivation can be modulated by voltage due to its docking site being allosterically linked to the DIVS4 voltage sensor (Smith, Yu, & Goldin, 1997). Additionally, fast inactivation can also be modulated through interactions between the C-terminal tail and the blocking particle, as well as the identity of associated  $\beta$ -subunits and cell type (Cormier et al., 2002; Qu et al., 2001). Slow inactivation occurs through a less well understood mechanism, but is generally thought to be mediated by structural rearrangements of the pore itself (Goldin, 2003). Despite the specificity to the pore domain, targeted mutagenesis studies demonstrate that regions throughout the structure outside of the pore are also able to modulate slow inactivation, reminiscent of the effects caused by various point mutations throughout the structure of Piezo observed in channelopathies.

### **1.9.2 Case study: Inactivation of voltage gated potassium channels**

Continuing in the context of action potentials, voltage gated potassium channels (Kvs) allow the passage of  $K^+$  out of the neuron in response to membrane depolarization, leading to repolarization of the cell back to its resting potential. The kinetics by which Kvs inactivate and recover from inactivation are therefore critical in the regulation of neuronal excitability. Kvs are formed by four identical pore forming

subunits of 6-transmembrane domains that are each equipped with a voltage sensor akin to S4 in Navs. Also similar to Navs, Kvs exhibit a fast and slow inactivation, which in this context are more commonly referred to as N-type and C-type inactivation, respectively (Kurata & Fedida, 2006). N-type inactivation is named for the pore blocking particle formed by its N-terminal tail and is mechanistically analogous to the 'ball and chain' mechanism described above, whereby the blocking particle binds to an intracellular cavity accessible in the channel's open state. Interestingly, N-type inactivation can also be mediated by auxiliary  $\beta$ -subunits as well, and PIP2 has also been shown to attenuate N-type inactivation possibly by sequestering the blocking particle (Cox, 2005; Oliver et al., 2004).

Slow inactivation here is referred to as C-type inactivation, named in part for the C-terminal location of the pore domain, and is thought to be caused by conformational changes in the selectivity filter and extracellular pore access (Kurata & Fedida, 2006). While the precise mechanism is not well understood, several studies have provided evidence for various possibly cooperative mechanisms for this process. Extracellular concentration of  $K^+$  potentiates current despite it being an unfavorable chemical gradient, and it has been proposed that this occurs due to the ability of  $K^+$  to relieve the outer pore domain from inhibitory protonation and thus attenuate C-type inactivation, leading to increased ion permeation (Kehl et al., 2002). Other studies demonstrate the extracellular  $K^+$  occupy an ion binding site with high affinity near the extracellular

mouth of the pore, leading to decreased permeation and inactivation (Starkus et al., 1997). Mutations and crosslinking of the extracellular pore and selectivity filter alter inactivation kinetics, and structural models have captured this domain in multiple conformations as well (Larsson & Elinder, 2000). Some evidence of cooperativity between N-type and C-type inactivation have also been described, as C-type inactivation is facilitated by N-type inactivation and actually determines the time course of recovery from inactivation for both modes (Baukrowitz & Yellen, 1995).

### **1.9.3 The challenge: Inactivation of Piezo ion channels**

The mechanism(s) of Piezo inactivation are far from reaching the level of clarity that has been established for the presented case studies. Certainly the overall architecture and structural details of Piezo channels already suggest that some of these mechanisms may be present. Additionally, one study has shown that Piezo1 can be characterized with two inactivation kinetics, suggesting the possibility of two mechanisms as well (Lewis et al., 2017). However, more complete structural models and structures captured in different conformations will be necessary to test these hypotheses further. A puzzling large collection of modulators have been shown to influence the kinetics of inactivation in Piezos, and the unusually large size of the protein as well as its diverse pattern of expression throughout different organ systems add to the complexity in studying the mechanism of inactivation. Of course this mechanism is not limited to

those already described, but reviewing these examples will help to form testable hypotheses addressing this problem.

## ***1.9 Open questions and aims***

This dissertation aims to answer the questions of what structures mediate the processes of activation and inactivation in Piezos, and how do these structures confer their respective functions to the channel. Defects in inactivation for other ion channels cause changes in cell excitability, frequently leading to diseases such as epilepsy and neuropathic pain. Channelopathies in Piezo confirm that this same mechanism can lead to disease as well, so understanding how inactivation occurs in Piezo already has direct an impact on human health. With the long term goal of treating disease, a question that must be asked is- can distinct structures in Piezo be modulated as a therapeutic strategy? Piezo has a rather ubiquitous role throughout the body, so Piezo-specific therapies may actually have impact on an incredibly wide span of health disorders. However in contrast, this thought poses the question of- is it the pharmacology of Piezo a feasible strategy to target one specific tissue or cell type without impacting Piezo function in the rest of the body? Additionally, why do mutations that lead to severe disorders in one organ system appear to be inconsequential for other systems in the same organism? One possibility is that the modulation of inactivation allows one homolog of Piezo to function differentially in each system depending on the conditions of its cellular environment, thus enabling a seemingly non-specialized channel (non-selective and

activated by many forms of force) to serve very specialized functions. One of the first steps towards understanding the mechanism of inactivation in Piezos is to identify the structures involved. This dissertation focuses on this aim and presents some of the first structure-function relationships that give insight into channel inactivation.

## **2. Localized force application reveals mechanically sensitive domains of Piezo1**

This chapter has been adapted from (Wu et al., 2016).

### ***2.1 Introduction***

Within the first five years of the discovery of Piezo proteins as pore forming subunits of a novel mechanically gated ion channel, Piezos had already been implicated in several biological processes involving mechanical sensing such as the sense of touch, proprioception, and cardiovascular development (Li et al., 2014; Maksimovic et al., 2014; S. S. Ranade et al., 2014; Woo et al., 2014, 2015). Additionally, a cryo-EM model of Piezo1 had revealed its macroscopic organization, highlighting various interesting structural domains, and lateral membrane tension had been demonstrated to be its activating stimulus (Ge et al., 2015; Lewis & Grandl, 2015). It seemed clear that the next question to be addressed was- how do Piezo channels function? Because Piezo channels are an entirely new family of ion channels, little could be drawn from the understanding of structure-function relationships for other well studied channels. Our first goal was therefore to identify the structural features that allow Piezos to sense force and transduce this into the molecular movements that govern channel activation.

We hypothesized that Piezo channels had distinct force sensing domains that were highly sensitive to localized application of force, whereas others would be less sensitive in comparison. Our rationale for this hypothesis draws from examples such as

voltage-gated ion channels which have distinct ‘voltage sensing domains’ that serve the purpose of sensing stimulus and transducing it into channel opening (Long et al., 2005). We further reasoned that mechanical perturbation of such domains may induce changes in channel function.

To test this, we developed a method by which localized force is applied through magnetic nanoparticles to distinct domains of Piezo1 while recording electrophysiological response to pressure. With this method, we identified domains that surprisingly caused gross alteration in the kinetics of channel inactivation, while mechanical perturbation of other domains did not appear to have such effects. When analyzed in detail, we revealed that one of these domains also affected the kinetics of pressure-dependent channel activation, highlighting its importance in the channel’s ability to sense and transduce mechanical force.

## **2.2 Experimental Methods**

### **2.2.1 Cloning and characterization**

Locations for inserting bungarotoxin binding sites (BBS) were selected by identifying poorly conserved residues in *Mus. musculus* (Mm) Piezo1 compared to *R. norvegicus*, *H. sapiens*, *M. mulatta*, *C. lupus*, and *G. gallus* within predicted extracellular sites (TMHMM). The 13 amino acid BBS (WRYYESSELEPYPD) or the 10 amino acid myc tag (EQKLISEEDL) was cloned into MmPiezo1-IRES-EGFP in the pcDNA3.1(-) vector using the QuikChange II XL Site-Directed Mutagenesis kit (Agilent).

A BBS was cloned into amino acid position 120 of MmKir2.1 and amino acid positions 197 (Kv1.2-BBS-S1-S2), (Kv1.2-BBS-S3-S4), and 350 (Kv1.2-BBS-S5-PH) of *H. sapiens* Kv1.2 in the pcDNA3.1(-) vector (Andolfo et al., 2013). All cloning primers were PAGE purified (Sigma). All clones were fully sequence verified (Genewiz, Inc.) and DNA maxi-prepped for transfection (Promega).

See Appendix for primer sequences.

### **2.2.2 Cell culture**

Human embryonic kidney HEK293T cells (ATCC # 3579061) were provided and authenticated (STR authenticated and verified mycoplasma-free) by the Duke Cell Culture Facility. Cells were cultured at a seeding density of 50,000 cells per well in a 24 well plate in DMEM-HG (Life Technologies) supplemented with 10% heat-inactivated fetal bovine serum (Clontech), 50 units/ml pen-icillin and 50 mg/ml streptomycin (Life Technologies), and grown at 37 °C on Poly-L-lysine and laminin coated coverslips (Sigma). Cells were transiently transfected with MmPiezo1-IRES-EGFP constructs (1.5 µg) in the presence of 10 µM ruthenium red using Fugene6 (Promega) according to manufacturer protocol. The Kir2.1-BBS construct was co-transfected with wild-type Piezo1-pIRES-EGFP at a 1:1 mass ratio. The Kv1.2-BBS construct was co-transfected with EGFP at a 1:0.5 molar ratio. Transfected cells were recorded or immunostained 36-72 hours post-transfection.

### **2.2.3 Nanoparticle labeling**

Nanoparticle labeling process is adapted from a previous study on L-type calcium channels. Transfected cells were washed twice with Phosphate Buffered Saline (PBS) and incubated for 15 min at 37 °C in PBS containing 10 µg/mL  $\alpha$ -bungarotoxin biotin-XX conjugate (1:100) (B1196; Molecular Probes) and 10 mM HEPES. Cells were then washed 3x with PBS for 5 min each, then incubated at room temperature (RT) while rocking gently for 15 min in PBS containing 10 µg/mL 75 nm streptavidin-coated magnetic nanoparticles (1:100) (MHS-075-05; OceanNanoTech) and 10 mM HEPES. Cells were then washed 2x with PBS and kept at RT during recording for no longer than 1.5 hours.

### **2.2.4 Immunostaining**

Nanoparticle-labeled cells were fixed with 4% paraformaldehyde for 30 min at RT and then blocked with 10% normal goat serum (NGS) for 15 min at RT. Cells were then incubated in 1% NGS containing 1:100 anti-streptavidin antibody (S6390; Sigma) for 1 hour at RT, then washed 3x with PBS and incubated at RT in 1% NGS containing 1:1000 Alexa Fluor 594-conjugated anti-rabbit antibody (A-11012; Molecular Probes) for 1 hour in the dark. Cells were then washed 2x in PBS and labeled with 1:100 Alexa Fluor 633-conjugated Wheat Germ Agglutinin (WGA) (W21404; Molecular Probes) for 10 min at RT for membrane visualization. Cells were washed 3x with PBS, mounted with Fluoromount-G (SouthernBiotech) on glass slides, and imaged on a Zeiss 780 inverted

confocal microscope at 63x magnification. Mean fluorescence intensity was measured along the bounding cell membrane with a custom-written script in Fiji image processing software.

The custom Fiji script first set a threshold limit on the GFP channel of images to identify GFP positive cells. The threshold processed image was then created into a binary image and filtered with preset Fiji scripts “watershed” and “erode” to separate and delineate individual cells. Individual objects in the resulting image were then used to define cell shaped ROIs, and the preset Fiji script “band” was used to create a 1  $\mu\text{m}$  thick band ROI encircling each cell. Finally, the mean fluorescence intensity was measured within the band for the corresponding immunolabeled nanoparticle channel. The ROIs were visually checked against WGA staining to ensure that they were accurately measuring the cell membrane.

### **2.2.5 Double labeling**

Efficiency of nanoparticle labeling was tested by first labeling Piezo1-BBS constructs with nanoparticles, and then incubating with 1:100 Alexa Fluor 647-conjugated  $\alpha$ -bungarotoxin at a 10  $\mu\text{g}/\text{mL}$  concentration in PBS and 10 mM HEPES (B35350; Molecular Probes) at RT for 15 minutes while rocking. Cells were then washed 3x with PBS for 5 min each, fixed with 4% PFA, and immunostained against streptavidin. For comparison, a separate set of cells were labeled with Alexa Fluor 647-

conjugated  $\alpha$ -bungarotoxin alone. Membrane fluorescence was measured with the custom Fiji script. Percent labeling efficiency was calculated by:

$$\% \text{ efficiency} = \left( 1 - \frac{\text{fluorescence (nanoparticles, then BTX647)}}{\text{fluorescence (BTX647 alone)}} \right) \times 100$$

### 2.2.6 Myc-tag labeling

Cells transfected with the Piezo1-myc-2422-pIRES-EGFP construct were washed once with pre-warmed culture medium and then incubated in warm medium with 1:50 anti-myc antibody (c-myc 9E11, Santa Cruz Biotech) for 20 min at 37 °C. Cells were then washed 2x with warm media and 1x with PBS and kept at RT for recording. For visualization, cells were incubated with 1:200 AlexaFluor546-conjugated anti-mouse antibody (A-11030; Molecular Probes) while rocking gently at RT for 10 min. Cells were then washed 3x in PBS, fixed with 4% PFA, mounted, and imaged with an inverted confocal microscope.

### 2.2.7 Electromagnetic needle

The electromagnetic needle was constructed from a HyMU-80 alloy (Carpenter Technology) core (100 mm length, 4.5 mm diameter) and tapered to a ~10  $\mu$ M tip with a diamond grinder. The electromagnetic coil was made with N = 200 turns of enameled AWG 24 copper wire, averaging 5 layers with 40 turns per layer, around a custom made brass frame (30.1 mm length, 7.5 mm inner diameter, 14.5 outer diameter). The copper wire was fixed in place with an epoxy resin coating, and the brass frame with copper wire coil was then sleeved over and clamped onto the HyMU-80 needle 25 mm from the

tip of the needle. The electromagnetic coil was then connected to a 12 V DC regulated power supply (301911, Jameco), generating a maximum current of 5 A through the coil. From these parameters, we calculated the magnetic field strength  $\mathbf{B}$  inside the coil to be:

$$\mathbf{B} = \mu_0 \frac{N}{L} I \approx 40 \text{ mT}$$

Where  $\mu$  is magnetic permeability,  $N$  is number of turns,  $L$  is the length of the coil, and  $I$  is current.

The distance of the needle tip from the patch surface was measured by the displacement readout of the micromanipulator (Sutter Instruments) between the cell surface and the experimental position over several trials.

### **2.2.8 Magnetic force calibration**

Fluorescent labeling of streptavidin-coated nanoparticles was achieved by first magnetically separating nanoparticles from solution with a permanent magnet (K&J Magnetics) for 5 minutes and washing once with PBS. Nanoparticles were then blocked with 10% NGS for 15 minutes while rotating at RT and then magnetically separated again. Next, nanoparticles were resuspended in 1% NGS containing 1:50 anti-streptavidin antibody (S6390; Sigma) and incubated for 1 hr while rotating at RT. Nanoparticles were then magnetically separated and washed 3x with PBS, then resuspended in 1% NGS containing 1:500 AlexaFluor594-conjugated anti-rabbit antibody (A-11012; Molecular Probes). Nanoparticles were magnetically separated and washed 3x once again before resuspending in PBS. For force measurements, 5  $\mu$ l of nanoparticle

solution was thoroughly mixed with 95  $\mu\text{l}$  of 100% glycerol and placed on a glass coverslip for imaging.

The magnetic force of the electromagnetic needle on 50, 75, 100, and 200 nm diameter magnetic nanoparticles (OceanNanoTech) was estimated by fluorescently labeling and pulling each size nanoparticle separately through 95% glycerol (Sigma), with 5 A of current supplied to the electro-magnet, and measuring their velocities within a 50  $\mu\text{m}$  radius from the tip of the needle. For 75 nm nanoparticles, this measurement was repeated with adjusting the supplied current to 1, 2, 3, and 4 A in separate measurements. In this experiment the magnetic force equals the drag force, which was calculated with Stokes law:

$$\mathbf{F}_d = 6\pi \mu R v$$

where  $\mu$  the dynamic viscosity,  $R$  the nanoparticle radius, and  $v$  the velocity. A force  $\mathbf{F} = 9.9 \pm 0.7$  pN was calculated for nanoparticles of 75 nm diameter at 5 A of supplied current.

For comparison, we calculated the Coulomb force  $\mathbf{F}_c$  on a voltage sensor domain containing four elementary charges, embedded in a membrane bilayer of 4 nm thickness and exposed to a physiological transmembrane voltage of 60 mV:

$$\mathbf{F}_c = 4 \times 1.6 \cdot 10^{-19} \text{C} \times \frac{60 \text{ mV}}{4 \text{ nm}} = 9.6 \text{ pN}$$

The gating energy  $E$  transduced by an ideal (Hooke) spring of 1 nm length under a force of 10 pN is substantially larger than the thermal energy at room temperature (300 K):

$$E_{\text{gating}} = 10 \text{ pN} \times 1 \text{ nm} = 1 \cdot 10^{-20} \text{ J} > E_{\text{thermal}} = k_{\text{B}}T = 0.4 \cdot 10^{-20} \text{ J}$$

## 2.2.9 Electrophysiology

Cell-attached recordings for all experiments were performed at RT in bath solution containing (in mM) 140 KCl, 10 HEPES, 1 MgCl<sub>2</sub>, and 10 Glucose, pH = 7.3 with KOH. Pipette buffer for Piezo1 experiments contained (in mM) 130 NaCl, 5 KCl, 10 HEPES, 1 CaCl<sub>2</sub>, 1 MgCl<sub>2</sub>, and 10 TEA-Cl, pH = 7.3 with NaOH. Pipette buffer for Kir2.1 and Kv1.2 experiments contained (in mM) 135 NaCl, 5 KCl, 10 HEPES, 2.8 Na-acetate, 1 CaCl<sub>2</sub>, and 1 MgCl<sub>2</sub>, pH = 7.3 with NaOH. Patch-clamp recordings were carried out with an EPC10 amplifier and Patchmaster software (HEKA Elektronik) and data were sampled at 5 kHz and filtered at 2.9 kHz. Pressure was controlled with a high-speed pressure-clamp system (ALA Scientific Instruments) connected to Patchmaster software. Pipette resistances ranged from 2 to 4 MΩ, and patches were held at -80 mV for the duration of the experiment. Pressure pulses were given at 10 mmHg steps from 0 to -70 mmHg for 200 ms, with a +5 mmHg pulse for 5 s between each step to minimize resting membrane tension (Lewis & Grandl, 2015). A rest interval of at least 1 min was given between two consecutive pressure-step protocols (i.e. before and after magnetic field application). Following an initial pressure-step protocol, the electromagnet was brought within close vicinity ( $54.7 \pm 5.5 \mu\text{m}$ ) directly above the cell-attached patch with a second micromanipulator and was manually switched on for at least 5 s before and for the duration of the second recording.

Kv1.2 channels were recorded with a voltage-step protocol from -80 mV to +30 mV for 300 ms, separated by a 600 ms period at -80 mV. Within each voltage step at 100 ms, a negative pressure stimulus of -60 mmHg was applied for 100 ms, then returned to 0 mmHg for the remainder of the voltage-step.

### 2.2.10 Electrophysiology analysis

Analysis was performed with Igor Pro 6.22A (WaveMetrics). Baseline currents before pressure stimulation were subtracted off-line and peak currents measured at each pressure. The pressure of half-maximal activation ( $P_{50}$ ) was calculated by normalizing each set of peak currents to the maximum value for each individual cell and fitting the data with a Boltzmann function:

$$I = I_{\min} + \frac{I_{\max}}{1 + \exp\left(\frac{P_{50} - P}{k}\right)}$$

where  $I_{\min}$  and  $I_{\max}$  are the minimum and maximum current amplitude,  $P$  is pressure and  $k$  is the slope. The  $P_{50}$  values for each individual cell were averaged and compared by ANOVA and a non-parametric multiple comparison test.

Inactivation was analyzed by calculating the normalized difference of the baseline-subtracted maximal current amplitude upon a -60 mmHg pressure step and the average current amplitude 150 ms later:

$$\% \text{ inactivation} = \left( \frac{\text{peak current} - \text{decayed current}}{\text{peak current}} \right) \times 100$$

A paired t-test was used to determine statistical significance of each construct.

The absolute changes in inactivation without and with the magnetic force were calculated using:

$$\text{change in \% inactivation} = \% \text{ inactivation}_{\text{with magnet}} - \% \text{ inactivation}_{\text{without magnet}}$$

and values were tested for statistical significance by ANOVA followed by Tukey-Kramer comparison.

Time constants for activation  $\tau_1$  and inactivation  $\tau_2$  were obtained by fitting current  $I$  with a double exponential function with bounds after the onset and before the offset of the pressure stimulus:

$$I = I_0 + I_1 \exp\left(\frac{-(t - t_0)}{\tau_1}\right) - I_2 \exp\left(\frac{-(t - t_0)}{\tau_2}\right)$$

Time constants for deactivation  $\tau_3$  were obtained by fitting the current following 40 ms after offset of the pressure stimulus with a single exponential function:

$$I = I_0 - I \exp\left(\frac{-(t - t_0)}{\tau_3}\right)$$

Fits of deactivation ( $\tau_3$ ) may have been overestimated due to above threshold oscillations at the offset of the pressure clamp stimulus. A paired t-test was used to determine statistical significance for each construct.

Maximal currents for Kv1.2 were measured from a P/N leak subtracted voltage step protocol from -80 to +30 mV for 300 ms divided into 100 ms periods at 0 mmHg, -60 mmHg, and 0 mmHg pressure stimulus. A 600 ms period of rest between each step was held at -80 mV. This protocol was repeated once on each cell first without, then with a

magnetic field applied. Reversal potentials were extrapolated with a tail current protocol. The calculated conductances for each period and condition were normalized and fit to a Boltzmann function to determine  $V_{1/2}$  values. Differences in  $V_{1/2}$  values and normalized maximal conductance were analyzed with a paired t-test.

### **2.2.11 NP<sub>o</sub> and single channel analysis**

NP<sub>o</sub> was calculated by measuring the average current amplitude during a 4 second period of the +5 mmHg prepulse at the onset of each pressure step protocol and dividing by the maximum current elicited by a saturating -60 mmHg pressure step.

Single channel amplitudes were measured by performing a Gaussian multi-peak analysis (IgorPro, Wavemetrics) on histogram plotted current amplitudes over a 1 s period exhibiting single channel openings. Conductance was then calculated using the holding potential of -80mV.

### **2.2.12 Statistical analysis**

For immunostaining experiments, a minimum of n = 8 cells and two transfections was analyzed for each individual immunostaining study for a maximum SEM of less than 20% the normalization standard and to account for day to day variability. All analyzed electrophysiological recordings had a seal resistance of at least 1 GΩ. Recordings for Piezo1 were only analyzed for patches with maximal pressure-induced currents of at least 40 pA to prevent poor fit. Recordings for Kv1.2 were only analyzed for patches with maximal voltage-induced currents of 50 pA (non-transfected cells, 0/30;

wild-type Kv1.2, 8/15; Kv1.2 -BBS-S1-S2, 9/24; Kv1.2 -BBS-S3-S4 8/47; Kv1.2 -BBS-S5-PH, 0/14). A minimum of n = 8 (2 transfections) for Piezo1 experiments and n = 5 cells (3 transfections) for Kv1.2 experiments were analyzed for each individual electrophysiology study for a normal distribution of values for across measurements.

Statistical analysis was performed with paired or unpaired Student's t-test and one-way analysis of variance followed by either a non-parametric multiple comparison or Tukey-Kramer comparison. Results are expressed as mean  $\pm$  SEM. Significant thresholds were set at  $p < 0.01$ ,  $p < 0.001$ , and  $p < 0.0001$ , as defined in the text.

### ***2.3 Localized force application by magnetic nanoparticles***

In order to probe mechanical sensitivity of Piezo1 ion channels with sub-molecular resolution, we generated a highly localized pulling force to specific domains of Piezo1 by attaching superparamagnetic nanoparticles and exposing the complex to a magnetic field while measuring channel activity electrophysiologically. Specifically, we engineered constructs of Piezo1-IRES-EGFP that each contained a 13 amino acid (aa.) bungarotoxin binding sequence (BBS) within a predicted extracellular domain, further referred to as Piezo1-BBS 18. We first treated HEK293T cells expressing Piezo1-BBS constructs with biotinylated bungarotoxin, which binds to the BBS with high affinity ( $K_d \sim 15$  nM) (Scherf et al., 2001). Next, we applied 75 nm diameter streptavidin-coated nanoparticles to the cells, which in turn bind the biotinylated bungarotoxin ( $K_d \sim 0.01$  pM), linking the targeted domain to the nanoparticle (Figure 8). We reasoned that due to

the comparatively large size, each Piezo1 channel can accommodate at most one single nanoparticle (Figure 9).

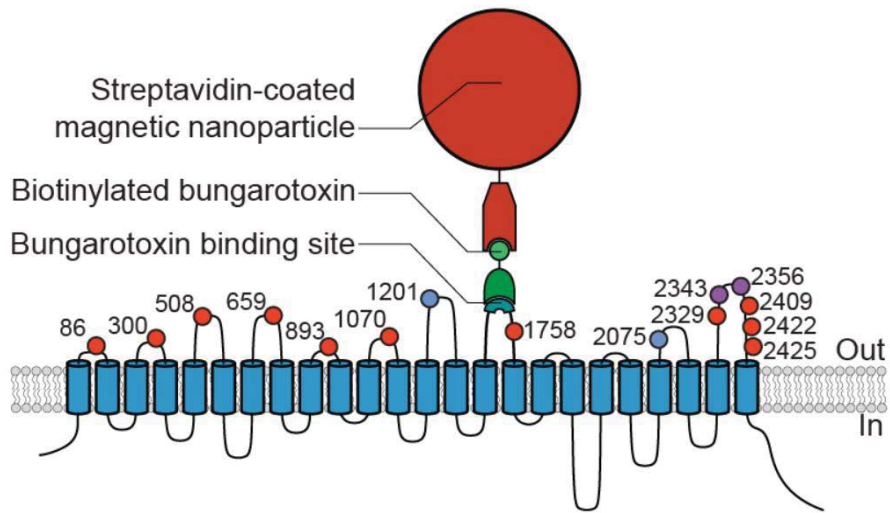


**Figure 8: Nanoparticle labeling strategy. Piezo1 transmembrane topology with aa. locations of BBS insertions (red, labeled and functional; blue, non-labeled; magenta, non-functional) and schematic of bead labeling strategy.**

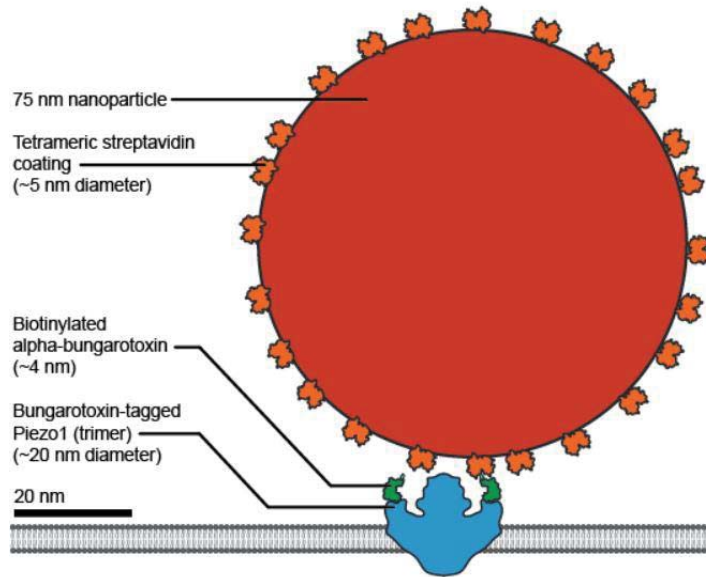


**Figure 9: Scale diagram of BBS-Piezo1 binding complex. Diagram depicting to-scale relationships of BBS-Piezo1, biotinylated bungarotoxin, and streptavidin-coated nanoparticle in complex.**

To probe the specificity of nanoparticle labeling, we immunostained nanoparticles bound to cells transfected with Piezo1-BBS constructs or wild-type Piezo1, which does not contain any BBS, and compared their near-membrane fluorescence (Figure 10A). All but two Piezo1-BBS constructs (those with BBS tags inserted at residue positions 1201 and 2075 (BBS-1201 and BBS-2075)) exhibited a fluorescence intensity that was at least two times higher as compared to the levels present on wild-type Piezo1 expressing cells and were used for further experiments (Figure 10B).

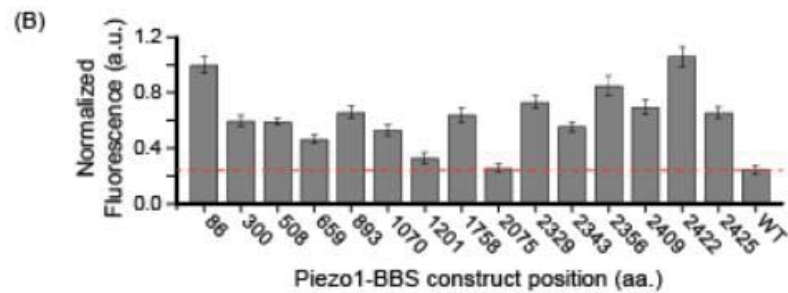
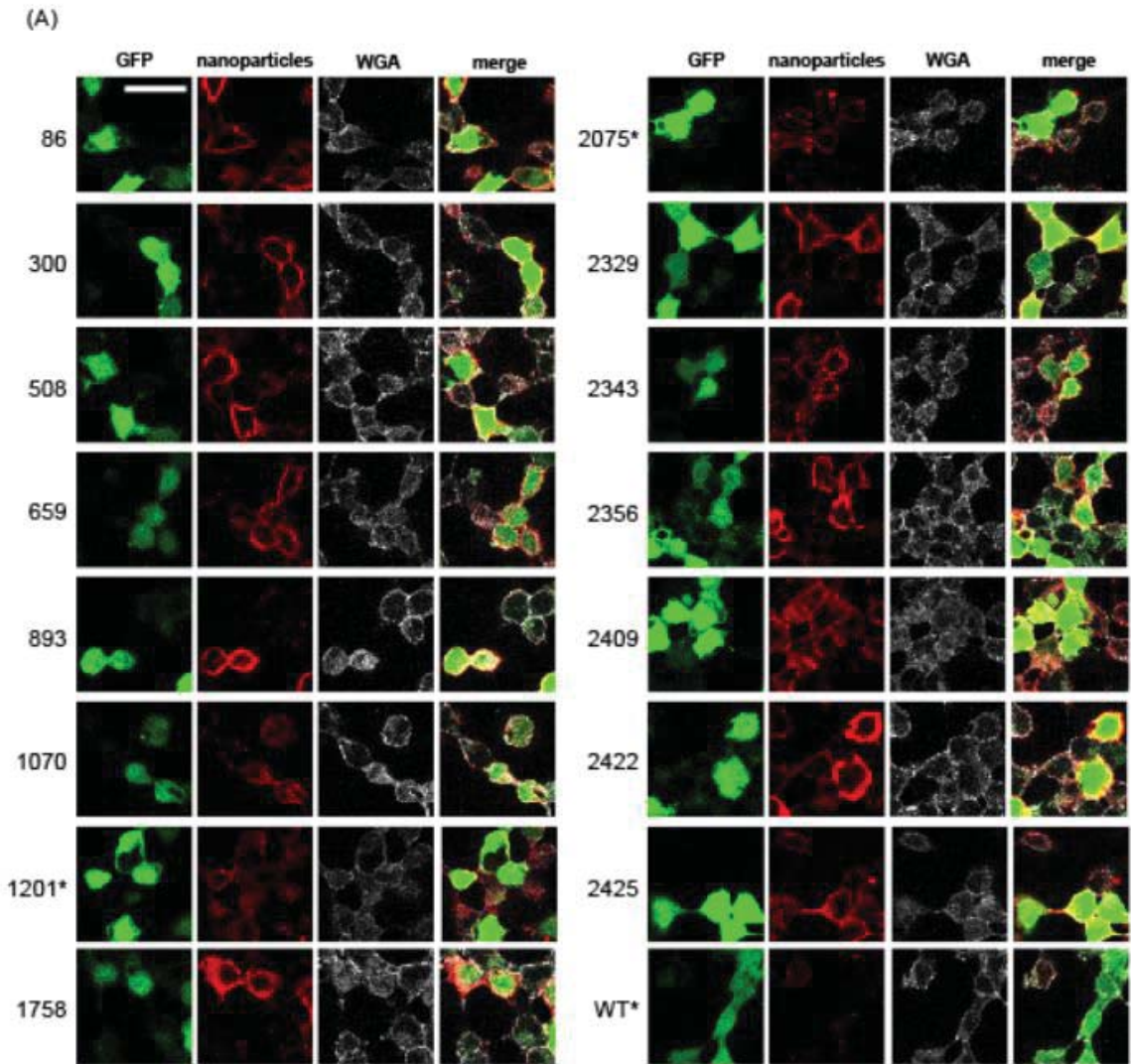


Figure 10: Specificity of nanoparticle labeling. (A) Representative images of HEK293T cells expressing Piezo1-BBS constructs, live-labeled with streptavidin-coated nanoparticles, immunostained against streptavidin, and WGA labeled for

membrane localization (\*, insignificant labeling; green, GFP; red, anti-streptavidin; gray, WGA). (B) Mean fluorescence intensity normalized to BBS-86 (a.u.) of nanoparticle labeling along the cell membrane for all constructs compared to wild-type Piezo1 (WT, red line) (n = 10 cells per transfection, 2 – 5 transfusions; p < 0.0001 for all constructs except BBS-1201 and BBS-2075 (p > 0.01), one-way ANOVA and NP multiple comparison).

Then, to probe the efficiency of nanoparticle labeling, we labeled unoccupied binding sites of all Piezo1-BBS constructs with a fluorescently-conjugated bungarotoxin either directly or after the binding of nanoparticles (Figure 11A). We observed for all constructs prior nanoparticle labeling reduced fluorescence by 60-80% (Figures 11B-C). Finally, to probe for possible nanoparticle dissociation or internalization, we immunostained nanoparticle-labeled cells transfected with one representative construct (BBS-2422) at various time points after labeling. We observed consistent fluorescence intensity ( $1.04 \pm 0.08$  a.u.) along the membrane over a time period of at least 1.5 hours (Figure 12). We therefore concluded that labeling of Piezo1-BBS constructs with magnetic nanoparticles was overall specific, efficient, and stable enough to use the nanoparticles as localized force transducers.

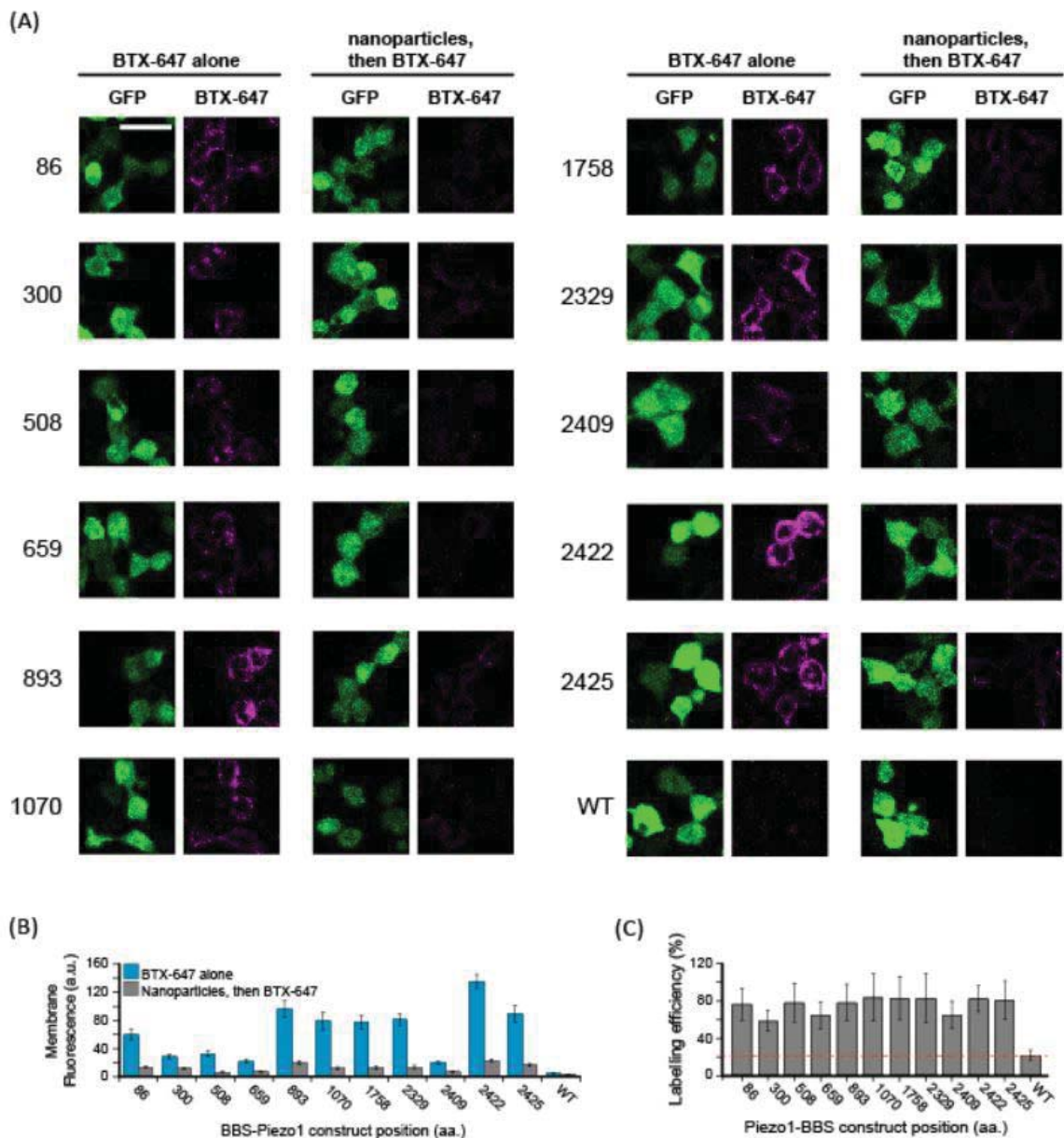
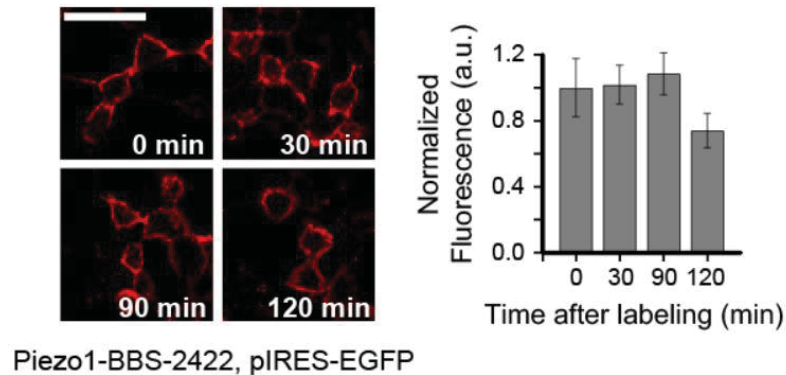


Figure 11: Efficiency of nanoparticle labeling. (A) Representative images of HEK293T cells expressing Piezo1-BBS constructs, live-labeled with either bungarotoxin (BTX)-Alexa Fluor 647 alone or first with nanoparticles, then followed by BTX-647 (green, GFP; magenta, BTX-647). (B) Membrane fluorescence without (blue) and with (gray) prior nanoparticle labelling. (C) Quantified labeling efficiency for all Piezo1-BBS constructs in comparison to WT (red line) ( $n = 12$  cells each, 1 transfection;  $p < 0.0001$ , one-way ANOVA and NP multiple comparison). Error bars are SEM. Scale bar is  $30 \mu\text{m}$ .



**Figure 12: Stability of nanoparticle labeling. Representative fluorescent images of HEK293T cells transfected with BBS-2422 as a function of time after surface labeling (red, anti-streptavidin) and mean membrane fluorescence intensity normalized against  $t = 0$  time point plotted vs time. (n = 10 cells per transfection, 1 - 2 transfections; no significance between any time points,  $p > 0.01$ , one-way ANOVA and Tukey's multiple comparison).**

We next probed by pressure-clamp electrophysiology if Piezo1-BBS constructs retained normal mechanical sensitivity, peak current amplitudes, and inactivation kinetics as compared to wild-type Piezo1 (Figures 13A-C). The majority of the constructs retained channel properties similar to wild-type Piezo1. Only two constructs (BBS-2343 and BBS-2356 within one domain were non-functional, and for three other domains, we only obtained constructs with attenuated pressure sensitivity (P50) (BBS-1070 and BBS-1758) or altered inactivation kinetics (BBS-1070 and BBS-2329). We accommodated the rightward shift in P50 for BBS-1758 with a higher ranged pressure step protocol (-50 to -120 mmHg). We decided to study these constructs despite their altered function, because we reasoned that they might still be informative if external pulling force further alters channel function. Altogether, we created eleven functional and accessible constructs,

covering eight of the nine individual extracellular loops that were previously identified by affinity-tag accessibility experiments (Coste et al., 2015).

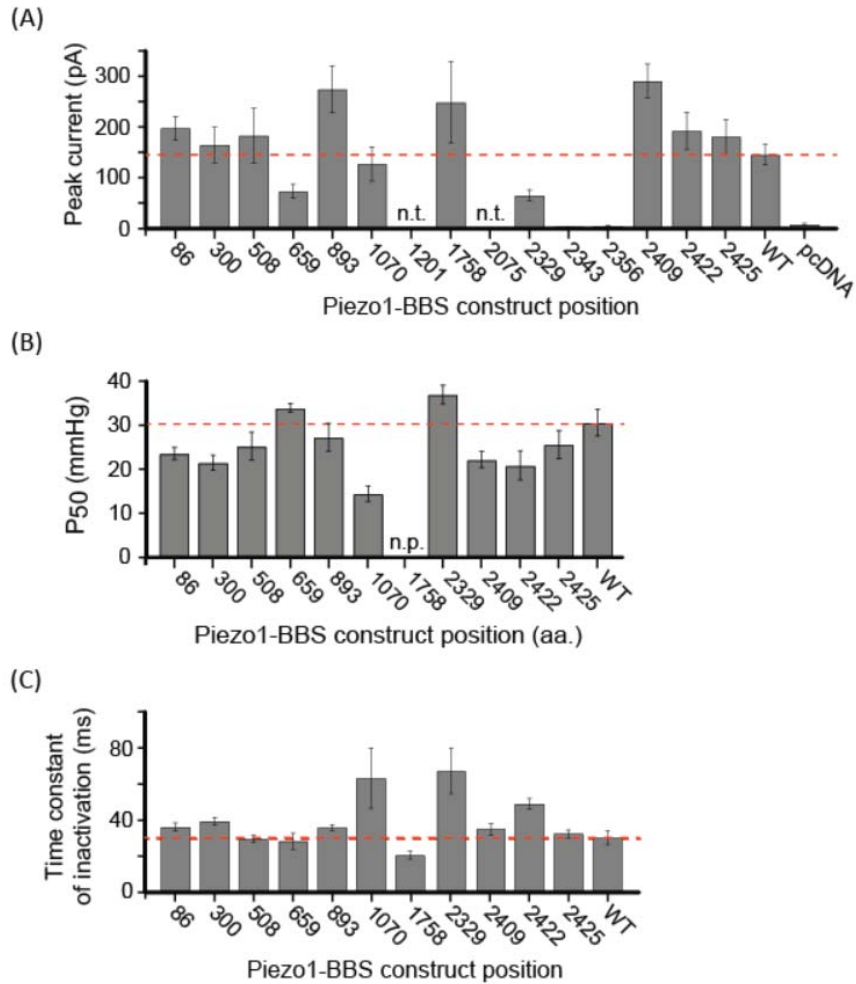


**Figure 13: Piezo1-BBS construct functionality. (A) Average peak current during a -60 mmHg pressure step (-110 mmHg step for construct 1758) (n = 8 - 21 cells) (n.t., not tested; BBS-2343 and BBS-2356 significantly lower than WT,  $p < 0.0001$ , one-way ANOVA and NP multiple comparison). (B) Average P<sub>50</sub> for each construct (n = 8 - 21 cells, 3 - 7 trans-fusions) in comparison to wild-type Piezo1 (red line) ( $p < 0.0001$  for BBS-1070, one way ANOVA and NP multiple comparison). Construct 1758 did not reach a plateau current (n.p.), and a P<sub>50</sub> value was not measured. (C) Average time constants of inactivation (BBS-1070 and BBS-2329 significantly greater than WT,  $p < 0.01$ , one-way ANOVA and NP multiple comparison). Red dotted lines denotes averages for wild-type Piezo1. Error bars are SEM.**

Finally, we engineered an electromagnetic coil (magnetic field  $B \sim 40$  mT) with an iron-nickel alloy core needle tapered to a  $<10$   $\mu\text{m}$  tip to generate a focused magnetic field gradient and positioned it  $54.7 \pm 5.5$   $\mu\text{m}$  above the tip of the patch pipette (Figures 14A-B) (Kollmannsberger & Fabry, 2007). This relatively large distance between the needle and membrane surface results in a magnetic pulling force that is predominantly perpendicular to the membrane plane, with only a small parallel component.

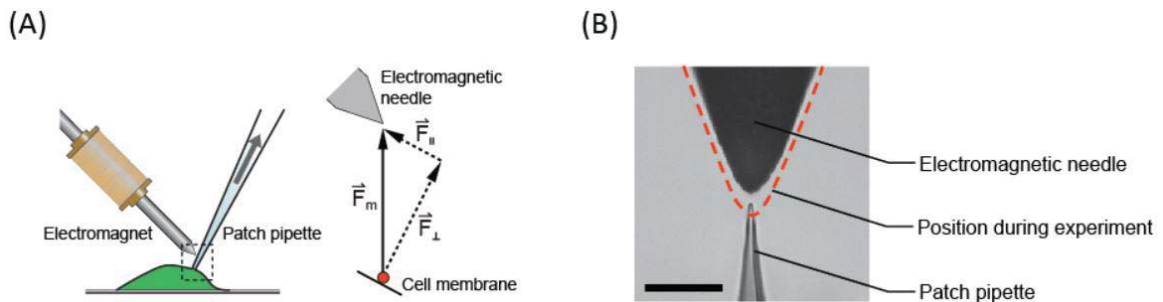


**Figure 14: Electromagnetic needle setup. (A) Diagram of patch-clamp pipette and electromagnetic needle and corresponding force diagram on nanoparticle ( $F_m$ , magnetic force vector;  $F_\perp$ , force vector normal to patch membrane;  $F_\parallel$ , force vector parallel to patch membrane). (B) Image of electromagnetic needle tip and patch pipette tip at 40x magnification. Dotted red line denotes position of needle above pipette tip during recording experiments. Scale bar is 50  $\mu\text{m}$ .**

## ***2.4 Magnetic force induces domain-specific loss of inactivation***

To measure the effect of magnetic pulling on Piezo1 channel function, we patched HEK293T cells expressing each Piezo1-BBS construct labeled with nanoparticles in the cell-attached configuration. We recorded currents in response to a pressure step protocol (0 to -70 mmHg with a +5 mmHg prepulse) we developed recently that

minimizes resting membrane tension, first without a magnetic field and then a second time in the presence of a magnetic field (Figure 15A).

As we expected, the magnetic field did not alter channel function when applied to wild-type Piezo1 lacking a BBS, demonstrating that Piezo1 channels have no inherent sensitivity to magnetic fields (Figure 15A). While some constructs were insensitive to magnetic force when labeled with nanoparticles, we found dramatic changes in channel function for certain constructs. Most strikingly, construct BBS-2422 revealed a substantial loss of inactivation upon magnetic force application, and an identical effect with the BBS at the proximal position in BBS-2425 confirmed region specificity (Figures 15A-B). A similar, albeit smaller, loss of inactivation was also apparent for BBS-86 and BBS-300. Although other mechanically sensitive sites may have been overlooked by our labeling strategy, which sparsely probes an unusually large protein and is restricted to extracellular domains, this result qualitatively supports our hypothesis that distinct sites within the Piezo1 channel are highly sensitive to localized force application, while others are less sensitive.

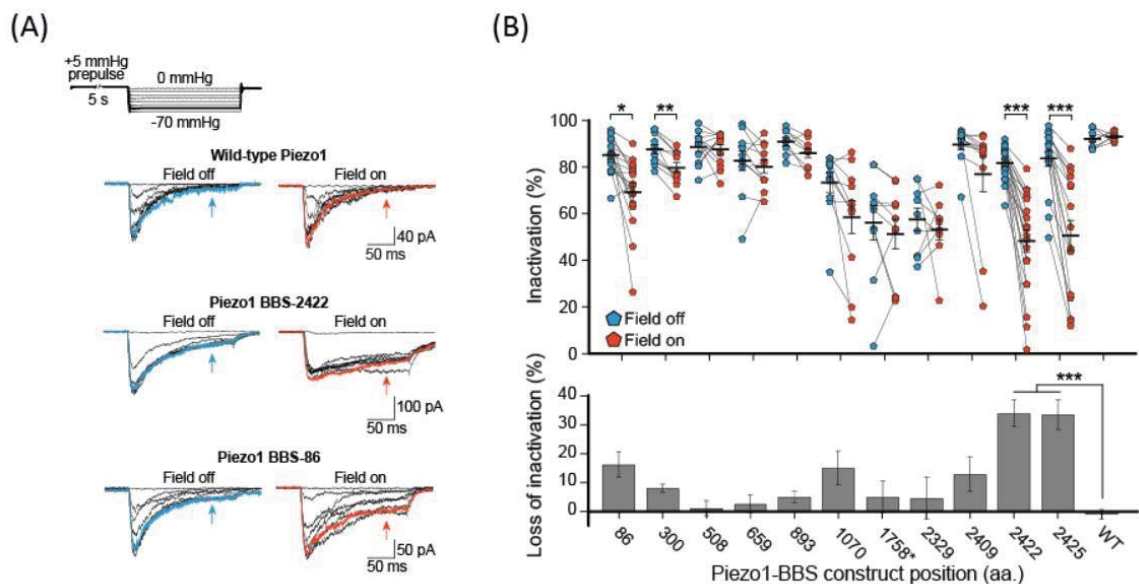


**Figure 15: Magnetic pulling force on Piezo1 slows inactivation. (A)** Representative current recordings of wild-type Piezo1, construct BBS-2422 and construct BBS-86 upon pressure-clamp stimulation from 0 to -70 mmHg (above) in the absence and presence of a magnetic field. Arrows denote inactivated current after 150 ms. Traces highlighted in bold represent -60 mmHg step and corresponding current (blue, field off; red, field on). **(B)** Inactivation at -60 mmHg (or -110 mmHg for BBS-1758) (top panel) for individual experiments and averages of constructs labeled with nanoparticles before (blue) and during (red) application of magnetic force (n = 8 - 21 cells, 3 - 7 trans-fusions; \*p < 0.01 \*\*p < 0.001, \*\*\*p < 0.0001, paired t-test). Average loss of inactivation (bottom panel) for data above (\*\*\*p < 0.0001, one-way ANOVA and Tukey's multiple comparison and NP multiple comparison). Error bars are SEM.

To quantify the loss of inactivation, we calculated the inactivation (see Methods) 150 ms after the peak current evoked by a saturating pressure step of -60 mmHg and its change upon magnetic force application (Figure 15B). For example, in BBS-2422 we found that the average inactivation decreased strongly (from  $76.3 \pm 2.0$  % (field off) to  $42.9 \pm 4.3$  % (field on), n = 19 cells, p < 0.0001, paired t-test), while in BBS-508 the average inactivation remained unchanged ( $85.6 \pm 2.1$ % (field off) and  $82.8 \pm 2.7$ % (field on), n = 12

cells,  $p > 0.01$ , paired t-test). This result shows quantitatively that inactivation, which is a hallmark of Piezo1 channel function, can be significantly inhibited by localized magnetic force application. Among all Piezo1-BBS constructs, the average loss of inactivation was greatest for BBS-2422 and BBS-2425. Additionally, we analyzed the change in maximum current amplitude and in pressure sensitivity ( $P_{50}$ ) in the presence of a magnetic field for all constructs and found, apart from a small decrease in current amplitude for BBS-2422 ( $22.0 \pm 5.0\%$ ;  $p < 0.01$ , paired t-test), no significant changes (Figures 16A-B).

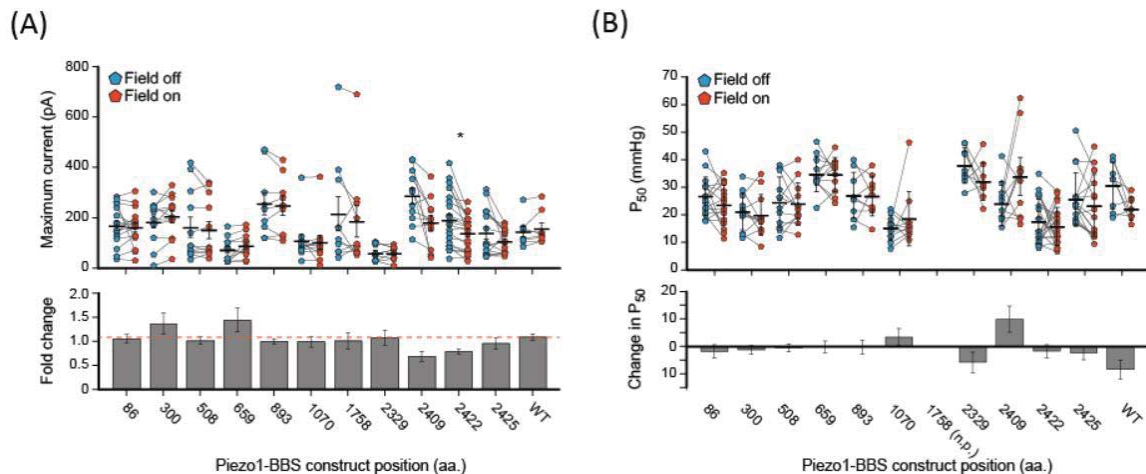


**Figure 16: Effect of magnetic pulling on BBS-constructs. (A) Average maximum current amplitudes before and during a magnetic field stimulation (above) (\*,  $p < 0.01$ , paired t-test) and fold change in amplitude (below) ( $p > 0.01$  for all constructs, one-way ANOVA and Tukey's comparison) ( $n = 8 - 21$  cells) (B)  $P_{50}$  values before and during magnetic field stimulation (n.p.,  $P_{50}$  unavailable for BBS-1758,  $p > 0.01$  for all constructs, one-way ANOVA and Tukey's comparison). Error bars are SEM.**

To test whether the magnetic field could lead to direct channel activation, we analyzed the channel open probability ( $NP_o$ ) during the +5 mmHg prepulse period in the presence and absence of the magnetic field. We found  $NP_o < 1\%$  for all constructs for both

conditions, indicating that the channel was predominantly closed regardless of the presence of a magnetic field (Figure 17).

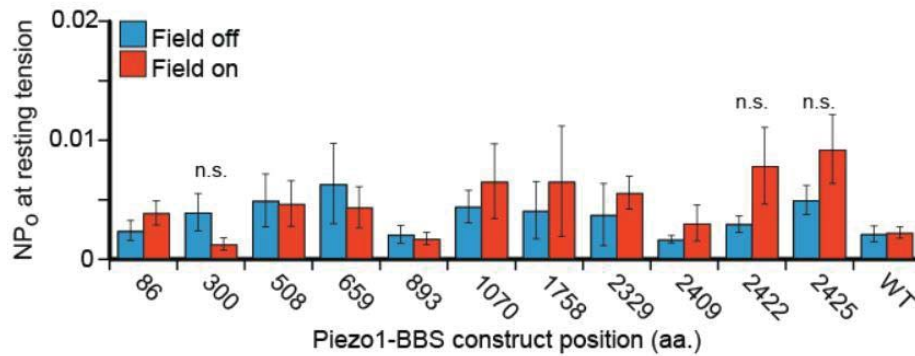


**Figure 17: A magnetic field does not directly activate Piezo1-BBS constructs at resting tension. NP<sub>o</sub> calculated from average current during a 4 second period at resting membrane tension (+5 mmHg) alone or in the presence of a magnetic field (n.s.  $p > 0.01$ , paired t-test). Error bars are SEM.**

Altogether, four extracellular sites within two domains emerged from our screen as significantly mechanically sensitive. BBS-86 and BBS-300 are both tagged proximal to the N-terminus, and BBS-2422 and BBS-2425 are tagged precisely on top of a large structurally unique extracellular domain located between the two predicted pore helices that likely forms part of the ion permeation pathway (Figure 18) (Ge et al., 2015; Kamajaya et al., 2014). Due to the robust effect we observed upon localized force application at BBS-2422 and the presence of human single-point mutations found within and surrounding this extracellular domain that cause loss of inactivation, we decided to further focus on construct BBS-2422 to better understand how localized force acts on Piezo1 function mechanistically (Volkers, Mechioukhi, & Coste, 2014).

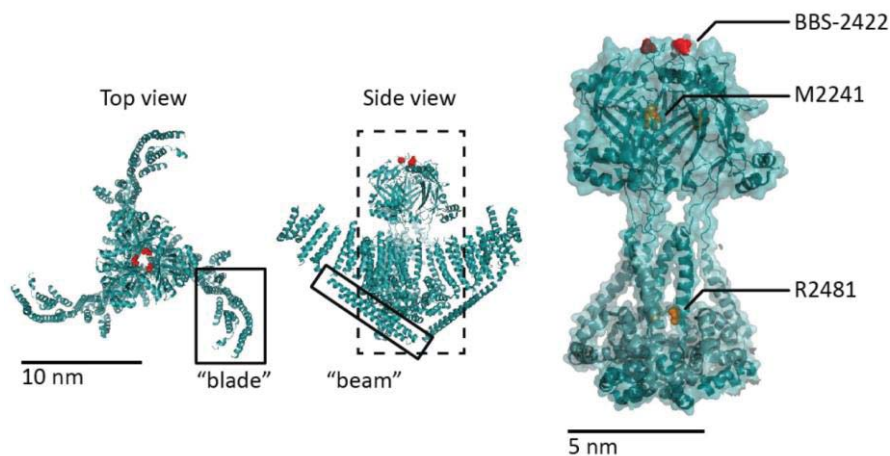


**Figure 18: Point mutations in the CED and pore domain. Top and side views (left and middle panels) of MmPiezo1 cryo-EM study (PDB 3JAC) with approximate location of aa. position 2422 highlighted in red. Previously named “blade” and “beam” are boxed. Predicted pore region (right) with overlaid electron density, highlighting 2422 position in red and alignment of human Piezo1 inactivation point mutations in yellow (M2242 and R2481 in mouse).**

## ***2.5 Magnetic force acts directly on channel domains***

Measuring the magnitude of the applied pulling force might allow for inferences about its effects on protein stability and function. To calibrate our setup, we labeled the 75 nm magnetic nanoparticles with Alexa Fluor 594 and measured their velocity through glycerol in the magnetic field of our setup. Using Stokes’ law, we calculated the drag force on 75 nm nanoparticles to be  $9.9 \pm 0.7$  pN, setting the upper limit of the total force applied to a single Piezo1 channel (Figure 19A). By performing this measurement on nanoparticles of 50, 100, and 200 nm diameter, we found that force increases with particle size, which is expected given that the magnetic susceptibility is the same for all bead sizes (Ocean NanoTech). Additionally, we measured the applied force for varying current amplitudes through the electromagnetic coil (Figure 19B). Supplying a current of

1 A reduced the force to  $2.6 \pm 0.2$  pN, which is comparable to the force of ambient thermal energy alone (see Methods). With this force we were unable to elicit a slowing of inactivation on BBS-2422, supporting the notion that the functional effect we observe is due to a force magnitude that exceeds basal conditions (Figure 19C).

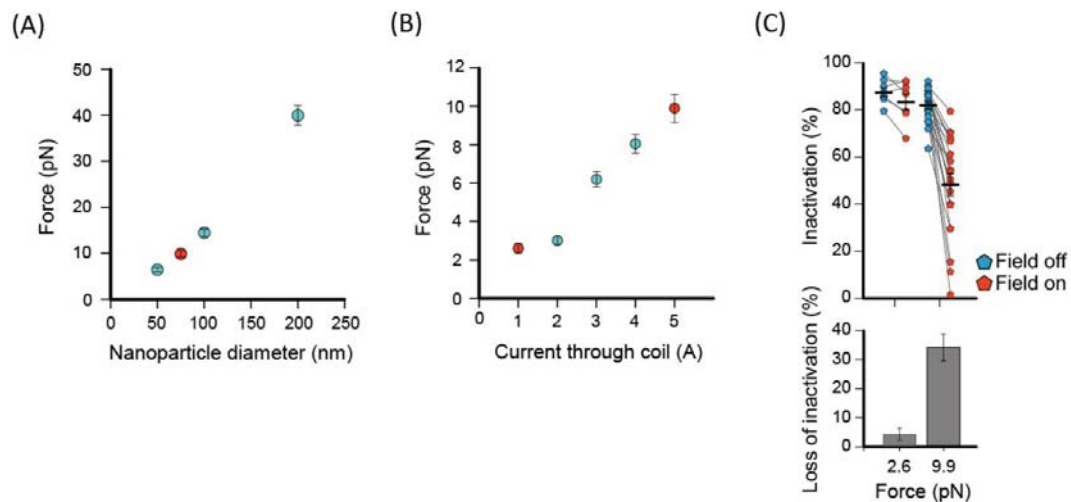


**Figure 19: Calibration of magnetic force. (A) Measured force on fluorescently labeled magnetic nanoparticles (red, 75 nm diameter; n = 15 nanoparticles per size). (B) Measured force on fluorescently labeled 75 nm diameter magnetic nanoparticles under varying current supply to electromagnet (red, 1 A and 5 A analyzed in next panel; n = 15 nanoparticles per condition). (C) Inactivation and averages of individual experiments (top) and average differences (bottom) of BBS-2422 with ~25% (1 A;  $2.6 \pm 0.2$  pN; n = 8 cells, 4 transfections) and 100% (5 A;  $9.9 \pm 0.7$  pN; n = 21 cells, 7 transfections) magnetic force with a -60 mmHg pressure step. Error bars are SEM.**

Next, we considered the possibility that steric effects of nanoparticle labeling may induce changes in channel activity. We observed for constructs BBS-86, BBS-300, BBS-2422 and BBS-2425 that nanoparticle labeling alone (i.e. in the absence of a magnetic field), did not induce a loss of inactivation upon two consecutive pressure step

stimulation protocols. Similarly, the presence of a magnetic field alone (i.e. without prior nanoparticle labeling) also did not elicit a loss of inactivation (Figure 20).

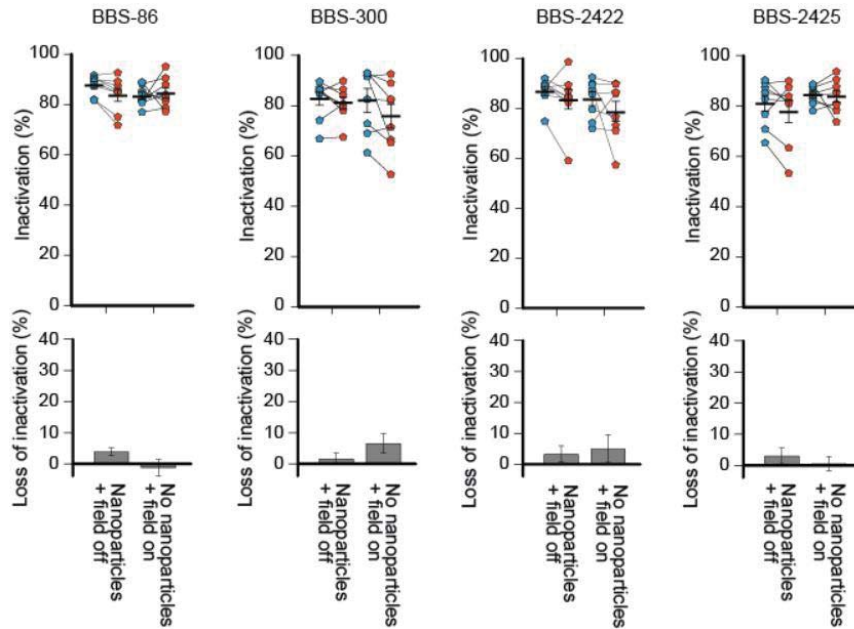


**Figure 20: Effect of magnetic field and nanoparticle labeling separately. Inactivation of individual constructs BBS-86, BBS-300, BBS-2422, and BBS-2425 with nanoparticle labeling alone (magnetic field off) or in the presence of a magnetic field alone (no nanoparticles) ( $p > 0.01$  all comparisons, paired t-test). Error bars are SEM.**

To further address the possibility of steric hindrance, we engineered a Piezo1-IRES-EGFP construct with a myc-tag binding sequence at residue 2422 (Piezo1-myc-2422) that we could specifically conjugate with a 10 nm-sized anti-myc antibody (Figure 21). The pressure sensitivity and inactivation ( $P50 = 18.5 \pm 2.4$  mmHg,  $80.9 \pm 3.1\%$ ,  $n = 8$  cells) of this construct were not affected by labeling it with the anti-myc antibody ( $P50 = 19.6 \pm 1.7$  mmHg,  $86.4 \pm 2.8\%$ ,  $n = 8$  cells;  $p > 0.01$ , unpaired t-test). Together, these results

support that it is specifically the magnetic force application that affects Piezo function and not steric hindrance.

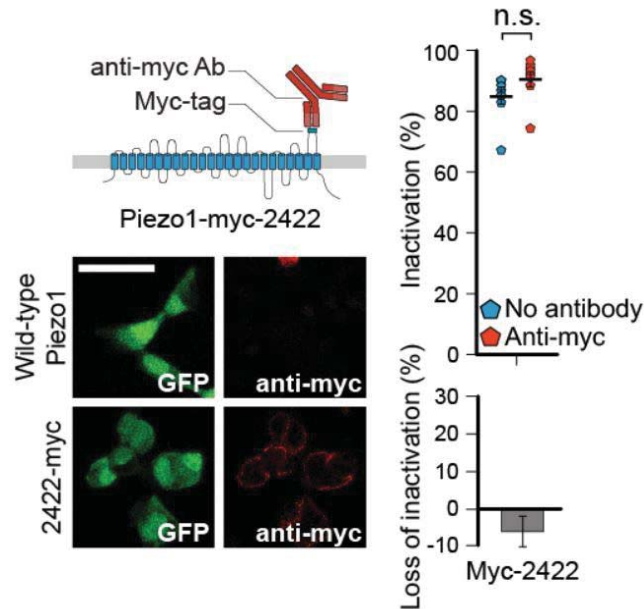


**Figure 21: Steric hindrance on CED does not affect Piezo inactivation.** Schematic of antibody labeling on Piezo1-myc-2422 (pIRES-EGFP) and representative images of HEK293T cells expressing wild-type Piezo1 (pIRES-EGFP) or Piezo1-myc-2422 construct (green, GFP; red, anti-myc). Percent inactivation and averages of individual experiments (top right) and average differences (bottom right) of myc construct labeled and unlabeled with c-myc antibody (n = 8 cells each, 2 transfections; n.s., p > 0.01, unpaired t-test). Scale bar is 30  $\mu$ m. Error bars are SEM.

We next hypothesized that Piezo function may be affected indirectly through pulling force transduced through the membrane bilayer. To test this we tagged the inwardly rectifying potassium Kir2.1 channel with a BBS (Kir2.1-BBS) on the first extracellular pore loop (S1-pore helix) and co-expressed it with wild-type Piezo1-pIRES-EGFP in HEK293T cells (Figure 22). We found that wild-type Piezo1 function (P50 = 24.6  $\pm$  2.7 mmHg, average maximal current = 148  $\pm$  44 pA, inactivation = 78.1  $\pm$  3.9%, n = 10

cells) was not affected by the force on Kir2.1 channels ( $P_{50} = 19.7 \pm 2.0$  mmHg, average maximal current =  $154 \pm 38$  pA, inactivation =  $74.8\% \pm 4.4$ ;  $p > 0.01$ , paired t-test). This result, together with the observation that the functional effects we detected were specific to each Piezo1-BBS construct, suggests that the pulling force is acting primarily on the tagged domain and not indirectly through the membrane bilayer.

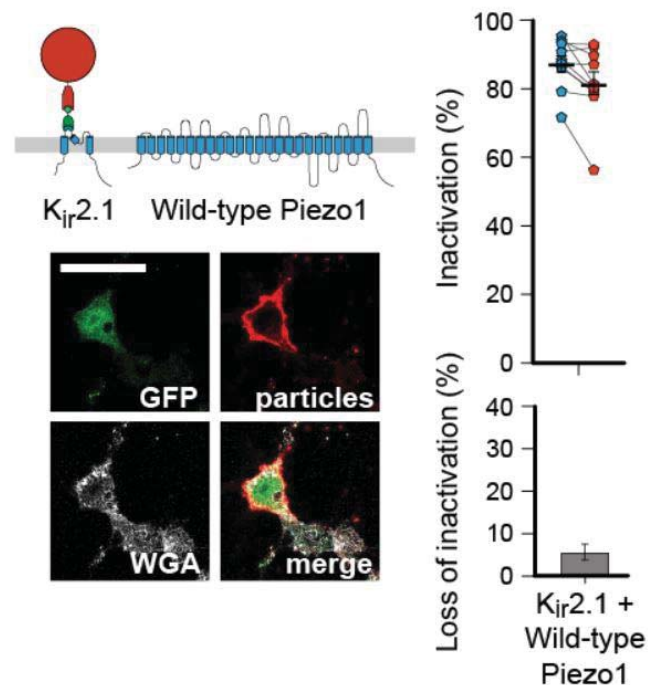


**Figure 22: Magnetic nanoparticles do not affect Piezos through membrane tethering.** Schematic of Kir2.1-BBS construct labeled with nanoparticles co-expressed with wild-type Piezo1 (pIRES-EGFP) and representative images of surface labeled HEK293T cells (green, GFP; red, anti-streptavidin; gray, WGA). Inactivation and averages of individual experiments (top right) and average differences (bottom right) for co-expressed Kir2.1-BBS and wild-type Piezo1 before and upon magnetic force ( $n = 10$  cells, 2 transfections). Scale bar is 30  $\mu$ m. Error bars are SEM.

Interestingly, the loss of inactivation is irreversible on a minute timescale (Figure 23). This is comparable to previous reports that a permanent loss of inactivation of wild-

type Piezo1 can be mechanically induced (Gottlieb et al., 2012). Such an effect suggests that magnetic pulling force on BBS-2422 may be accelerating an existing, but mechanistically unclear, tendency towards channel inactivation.

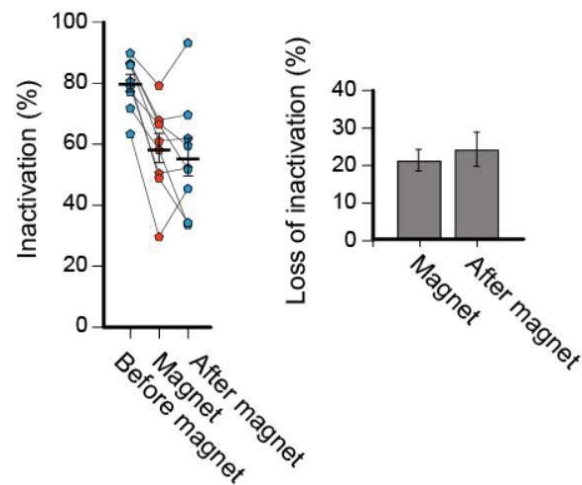


**Figure 23: Non-reversibility of magnetic pulling. Inactivation and averages of individual experiments (left) and average differences (right) for BBS-2422 recorded first without magnetic field, second with magnetic field, and third again without magnetic field (n = 9 cells, 5 transfections) Error bars are SEM.**

Structural studies showed that the BBS-2422 site is located near or along the ion permeation pathway (Ge et al., 2015). We found that the single channel conductance  $g$  of BBS-2422 ( $g = 32.5 \pm 0.7$  pS;  $n = 10$  cells) remained unchanged by magnetic pulling force ( $g = 31.3 \pm 0.3$  pS;  $n = 10$  cells;  $p > 0.01$ , paired t-test), therefore suggesting that mechanical perturbation of the extracellular domain containing residue 2422 is directly affecting the mechanism of inactivation independently of ion permeation (Figure 24).

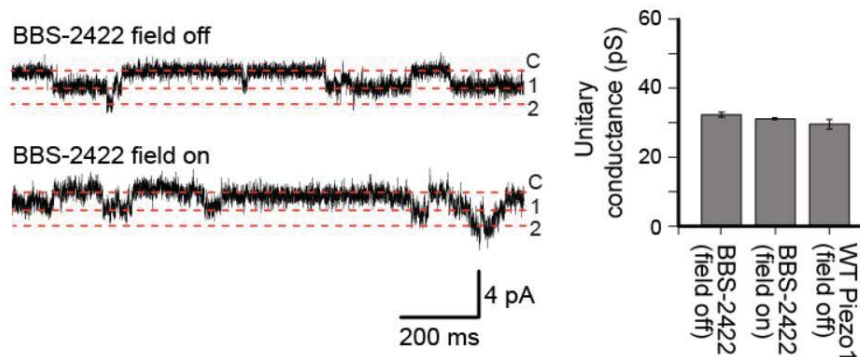


**Figure 24: Magnetic pulling does not affect single channel conductance.** Representative single channel recordings for BBS-2422 at resting tension with and without a magnetic field and quantification of single channel conductance (n = 9 cells, 4 transfections). Error bars are SEM.

## ***2.6 Magnetic force specifically perturbs mechanical gating***

We next aimed to test whether the observed functional effects from a magnetic pulling force were specific to a mechanism of mechanical activation or rather a nonspecific conformational change. To test this, we inserted a BBS into the extracellular loops of the voltage-activated ion channel Kv1.2 (Kv1.2-BBS). While this channel is not known to be mechanically activated, a previous study has shown that mechanosensitivity can be conferred by fusing it with the mechanosensitive ankyrin repeat domain of NOMPC, and another study has shown that activation can be modulated when stimulated with pressure, suggesting that this channel may be a strong candidate for modulation by a magnetic pulling force (Hao et al., 2013; Zhang et al., 2015). Specifically, a BBS was inserted into the extracellular loops S1-S2 (Kv1.2-BBS-S1-S2) and S3-S4 (Kv1.2-BBS-S3-S4) of the voltage-sensing domain, which undergoes a well-characterized conformational change upon depolarization leading to channel activation,

as well as the S5-pore-helix (Kv1.2-BBS-S5-PH) of the pore domain (Figure 25A) (Long et al., 2005). Nanoparticle labeling was specific to constructs Kv1.2-BBS-S1-S2 and Kv1.2-BBS-S3-S4 constructs, but failed to label Kv1.2-BBS-S5-PH (co-transfected with EGFP) (Figure 25B).

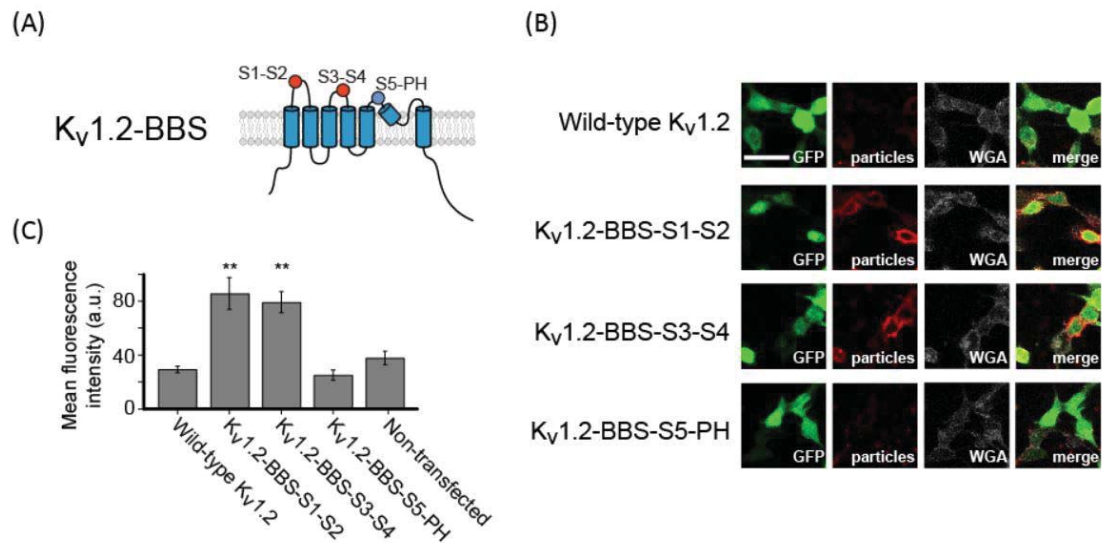


**Figure 25: Kv1.2-BBS nanoparticle labeling. (A) Kv1.2 transmembrane topology with aa. locations of BBS insertions (red, labeled and functional; blue, non-labeled and non-functional). (B) Representative fluorescent images of HEK293T cells immunostained against nanoparticles for Kv1.2-BBS constructs vs wild-type Kv1.2 (green, GFP; red, nanoparticles; gray, WGA). (C) Quantification of mean fluorescence intensity along cell membrane compared against non-transfected cells (n = 15 cells each, 3 coverslips; \*\*p < 0.001, unpaired t-test). Error bars are SEM. Scale bar is 30  $\mu\text{m}$ .**

We recorded voltage-activated currents from nanoparticle-labeled Kv1.2-BBS transfected HEK293 cells in a cell-attached configuration, while additionally applying a transient -60 mmHg pressure stimulus, analogous to our studies on Piezo1, at each voltage step (Figure 26A). As with Piezo1, these recordings were performed first without and then with a magnetic force  $F = 9.9 \pm 0.7$  pN applied.

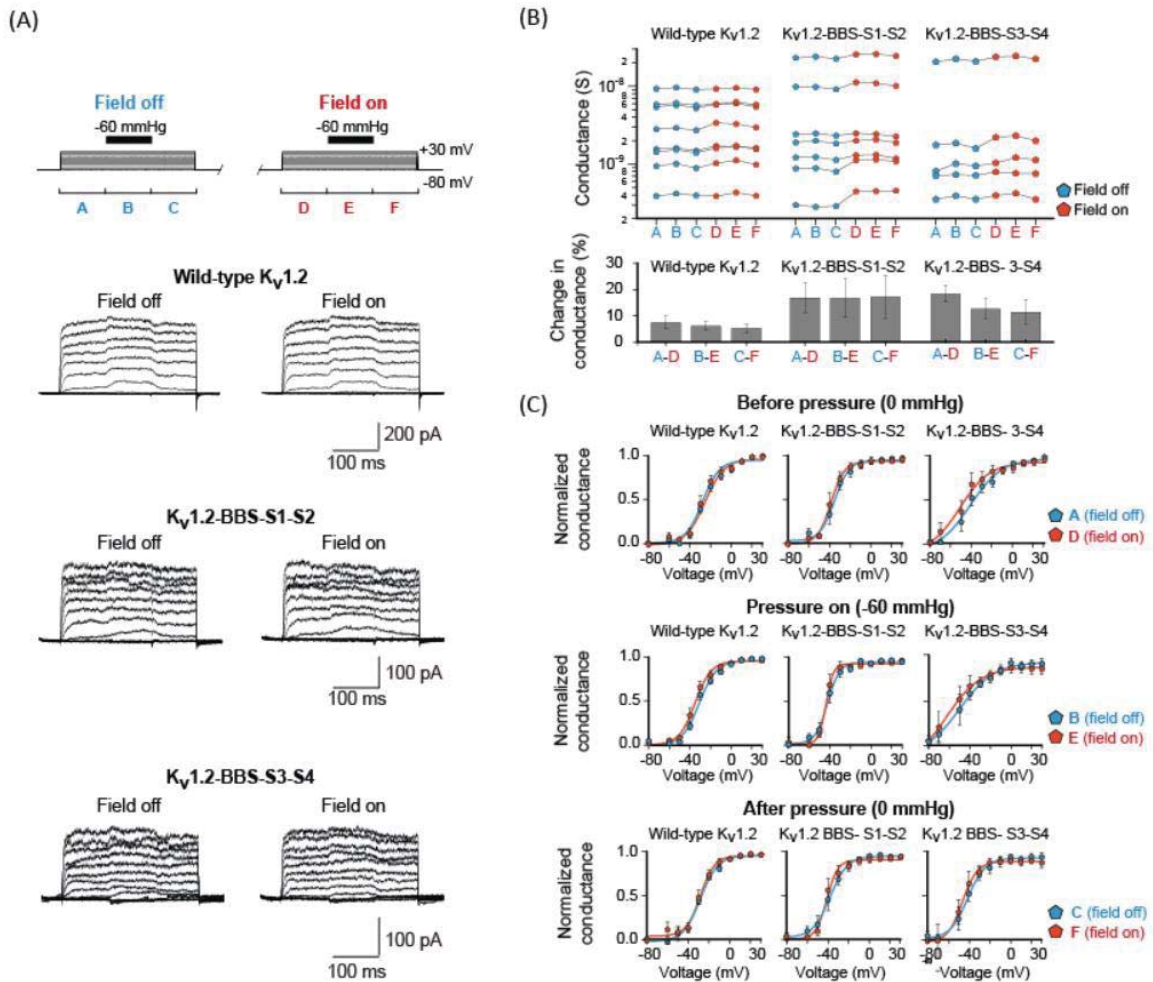


Figure 26: Magnetic pulling does not affect Kv1.2-BBS. (A) Voltage-step and pressure-pulse protocol with representative current traces for wild-type Kv1.2, Kv1.2-BBS-S1-S2 and Kv1.2-BBS-S3-S4. Periods A, C, D, and F mark voltage stimulation alone, while B and E are marking simultaneous voltage-stimulation and pressure-stimulation (field off for A-C, field on for D-F). (B) Maximal conductances of individual recordings ( $p > 0.01$  for comparisons between pairs A-D, B-E, and C-F for all constructs, paired t-test) and mean percent changes ( $n = 5 - 8$  cells, 2 transfections each;  $p > 0.01$  for comparisons of between corresponding values compared to wild-type Kv1.2, unpaired t-test). (C) Normalized average G/V curves for periods A (field off) vs D (field on), B (field off) vs E (field on), and C (field off) vs F (field on) ( $p > 0.01$  for comparisons of  $V_{1/2}$  in each panel, paired t-test). Error bars are SEM.

In the absence of magnetic force, maximal conductance from wild-type Kv1.2 expressing cells increased slightly and reversibly upon pressure stimulation ( $5.3 \pm 0.6$  % increase upon pressure onset; and  $2.6 \pm 0.8$  % decrease upon pressure release;  $p < 0.0001$ ,  $n = 8$  cells, paired t-test), which recapitulates an inherent mechanical modulation that had been reported before (Figure 26A-B) (Hao et al., 2013). As expected for a wild-type channel not binding magnetic nanoparticles, magnetic force application did not induce any further statistically significant changes in mean maximal conductance or voltage sensitivity before, during, or after pressure stimulation (change in conductance =  $7.5 \pm 2.6$  % (before),  $6.2 \pm 1.8$  % (during),  $5.3 \pm 1.7$  % (after); for all pairs  $p > 0.01$ ,  $n = 8$  cells, paired t-test) (Figure 26B). Likewise, we did not detect a statistically significant change in conductance, though an increasing trend is observed, or voltage sensitivity upon magnetic stimulation at each stage of the stimulation protocol for both constructs targeting the voltage sensor domain: Kv1.2-BBS-S1-S2 (change in conductance =  $17.0 \pm 5.6$  % (before),  $16.8 \pm 7.5$  % (during),  $17.3 \pm 8.1$  % (after); for all pairs  $p > 0.01$ ,  $n = 7$  cells, paired t-test) and Kv1.2-BBS-S3-S4 (change in conductance =  $18.5 \pm 3.2$  % (before),  $12.8 \pm 3.8$  % (during),  $11.5 \pm 4.7$  % (after); for all pairs  $p > 0.01$ ,  $n = 5$  cells, paired t-test) (Figure 26C and Table 1). Also, wild-type Kv1.2 and both Kv1.2-BBS constructs did not exhibit any inactivation, and again this property was unaffected by magnetic stimulation. Construct Kv1.2-BBS-S5-PH, targeting the pore domain, did not exhibit any currents above those measured in non-transfected cells, which was consistent with its lack of

nanoparticle labeling, showing that Kv1.2 did not tolerate insertion of BBS into the very short extracellular pore loop. Together, these results support that our approach specifically identified mechanically sensitive regions of Piezo1.

**Table 1: Magnetic pulling does not affect voltage sensitivity of Kv1.2-BBS constructs. Mean  $V_{1/2}$  values for wild-type Kv1.2 and Kv1.2-BBS constructs ( $p > 0.01$  for comparisons between pairs A-D, B-E, and C-F; wild-type Kv1.2,  $n = 8$ ; Kv1.2-BBS-S1-S2,  $n = 7$ ; Kv1.2-BBS-S3-S4,  $n = 5$ ; paired t-test.)**

Mean $V_{1/2}$ (mV) for Kv1.2 and Kv1.2-BBS constructs						
	Field off			Field on		
	A (0 mmHg)	B (-60 mmHg)	C (0 mmHg)	D (0 mmHg)	E (-60 mmHg)	F (0 mmHg)
Wild-type Kv1.2	-24.4 ± 2.7	-30.4 ± 1.9	-29.3 ± 2.2	-27.4 ± 2.9	-34.3 ± 2.3	-30.5 ± 2.6
Kv1.2-BBS-S1-S2	-33.8 ± 2.5	-41.6 ± 3.8	-35.7 ± 2.7	-38.9 ± 3.8	-45.8 ± 4.1	-43.6 ± 4.8
Kv1.2-BBS-S3-S4	-39.7 ± 4.9	-44.9 ± 5.5	-41.9 ± 3.8	-42.0 ± 4.7	-46.8 ± 5.3	-43.1 ± 3.4

Finally, to understand how magnetic force interferes with mechanical gating by membrane tension thermodynamically, we analyzed the effect of magnetic force application on the kinetics of BBS-2422 channel activation, inactivation, and deactivation elicited by a pressure step (Figure 27A). We found that magnetic force significantly increases the time constants of activation ( $4.2 \pm 0.3$  ms (field off) and  $6.1 \pm 0.7$  ms (field on),  $p < 0.01$ , paired t-test) and inactivation ( $49.0 \pm 3.1$  ms (field off) and  $66.5 \pm 6.2$  ms

(field on),  $p < 0.01$ , paired t-test), while leaving deactivation unchanged ( $11.9 \pm 1.5$  ms (field off) and  $14.6 \pm 1.6$  ms (field on),  $p > 0.01$ ,  $n = 19$  cells, paired t-test) (Figure 27B).

These results suggest that the application of a magnetic pulling force not only slows inactivation specifically through a mechanosensitive domain, but also directly inhibits mechanical activation by membrane tension.

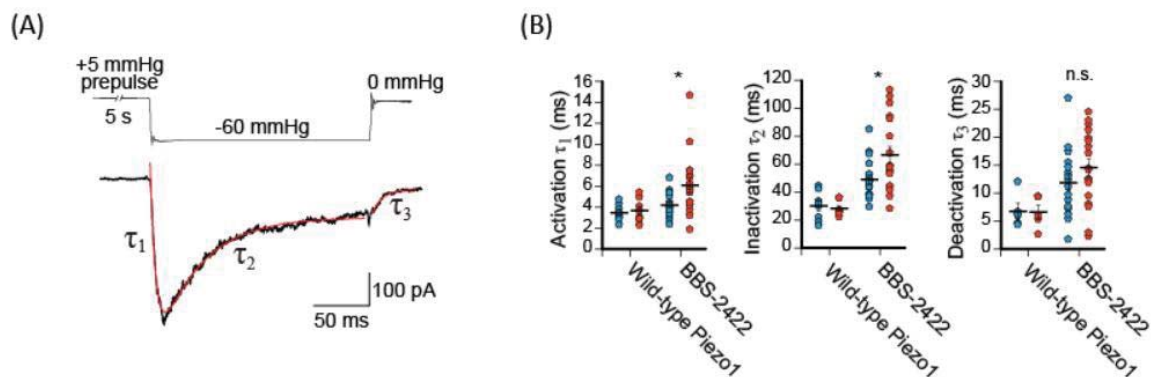


**Figure 27: Magnetic force affects mechanical activation. (A) Representative current trace of BBS-2422 upon stimulation by a -60 mmHg pressure step and exponential fit functions (red) with time constants of activation ( $\tau_1$ ), inactivation ( $\tau_2$ ), and deactivation ( $\tau_3$ ). (B) Time constants and averages of activation, inactivation, and deactivation obtained from individual experiments without magnetic field (blue) and upon magnetic field (red) for wild-type Piezo1 ( $n = 8$  cells, 3 transfections) and construct BBS-2422 ( $n = 17$  cells, 7 transfections; \* $p < 0.01$ , n.s.,  $p > 0.01$ , paired t-test). Error bars are SEM for all panels. Scale bars are  $30 \mu\text{m}$ .**

## 2.7 Discussion

We set out to identify domains with high mechanical sensitivity in Piezo1.

Current experimental methods do not allow force application on defined sub-molecular structures simultaneous to functional characterization. Here, we apply a force of  $\sim 10$  pN to specific extracellular domains, while measuring channel function electrophysiologically. Atomic force microscopy experiments have shown that

destructive forces that extract an entire transmembrane domain from the lipid bilayer (100-150 pN) or that cause domain unfolding (50-200 pN) are much larger, which is consistent with our finding that none of the tested constructs loses its ability to be mechanically activated under magnetic force application (Hoffmann et al., 2013; Müller et al., 2009). Rather, the force in our experiments is comparable to the Coulomb force acting on a single voltage sensor domain of a voltage-gated potassium channel under physiological conditions (~10 pN; see Methods) or the force acting on a 1 nm long gating spring to open a mechanically activated ion channel (~10 pN; see Methods) (Sukharev & Corey, 2004).

Lower forces were indistinguishable from ambient thermal energy and thus did not affect channel behavior. Higher forces could have allowed us to investigate the upper limits of local force application on Piezo1, but the electromagnetic coil in these experiments was already operated near the fusing current. Given this limitation, our measurements of magnetic pulling force on different sized nanoparticles show that the 75 nm diameter size nanoparticles meet a balance by minimizing size while still providing a physically relevant magnitude of force. One related potential caveat in our study arises from the possibility that multiple channels or subunits may be bound to a single nanoparticle. In this case, the force transduced by one nanoparticle would be distributed among these channels, likely rendering the force negligible and therefore resulting in wild-type Piezo1-like behavior. However, the fact that each channel is

maximally labeled to a single nanoparticle is at the same time advantageous, because each labeled channel is then modulated identically.

Our unbiased screen reveals four mechanically sensitive sites in two distinct domains of Piezo1. Sites 86 and 300, located at the proximal N-terminus, mark an intriguing location because it resonates with the theoretical mechanism of a gating spring that provides maximal force sensitivity at the outermost end of a lever structure (Sukharev & Corey, 2004). Additionally, an effect in this region also supports structural data suggesting that the numerous transmembrane domains are in fact organized as a 'blade' structure possibly involved in mechanosensing (Ge et al., 2015). Sites 2422 and 2425 are part of the outer pore domain, which raises the possibility that mechanisms of inactivation found in other ion channels, such as pore blocking (N-type inactivation) or collapse of the selectivity filter (C-type inactivation), are also at work in Piezos (Hoshi, Zagotta, & Aldrich, 1991). The fact that single channel conductance stays unchanged in BBS-2422, which likely interacts directly with the pore region, suggests that it is less likely that the pore helices are being pulled apart by the magnetic force as part of an irreversible structural change. Rather, the lack of an effect on single channel conductance suggests that we are facilitating a natural movement of the channel by specifically targeting mechanosensitive sites. It is possible, however, that the domains we have identified are critical for channel function but not necessarily its native

mechanosensitivity. Therefore we can currently only conclude that these domains are themselves mechanically sensitive, but not necessarily the “mechanosensors” of Piezo1.

Despite the N-terminus and the outer pore clearly being structurally distinct, it is interesting that these two regions both affect the process of inactivation, though it is still unclear whether this occurs through a common mechanism. A clue for a potential allosteric interaction between these regions may be found in the intracellular ‘beam’ structures revealed in the cryo-EM model that span the length of each subunit and through which membrane tension acting on the “blade” structures could be transmitted to the pore (Ge et al., 2015). In our study, we see that pulling either the N- or C-terminal domain away from the membrane induces a stabilization of the open state upon activation by pressure, which manifests itself as a loss of channel inactivation. One possible mechanism by which this occurs could involve a “lever and hinge” mechanism by which the “blade” domain functions as a stiff lever with its movements allosterically connected to the central pore. Accordingly, our manipulation with a magnetic pulling force may imitate a native tension-induced movement of Piezo1.

Magnetic pulling only affected function of the mechanically activated Piezo1 channel, and not that of the voltage activated Kv1.2, even under the added mechanical stress of increased membrane tension. Along with our observation that the effects of magnetic pulling on Piezo1 are confined to only certain domains, this finding suggests that the sites our screen identified in Piezo1 might specifically contribute to sensing

mechanical stimulation. Still, it is likely that targeting other specific sites within Kv1.2 or in entirely different channels could reveal structures not unique to Piezo that can be mechanically perturbed. Our experiments on Kv1.2 are thus merely a first test for specificity, and future broad application of magnetic pulling could be used to investigate the fundamental principles of mechanical sensitivity in other ion channel proteins. In light of our findings in Piezo1, it is quite remarkable that we did not observe acute channel activation with the onset of magnetic pulling force, but rather a slowing of activation in BBS-2422. Taken with the idea that a slowing of inactivation indicates a stabilization of the channel's open conformation, this may indicate that perturbing the domains identified in our screen may affect channel activation and inactivation through mechanistically distinct pathways.

Ultimately, we identify two mechanically sensitive domains, and it is possible that more domains remain to be uncovered with more controlled labeling stoichiometry, probing of intracellular sites, or higher forces. This finding sets a direction for future studies in understanding the mechanism of mechanical activation in Piezo ion channels. Finally, this study provides the first evidence for a structural component of inactivation in Piezos and an unexpected framework for future studies of this intriguing process.

### **3. Inactivation of mechanically activated Piezo1 ion channels is determined by the C-terminal extracellular domain and the inner pore helix**

#### ***3.1 Introduction***

The process of inactivation for Piezo ion channels was first observed upon their initial characterization in 2010 (Coste et al., 2010). Upon mechanical stimulation, Piezo channels activate allowing current to rise and then decay while still in the presence of stimulus. In principle, this decay in current could be due to adaptation of the channel to the stimulus, or due to an intrinsic transition towards pore closure known as inactivation. While both processes are not mutually exclusive, it has been shown in at least one stimulation paradigm that adaptation has only a minor contribution in Piezo1 and that the predominant mechanism for current decay is indeed inactivation (Lewis et al., 2017).

In the first report of Piezo current, it was observed that the time course of inactivation was fast at negative potentials and slow at positive potentials, and Piezo1 inactivation at all voltages was slower than Piezo2 at the corresponding voltage (Coste et al., 2010). Since then, inactivation of Piezo channels has risen as a key subject of interest, as an increasing number of studies reveal its physiological roles. The change in overall current density through inactivation causes changes in stimulus sensitivity and allows for the generation of temporal frequency filtering of repetitive stimuli such as mechanical vibration (Lewis et al., 2017). Additionally, several point mutations that alter

inactivation kinetics in both Piezo1 or Piezo2 were identified from human patients of various diseases, such as red blood cell dehydration (xerocytosis) and Gordon syndrome (distal arthrogyriposis type 3) (Albuisson et al., 2013; Andolfo et al., 2013; Bae, Gnanasambandam et al., 2013; Coste et al., 2013; Lukacs et al., 2015; McMillin et al., 2014; Okubo et al., 2015; Zarychanski et al., 2012). Endogenous factors such as bradykinin, divalent ion concentration, and extracellular pH also affect inactivation, opening the possibility that Piezo function is physiologically regulated through this mechanism (Bae et al., 2015; Dubin et al., 2012; Gottlieb et al., 2012). Given its demonstrated importance for mechanotransduction and its direct link to disease, a molecular understanding of Piezo inactivation is critical for developing treatments for Piezo function-related defects.

It now seems likely that Piezos are strongly modulated by the process of inactivation in physiology, but what structures mediate inactivation and how this process occurs in Piezos is still unknown. We therefore set out to understand the structural mechanism for inactivation in Piezo channels. In this study we hypothesize that inactivation is mediated by specific domains within the protein structure. Support for this hypothesis is drawn from the previously presented study, in which we identified the CED as a protein domain that may play a role in inactivation. Due to its proximity to the pore domain, we studied the CED and pore helices with mutagenesis paired with electrophysiology to uncover if and how these domains contribute to inactivation. Ultimately, we identified two distinct structures that mediate the kinetics and voltage

dependence of inactivation. With structural correlates for inactivation, we can then begin to study the molecular movements that underlie the mechanism of inactivation and how these movements are altered by disease causing mutations of under different external modulators such as voltage.

## **3.2 Experimental Methods**

### **3.2.1 Construct subcloning and characterization**

Mouse Piezo1-pIRES-EGFP in pcDNA3.1(+) was obtained from Ardem Patapoutian and previously described (Coste et al., 2012). Mouse Piezo2 was synthesized to be codon-optimized for expression in human cells by Genewiz and ligated into pcDNA3.1(+) between restriction sites Kpn1 and Not1.

CED chimeric constructs were generated by first inserting AgeI restriction sites into regions flanking the CED of Piezo1 (after amino acid positions S2211 and G2459) and regions flanking the CED of Piezo2 (after positions S2614 and G2733), using the QuikChange Lightning Multi Site-Directed Mutagenesis Kit (Agilent). All primers were synthesized and desalted by Sigma Aldrich. The constructs were then digested with AgeI-HF (NEB), purified after gel electrophoresis, and re-ligated with T4 DNA ligase (NEB) to insert the Piezo2 CED into the Piezo1 backbone, and the Piezo1 CED into the Piezo2 backbone. Lastly, the AgeI restriction sites were removed with the QuikChange Lightning Multi Site-Directed Mutagenesis Kit (Agilent Technologies).

Piezo1 charge neutralization and reversal constructs, as well as all cysteine mutant constructs were generated by site-directed mutagenesis using the QuikChange Lightning Multi Site-Directed Mutagenesis Kit (Agilent Technologies).

CED deletion constructs were generated either by digesting, purifying after gel electrophoresis, and self-ligating Piezo DNA with inserted AgeI restriction sites as described for chimeras, or with the Q5® Site-Directed Mutagenesis Kit (NEB). CED deletion constructs for Piezo1 are as listed: P2223-S2450delinsTG, P2223-P2456delinsTG, L2212-L2461delinsTG, V2226-F2449delinsTG, R2295-K2422del, R2295-K2438del, P2253-K2422del, and P2253-K2438del, where 'insTG' indicates when an AgeI restriction site remained in the sequence. 'P2223-S2450delinsTG' was cloned into the background of the previously reported  $\alpha$ -bungarotoxin tagged Piezo1, Piezo1-BTX-86 for fluorescence imaging, or the background of the previously reported Piezo1-FLAG construct for NativePAGE electrophoresis (Syeda et al., 2016; Wu, Goyal, & Grandl, 2016). All other deletion constructs were in wild-type Piezo1. CED deletion constructs for Piezo2 were cloned into wild-type Piezo2 and are as listed: L2495-L2735delinsTG and V2509-F2723delinsTG.

PreScission Protease sites were inserted into Piezo1 by synthesizing the Piezo1 CED flanked with AgeI restriction sites and the sequence 5' CTGGAAGTTCTGTTCCAGGGGCCC 3' at amino acid positions Q2222 and P2456. AgeI sites were inserted into the Piezo1 vector as well at the described sites. Piezo1

vector and CED fragments were digested and re-ligated with AgeI-HF restriction enzyme (NEB) as described above. All constructs were sequence verified by Sanger sequencing (Genewiz).

### **3.2.2 Cell culture**

HEK293T-P1KO cells (Piezo1 knock-out human embryonic kidney cells) were obtained from Ardem Patapoutian and previously described (Dubin et al., 2017). Cells were cultured at a seeding density of 10,000 cells per well in a 24-well plate in DMEM-HG (Life Technologies) supplemented with 10% heat-inactivated fetal bovine serum (Clontech Laboratories), 50 U ml<sup>-1</sup> penicillin and 50 mg ml<sup>-1</sup> streptomycin (Life Technologies), and grown at 37 °C and 5% CO<sub>2</sub> on poly-L-lysine and laminin coated coverslips (Sigma Aldrich). Cells were transiently transfected with Piezo1 and Piezo1 mutants (1.5 µg) in the presence of 10 µM ruthenium red using Fugene6 (Promega) according to manufacturer protocol. Piezo2 and Piezo2 mutants were co-transfected with EGFP at a 1:0.5 mass ratio. Transfected cells were recorded 24-72 hours post-transfection.

### **3.2.3 Electrophysiology**

Patch-clamp recordings were performed using an EPC10 amplifier and Patchmaster software (HEKA Elektronik). Data were sampled at 5 kHz (cell-attached) or 10 kHz (whole-cell) and filtered at 2.9 kHz.

For whole-cell experiments, borosilicate glass pipettes (1.5 OD, 0.85 ID; Sutter Instrument Company) had a resistance of 2-4 M $\Omega$  when filled with pipette buffer solution containing (in mM) 133 CsCl, 10 HEPES, 5 EGTA, 1 CaCl<sub>2</sub>, 1 MgCl<sub>2</sub>, 4 MgATP, and 0.4 Na<sub>2</sub>GTP, pH=7.3 with CsOH. The bath solution for whole-cell experiments contained (in mM), 130 NaCl, 3 KCl, 1 MgCl<sub>2</sub>, 10 HEPES, 2.5 CaCl<sub>2</sub>, and 10 glucose, pH=7.3 with NaOH. For 'NMDG+ intracellular' recordings, all CsCl in the pipette solution was replaced with 133 mM NMDG+ and recorded with standard bath buffer. For 'NMDG+ extracellular' recordings, all NaCl and KCl in the bath buffer was replaced with 133 mM NMDG and recorded with standard pipette buffer. For whole-cell recordings, internal solution was allowed to dialyze for at least five minutes before recording to allow for GTP-mediated run-up of Piezo2 currents (Jia et al., 2013).

Cell-attached recordings for all experiments were performed at RT in bath solution containing (in mM) 140 KCl, 10 HEPES, 1 MgCl<sub>2</sub> and 10 Glucose, pH=7.3 with KOH. Pipette buffer for Piezo1 experiments contained (in mM) 130 NaCl, 5 KCl, 10 HEPES, 1 CaCl<sub>2</sub>, 1 MgCl<sub>2</sub> and 10 TEA-Cl, pH=7.3 with NaOH.

Mechanical stimulation was applied as previously described (Coste et al., 2010; Wu, Lewis, & Grandl, 2017). For poke stimulation cells were indented with a fire-polished glass pipette (tip diameter ~3-5  $\mu$ m) controlled by an amplifier-controlled piezo-electric driver (E625 LVPZT Controller/Amplifier; Physik Instrumente). The probe was initially positioned ~2-4  $\mu$ m from the cell and advanced at 0.5  $\mu$ m/ms in 1  $\mu$ m

increments at an 80° angle, while the cell was held at -80 mV, and the protocol was stopped and step increment was recorded after eliciting a current of greater than 100 pA. Cells were then stimulated with a voltage-step protocol from -100 mV to +100 mV, with a single indentation stimulus of the previously recorded increment at each voltage-step. For stretch stimulation negative pressure was applied through the patch pipette with an amplifier-controlled high-speed pressure clamp system (HSPC-1; ALA Scientific Instruments). Membrane curvature measurements were obtained as previously described (Lewis & Grandl, 2015).

For MTSET experiments, MTSET (Toronto Research Chemicals) was reconstituted in water from powder stock to a 400 mM stock solution and diluted in the cell-attached pipette buffer to a final concentration of 2 mM or 200  $\mu$ M. Pipette buffer was kept on ice for a maximum for 1.5 h during recording to minimize hydrolysis. TRPA1 experiments were performed in the whole-cell configuration with a bath buffer consisting of (in mM) 150 NaCl, 1 MgCl<sub>2</sub>, 1 EGTA, 10 HEPES, and 10 Glucose, pH=7.3 with NaOH, and internal buffer consisting of (in mM) 150 CsCl, 1 MgCl<sub>2</sub>, 10 EGTA, and 10 HEPES, pH= 7.3 with CsOH.

### **3.2.4 Fluorescence imaging**

The CED deletion construct 'Q2222-D2451delinsTG' and the previously reported construct Piezo1-BTX-86 were transiently transfected into HEK293T-P1KO cells for 48 hours (Wu, Goyal, & Grandl, 2016). For membrane surface labelling, cells were live-

labeled by washing twice with PBS, then incubating at 37 °C for 15 min in PBS containing  $\alpha$ -bungarotoxin conjugated with AlexaFluor-555 (B35451; Molecular Probes) at a final concentration of 10  $\mu$ g/mL and 10 mM HEPES. Cells were then washed 3 times for 5 min each and fixed with 4% paraformaldehyde for 30 min at room temperature in the dark. For cytoplasmic protein labeling, cells were first fixed in 4% PFA and then permeabilized with 0.25% Triton X-100 (201614; Thermo Fisher) and incubated with PBS containing 10  $\mu$ g/mL  $\alpha$ -bungarotoxin conjugated with AlexaFluor-647 (B35452; Molecular Probes) for 15 min in the dark at 37 °C for labeling in cytoplasmic protein. Cells for both experiments were washed 3 times for 5 min each and mounted with Fluoromount-G (SouthernBiotech) on glass slides, and imaged on a Zeiss 780 inverted confocal microscope at x63 magnification. Mean fluorescence intensity was measured along the bounding cell membrane or within the cytoplasm with a custom-written script in Fiji image processing software as previously described (Wu, Goyal, & Grandl, 2016).

### **3.2.5 Protein purification and NativePAGE gel**

The mouse Piezo1-Flag construct was obtained from Ardem Patapoutian and purified as previously described (Syeda et al., 2016). The CED deletion construct 'P2223-S2450delinsTGFLAG' was purified in the same manner. Purified protein samples were analyzed by nondenaturing gel electrophoresis using the NativePAGE novex (Invitrogen) system in accordance with the user manual. Specifically, samples were mixed with NativePAGE sample buffer and NativePAGE 5% G-250 sample additive and

run on a 3%-12% bis-tris gel at 150 V for 90 minutes. Following electrophoresis, the native gel was visualized by coomassie G-250 staining.

### 3.2.6 Data analysis

Analysis for was performed with Igor Pro 6.22A (WaveMetrics) and R + RStudio. Whole-cell electrophysiology recordings were analyzed for cells with a seal resistance of >500 MΩ and a series resistance of <10 MΩ. Cells with maximum currents less than 100 pA in whole-cell were excluded from analysis. Cell-attached recordings were analyzed for patches with a seal resistance of >1 GΩ, and cells with maximum currents less than 30 pA were excluded from analysis for percent inactivation.

The time constant of inactivation  $\tau$  was obtained by fitting a single exponential curve between the peak current and the stimulus offset:

$$I = I_0 - I \exp \frac{-(t - t_0)}{\tau}$$

The degree of inactivation for cell-attached recordings was analyzed as previously described with the function:

$$\% \text{ inactivation} = \left( \frac{\text{peak current} - \text{decayed current}}{\text{peak current}} \right) \times 100$$

With decayed current measured at 150 ms after the time of peak current (Wu, Goyal, & Grandl, 2016).

Gating charges  $z$  were calculated with the Faraday constant  $F = 96,485 \text{ s}\cdot\text{A/mol}$  and the gas constant  $R = 8.31 \text{ J/mol}\cdot\text{K}$  for a temperature  $T = 298 \text{ K}$ . Exponential functions were fit to inactivation time constants in the entire range of reported voltages.

### **3.2.7 Statistical analysis**

Statistical analyses were performed with paired or unpaired Student's t-tests, or one-way analysis of variance (ANOVA) when comparing three or more conditions. All data are reported as mean  $\pm$  SEM. Significance thresholds were set as  $p < 0.05$ , as described in the text.

### ***3.3 Voltage modulates Piezo1 and Piezo2 inactivation kinetics in a continuous manner***

To investigate the readily apparent voltage dependence of Piezo inactivation in greater detail, we performed whole-cell electrophysiology recordings on HEK293T-P1KO cells, which were engineered by CRISPR/Cas9 to lack endogenous Piezo1, and are thus devoid of mechanically activated currents (Dubin et al., 2017).

We mechanically stimulated cells transiently transfected with DNA encoding wild-type mouse Piezo1 by indentation with a blunt glass pipette, while holding the cells at potentials ranging from -100 mV to +100 mV (Figure 28A). Mean currents elicited by this protocol were large ( $1.37 \pm 0.22$  nA at -100 mV and  $1.5 \pm 0.34$  nA at +100 mV;  $n = 13$  cells), and exhibited the previously reported rapid activation and subsequent inactivation, the latter of which was well-fit by a single exponential function (IgorPro, Wavemetrics) (Figure 28A).

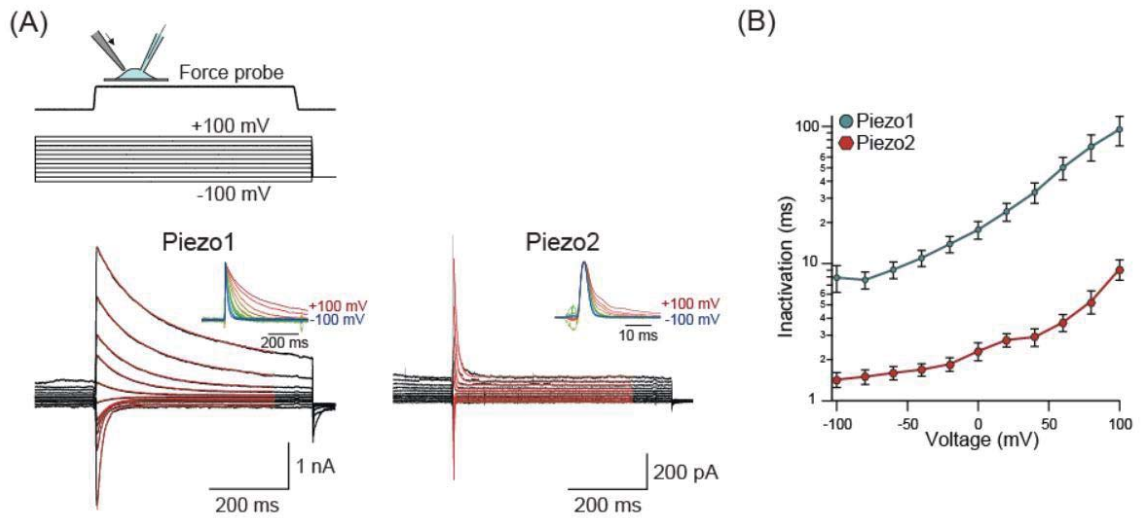


**Figure 28: Inactivation kinetics of Piezo1 and Piezo2. (A) Force probe indentation stimulation protocol and representative currents of whole-cell recordings from HEK293T-P1KO cells transiently transfected with wild-type mouse Piezo1 and Piezo2. Red lines are single exponential fits to the decaying currents. Insets show currents normalized to their peak amplitudes. (B) Mean inactivation time constants obtained from exponential current fits as a function of membrane potential for Piezo1 (n = 13 cells) and Piezo2 (n = 14 cells). Error bars are SEM.**

Importantly, we observed that the previously reported binary difference in inactivation kinetics between negative and positive potentials is more accurately described as a gradual change, i.e. over a wide range of membrane potentials, inactivation kinetics change exponentially as a function of voltage. Based on this exponential relationship, we applied a two-state mechanism of channel inactivation (open  $\leftrightarrow$  inactivated) and its associated inactivation rate constant  $\alpha = A \cdot \exp((E_{inact} - zFV)/RT)$  (see Methods) to calculate the effective charge ( $z = 0.31 \pm 0.02$  e) associated with voltage dependent inactivation. Identical experiments on wild-type mouse Piezo2 revealed a similar, albeit shifted, voltage dependence of inactivation

kinetics, with a calculated effective charge  $z = 0.24 \pm 0.02 e$  (Figure 28B). From these data we concluded that voltage dependence of inactivation might be generated by one single charged residue within the numerous predicted transmembrane domains within each monomer of the trimeric Piezo channels. The results also suggested that, although mouse Piezo1 and mouse Piezo2 share only ~53% sequence homology, the mechanism and perhaps also the structures giving rise to inactivation and its voltage dependence are identical in both proteins.

To determine whether the voltage dependence of inactivation was an effect of ion permeation, we recorded Piezo1 activity while substituting permeant cations on the intracellular ( $\text{Cs}^+$ ) or extracellular side ( $\text{Na}^+$  and  $\text{K}^+$ ) with the large cation NMDG<sup>+</sup>. This resulted in a  $-25 \pm 2$  mV shift in reversal potential towards more negative values (NMDG<sup>+</sup> extracellular) vs. a  $+22 \pm 1$  mV shift towards more positive values (NMDG<sup>+</sup> intracellular), respectively compared to the standard recording buffer ( $3.7 \pm 2$  mV) (Figure 29A). Importantly, we found that inactivation kinetics remained identical across all voltages ( $p \geq 0.05$ , one-way ANOVA followed by post-hoc Tukey test,  $n = 9-13$  cells) regardless of substitution with NMDG<sup>+</sup>, demonstrating that the voltage dependence of inactivation is autonomous of the driving force of ion permeation (Figure 29B).

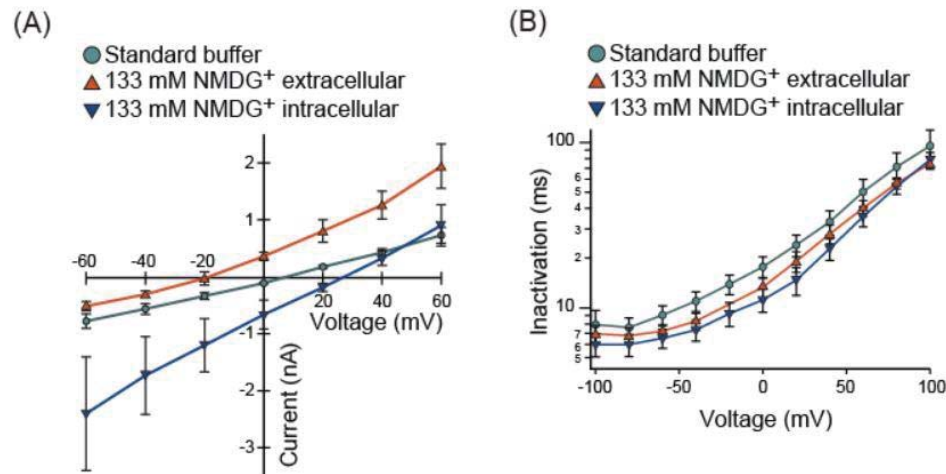


**Figure 29: Effect of ion permeation on inactivation. (A) Mean peak currents for Piezo1 during force probe stimulation and (B) mean inactivation time constants from single exponential fits, recorded with standard bath and pipette buffers ( $n = 13$  cells), NMDG<sup>+</sup> in the bath ( $n = 10$  cells), and NMDG<sup>+</sup> in the recording pipette ( $n = 9$  cells) as a function of membrane potential. Error bars are SEM.**

These results further suggest that Piezo ion channels inactivate in a voltage dependent manner that is likely mediated by intrinsic mechanisms within the Piezo protein itself. Previously, our group and two others demonstrated through complementary approaches that Piezo1 is activated by lateral membrane tension (Cox et al., 2016; Lewis & Grandl, 2015; Syeda et al., 2016). In our approach, we measured currents of cell-attached patches of HEK293T cells overexpressing Piezo1 at -80 mV, while simultaneously visualizing and measuring membrane geometry (Lewis & Grandl, 2015). In this setting, negative pressure applied to the patch pipette induces membrane curvature, thus increasing membrane tension and activating Piezo1. By analyzing these data with respect to current inactivation, we found that inactivation exhibited minimal dependence ( $\tau = 59 \pm 8$  ms to  $113 \pm 40$  ms) on membrane tension (Figure 30). This result

is in stark contrast to the strong modulation by voltage, which ranges over more than one order of magnitude, and thus shows that the mechanism of inactivation is specifically sensitive to modulation by voltage but not to tension in the membrane bilayer.

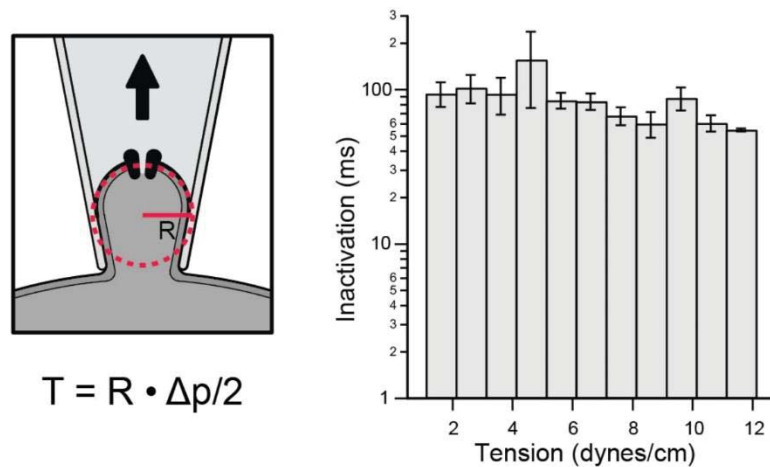


**Figure 30: Effect of membrane tension on inactivation.** Diagram of membrane radius measurement and tension derivation through LaPlace's law; R is radius and p is pressure. Mean time constants of inactivation binned as a function of membrane tension within the patch dome during cell-attached pressure clamp stimulation, from HEK293T transiently transfected with Piezo1. Data by A. Lewis. Error bars are SEM.

### ***3.4 The C-terminal extracellular domain is sufficient to confer inactivation kinetics***

Previous work from our lab implicated the C-terminal extracellular domain (CED) as a domain specifically important for Piezo1 inactivation, as we found that a pulling force of 10 pN applied to the upper part of the CED slows inactivation by ~40% (Wu, Goyal, & Grandl, 2016). In the primary sequence the CED is situated between the two pore helices and connected to them by linker regions that are highly conserved

amongst Piezo orthologues. A Piezo1 cryo-EM structure revealed that the CED is located directly on top of the permeation pathway, which is formed by the inner and outer pore-helices (Ge et al., 2015). We therefore hypothesized that the CED might be a structural determinant of inactivation kinetics.

To test this hypothesis, we pursued a chimeric strategy where we engineered a wild-type Piezo1 channel with the CED of Piezo2 (P1-P2CED), and a wild-type Piezo2 channel with the CED of Piezo1 (P2-P1CED) and measured channel activity induced by stimulating transfected cells with a blunt glass pipette in the whole-cell configuration (Figure 31A). Strikingly, a first qualitative examination of representative currents recorded at -60 mV and at +60 mV suggested that chimera P1-P2CED inactivates with kinetics similar to that of wild-type Piezo2, while chimera P2-P1CED adopts the inactivation kinetics of Piezo1 (Figures 31B-C). When stimulated at a holding potential of +100 mV, both chimeric constructs yielded peak current amplitudes that were statistically identical to those of wild-type channels (wild-type Piezo1:  $I_{\text{peak}} = 1.5 \pm 0.3$  nA; wildtype Piezo2:  $I_{\text{peak}} = 0.8 \pm 0.2$  nA; P1-P2CED:  $I_{\text{peak}} = 1.4 \pm 0.2$  nA; P2-P1CED:  $I_{\text{peak}} = 1.2 \pm 0.3$  nA), and no significant difference was measured across all tested voltages ( $p \geq 0.05$ , one-way ANOVA followed by post-hoc Tukey test,  $n = 13-14$  cells) (Figure 32A).

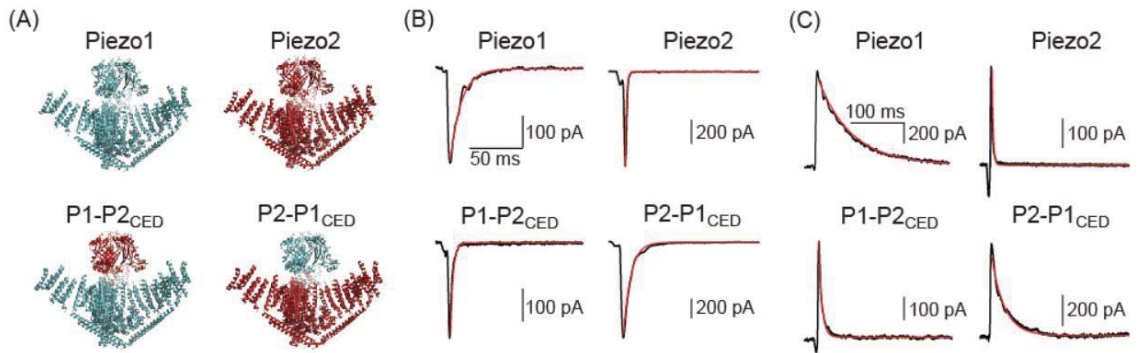


**Figure 31: The CED confers kinetics of inactivation. (A) Illustrations of chimeric constructs: the CED of wild-type Piezo1 (blue) and Piezo2 (red) are swapped to generate constructs P1-P2<sub>CED</sub> (Piezo1 with the CED of Piezo2) and P2-P1<sub>CED</sub> (Piezo2 with the CED of Piezo1). (B and C) Representative currents of whole-cell patches from wildtype Piezo1, Piezo2, P1-P2<sub>CED</sub>, and P2-P1<sub>CED</sub> elicited by a force probe stimulus at negative (-60 mV, (B)) and positive (+60 mV, (C)) holding potentials. Red lines are single exponential fits to the decaying currents.**

In order to obtain a detailed quantitative description we again fit inactivating currents with single exponential functions and plotted the time constants as a function of voltage (Figure 32). Indeed, chimera P2-P1<sub>CED</sub> was statistically identical in its inactivation kinetics to wild-type Piezo1 over the entire range of measured voltages from -100 mV to +100 mV ( $p \geq 0.05$  at each voltage, unpaired Student's t-test,  $n = 13-14$  cells). Inactivation kinetics for chimera P1-P2<sub>CED</sub> were identical to wild-type Piezo2 throughout negative and moderate positive potentials, while for more positive potentials (+40 mV to +100 mV), kinetics were intermediate between wild-type Piezo1 and wild-type Piezo2 (Figure 32B). These results show that the CED is in principal, sufficient for conferring the distinct inactivation time-courses between Piezo1 and

Piezo2, although structures or residues outside the CED must exist, at least in Piezo2, that also influence inactivation kinetics at positive potentials.

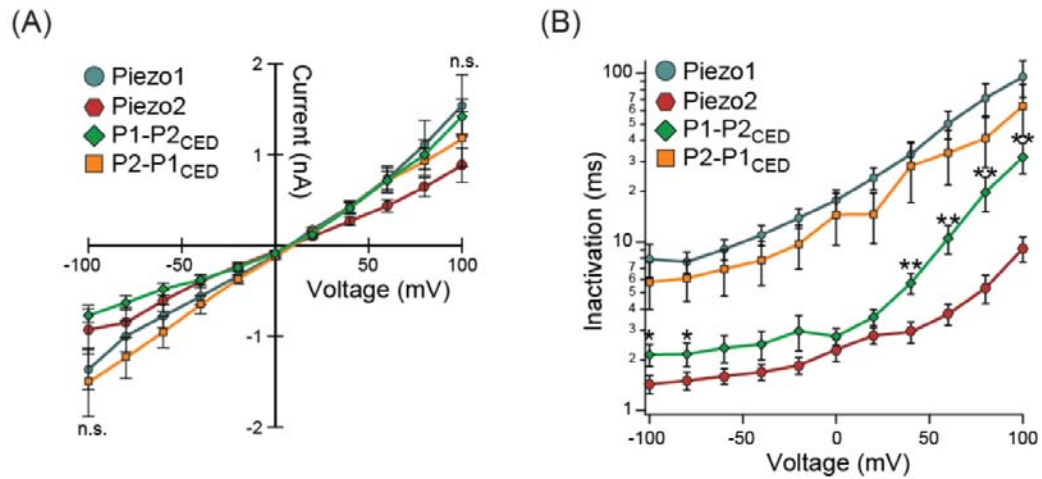


**Figure 32: Inactivation kinetics of chimeric constructs. (A) Mean peak currents elicited by force probe stimulation. (B) Mean inactivation time constants ( $\tau$ ) obtained with exponential fits from whole-cell recordings of HEK293T-P1KO cells transiently transfected with wild-type Piezo1 ( $n = 13$  cells), Piezo2 ( $n = 14$  cells), P1-P2CED ( $n = 14$  cells), and P2-P1CED ( $n = 14$  cells) as a function of membrane potential (n.s., no significance between all constructs,  $p \geq 0.05$ ; between Piezo2 and P1-P2CED,  $* p \leq 0.05$ ,  $** p \leq 0.005$ , one-way ANOVA followed by post-hoc Tukey's test). Error bars are SEM.**

The structure of the CED, first resolved in isolation by X-ray crystallography and later again by cryo-EM within the trimeric channel complex, reveals a cavity along the central axis of the CED and multiple large side fenestrations, raising the possibility that the CED mediates inactivation directly by acting as part of the permeation pathway (Ge et al., 2015; Kamajaya et al., 2014). However, we did not find any evidence for this function, as nine residues located within the central cavity, when individually mutated to cysteines and incubated with the cysteine modifying reagent MTSET, did not show

any statistically significant changes in peak current amplitude or the extent of inactivation (Figures 33A-C).

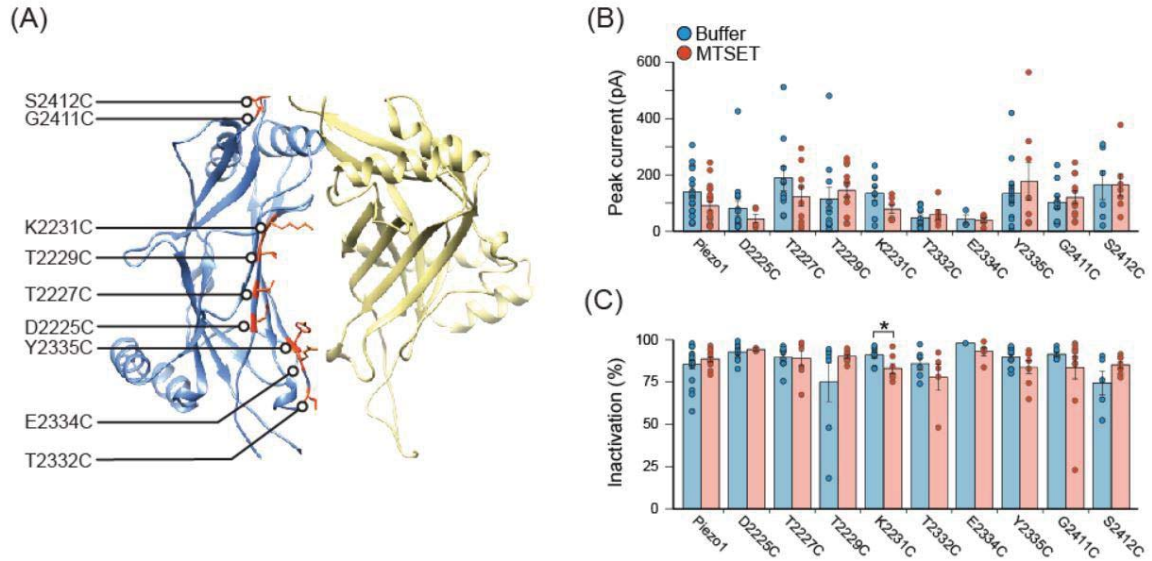


**Figure 33: Effects of MTSET modification in the CED. (A) Illustration of Piezo1 CED structure (only two subunits shown for clarity) with residues mutated individually to cysteines highlighted in red. (B) Individual and mean peak current amplitudes and (C) percent inactivation from cell-attached recordings of HEK293T-P1KO cells transiently transfected with Piezo1 cysteine mutants in 'A' stimulated with a -60 mmHg pressure stimulus (\*  $p \leq 0.05$ , unpaired Student's t-test). All data are mean  $\pm$  SEM. Data collected and analyzed with M. Young.**

In addition, several deletion constructs that we engineered to lack the CED had no mechanically activated currents (data not shown, see Methods for details). We examined one of these constructs (P2223-S2450delinsTG) further and found that it failed to locate to the plasma membrane, but had normal oligomerization as visualized by native gel electrophoresis (Figures 34A-B).

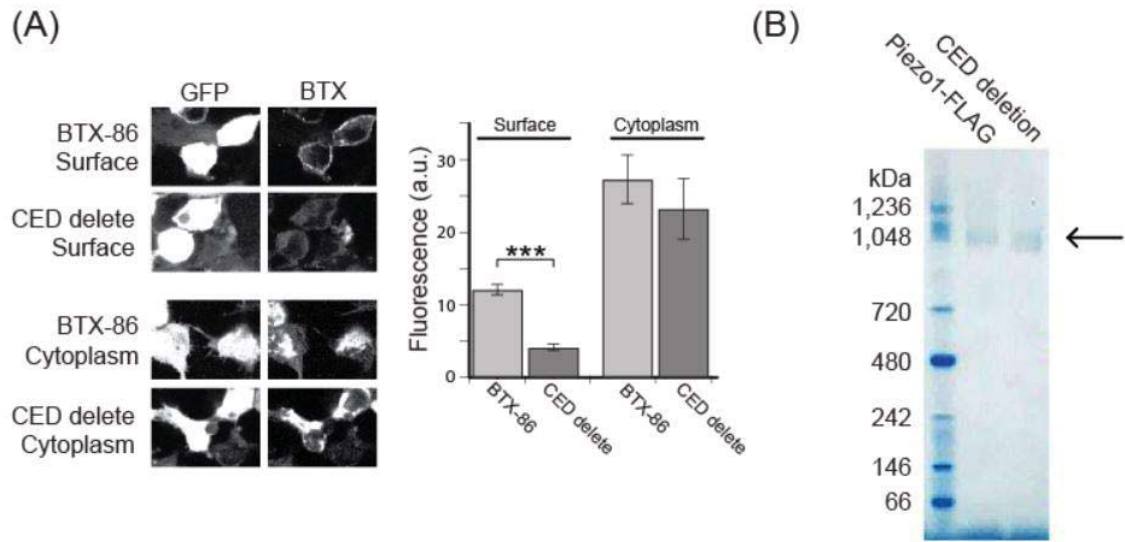


**Figure 34: Characterization of CED deletion.** (A) Representative images of HEK293T-P1KO cells transiently transfected with bungarotoxin-tagged Piezo1 (BTX-86) or CED deletion construct  $\Delta$ Q2222-D2451 (CED delete). GFP indicates transfected cells, BTX indicated labeling with  $\alpha$ -bungarotoxin conjugated with AlexaFluor 555 for surface labeling or AlexaFluor 647 for cytoplasmic labeling. Mean fluorescence intensity of  $\alpha$ -bungarotoxin on the plasma membrane surface or in the cytoplasm for indicated conditions (n = 18 cells, \*\*\* p  $\leq$  0.0005, unpaired Student's t-test). (B) FLAG-purified wild-type and CED deletion Piezo1 separated on a 3%-12% bis-tris non-denaturing gel and visualized by coomassie G-250 staining. Expected molecular weights of wild-type and CED delete Piezo1 are 876 kDa and 800 kDa, respectively (arrow). Error bars are SEM. Data collected by B. Kalmeta and A. Henderson.

These results suggest that the CED may be required for protein trafficking, but not assembly or stability, in addition to determining inactivation kinetics. Similarly, insertion of PreScission Protease sites into the highly conserved adjacent CED linker domains, with the goal of enzymatically cleaving the CED after initial membrane expression, also resulted in non-functional channels (data not shown, see Methods), altogether precluding a direct test for whether inactivation occurs in the absence of the CED.

### 3.5 A single lysine residue in the inner pore helix confers voltage dependence of inactivation to Piezo1

The amino acids giving rise to the effective charge we calculated to be associated with voltage dependent inactivation could be located within any of the 14-30 transmembrane domains, predicted from a structural model and hydrophathy profiles (Alper, 2017; Ge et al., 2015). However, due to our finding that the CED confers the distinct inactivation kinetics between Piezo1 and Piezo2, and that magnetic force application on the CED can directly slow inactivation, we focused our attention on the two transmembrane domains immediately connected to the CED known as the outer pore helix and the inner pore helix (Wu, Goyal, & Grandl, 2016). Specifically, we hypothesized that, similarly to magnetic force, Coulomb-forces generated by an electric potential on charged residues within these two helices may also influence inactivation kinetics (Figure 35).

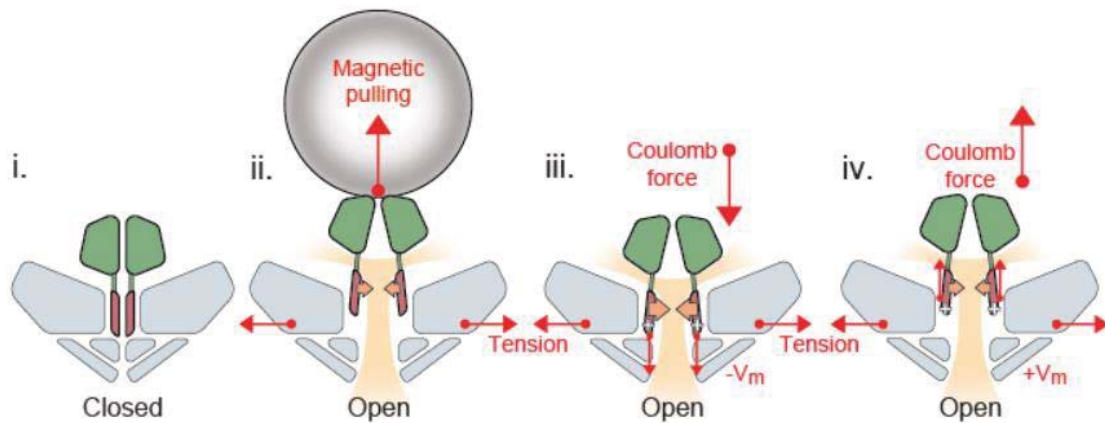
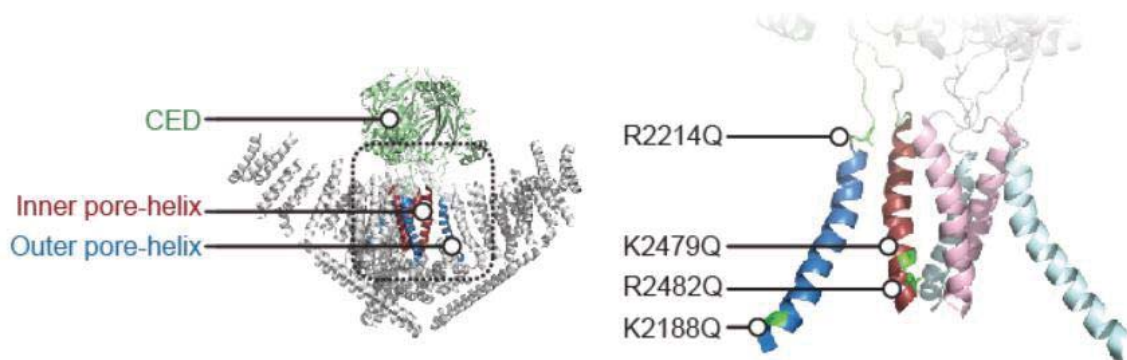


Figure 35: Schematic of open state modulation of inactivation. i) Piezo in closed state highlighting CED (green) and inner pore-helices (red). ii) Piezo in tension induced open state with CED under pulling force by magnetic bead. Orange arrows

represent force towards inactivation through pore helices. Movement of the CED away from the channel alters inactivation through interaction with the pore helices. Shaded yellow region depicts permeation pathways. iii) Piezo in tension induced open state at a negative holding potential. Larger orange arrows represent stronger force towards inactivation through pore helices. White plus signs represent positive charges within the pore helices. Coulombic force holds pore helices and adjacent CED in a fast inactivating state. iv) Piezo in tension induced open state held at a positive holding potential. Small orange arrows represent weaker force towards inactivation. Coulombic force induces displaced pore helices and CED similar to magnetic pulling to induce a slowly inactivating state.

To test this idea experimentally, we individually neutralized each of the four positively charged residues within these two helices by mutating them to glutamine (outer pore-helix: K2188Q, R2214Q; inner pore-helix: K2479Q, R2482Q), and measured how this affected the voltage dependence of inactivation (Figure 36).



**Figure 36: Charged residues in the pore helices. Illustrations of Piezo structure highlighting the CED (green), the inner pore-helix (red) and the outer pore-helix (blue) and four positively charged residues mutated to charge-neutral glutamines. Right panel is zoom in of boxed area shown on left depicting only pore helices.**

Strikingly, we found that neutralization of a single lysine (K2479Q) in the inner pore-helix resulted in consistent inactivation kinetics at all potentials between -100 and +100 mV ( $\tau = 5-9$  ms,  $n = 10$  cells) and calculation of the effective gating charge revealed that it

was virtually eliminated ( $z = 0.06 \pm 0.06 e$ ) (Figure 37). In contrast, the nearby mutation K2482Q caused a modest decrease in voltage dependence of the inactivation gating charge ( $z = 0.20 \pm 0.02 e$ ,  $n = 9$  cells). Channels with mutations K2188Q and R2214Q in the outer pore-helix exhibited inactivation kinetics and gating charges similar to that of wild-type Piezo1 (K2188Q:  $z = 0.26 \pm 0.03 e$ ,  $n = 8$  cells; R2214Q:  $z = 0.26 \pm 0.03 e$ ,  $n = 8$  cells) (Figure 37). This result shows that two charged residues in the lower part of the inner pore-helix of Piezo1 are important for the voltage dependence of inactivation, and in particular, that the single lysine residue K2479 is specifically required for it.

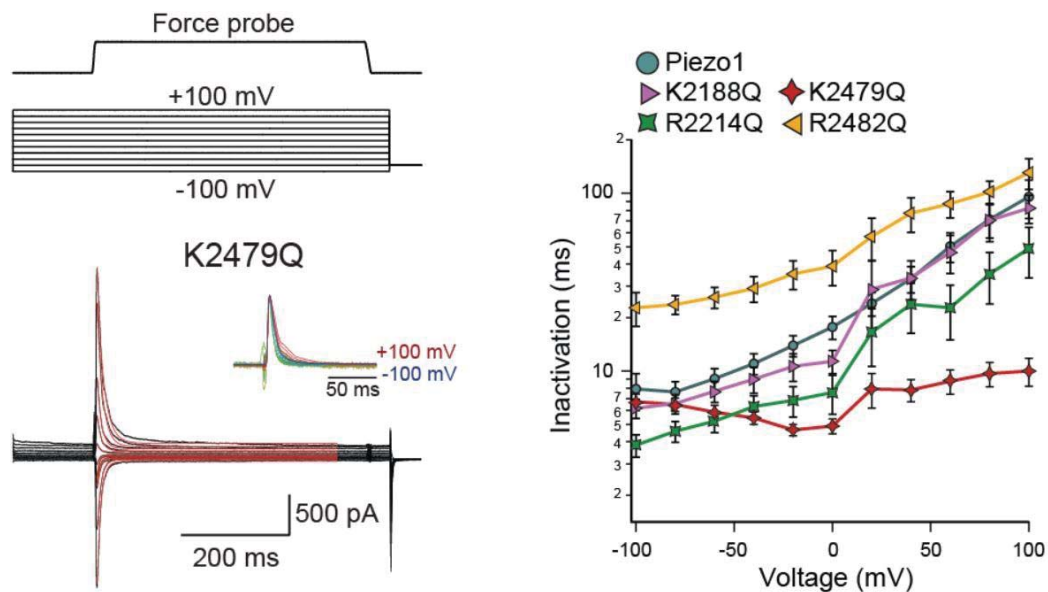


**Figure 37: Charge neutralization eliminates voltage dependency of inactivation. (Left) Force probe stimulus protocol and representative current trace of single point mutant K2479Q. Red lines are single exponential fits to the decaying currents. Insets show currents normalized to peak amplitudes. (Right) Mean inactivation time constants obtained from single exponential fits of force-probe induced current from whole-cell recordings of HEK293T-P1KO cells transiently transfected with wild-type Piezo1 ( $n = 13$  cells), and single-point mutants K2188Q ( $n =$**

8 cells), R2214Q (n = 8 cells), K2479Q (n = 10 cells), and R2482Q (n = 9 cells) as a function of membrane potential. Error bars are SEM.

We noticed that the charge neutralization of K2487Q resulted in inactivation kinetics similar to kinetics observed in wild-type Piezo1 at very negative voltages, i.e. -100mV. We next tested the effect of a charge reversal mutation on that same residue, K2479E. Interestingly, we found that this mutation not only ablates voltage dependence of inactivation similarly to K2479Q, but that it also sets inactivation kinetics to values similar those observed in wild-type Piezo1 at strongly positive potentials ( $\tau = 31\text{-}70$  ms between -100 and +100 mV, gating charge  $z = 0.06 \pm 0.06$  e, n = 8 cells) (Figure 38). This result supports the notion that voltage controls inactivation kinetics over a wide range, specifically through Coulomb-forces acting on the inner pore-helix.

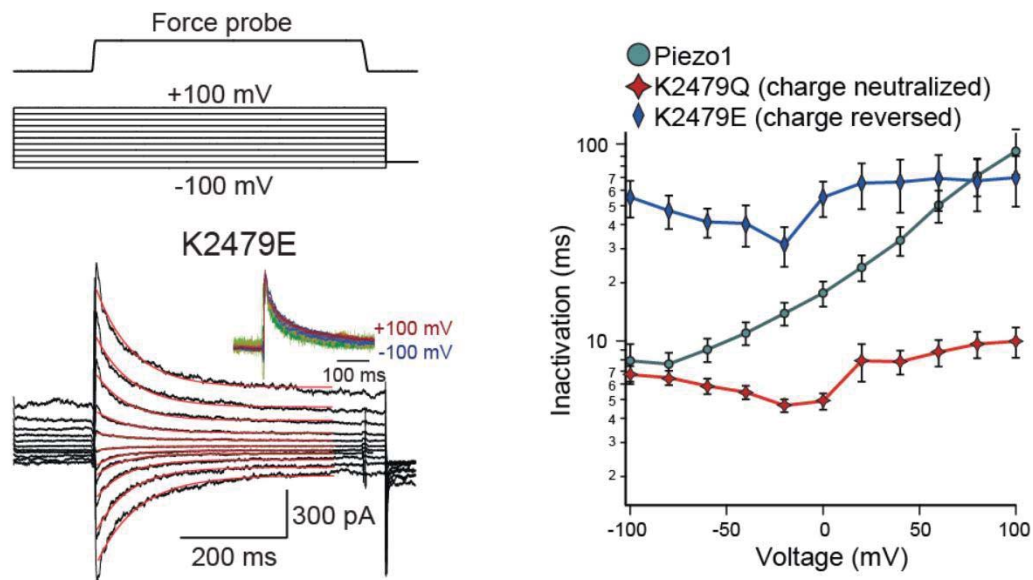


**Figure 38: Charge reversal clamps inactivation kinetics at slower values. Effects of charge reversal on inactivation. (Left) Force probe stimulus protocol and representative current trace of single point mutant K2479E. Red lines are single**

exponential fits to the decaying currents. Insets show currents normalized to peak amplitudes. (Right) Mean inactivation time constants from single exponential fits of current from whole cell recordings in HEK293T-P1KO cells transiently transfected with wild-type Piezo1 (n = 13 cells), and single-point mutants K2479Q (n = 10 cells), and K2479E (n = 8 cells) as a function of membrane potential. Error bars are SEM.

### ***3.6 MTSET accessibility to inner pore helix residue V2467 is voltage dependent***

The above results suggested to us that a conformational change within the inner pore helix, whether induced by magnetic force or by Coulomb force, might be a mechanism for determining inactivation kinetics in Piezo1. We therefore aimed next to directly test for such a voltage dependent conformational change. For this, we selected five residues in the upper part of the inner pore helix based on their predicted orientation with respect to the permeation pathway, mutated them individually to cysteines (F2460C, G2463C, Y2464C, V2467C, and G2468C) and probed for their accessibility to the extracellular solvent with the cysteine-modifying reagent MTSET in cell-attached recordings using pressure-clamp stimulation (Figure 39A).

We designed a first protocol, where we clamped cells at a constant potential of -80 mV for 120 s to allow for cysteine modification by 2 mM MTSET at negative potentials, followed by testing channel function with a standard pressure-step protocol (5 s prepulse of + 5 mmHg, followed by 200 ms steps from 0 mmHg to -70 mmHg) (Figure 39B). Identical experiments without MTSET in the buffer served as control.

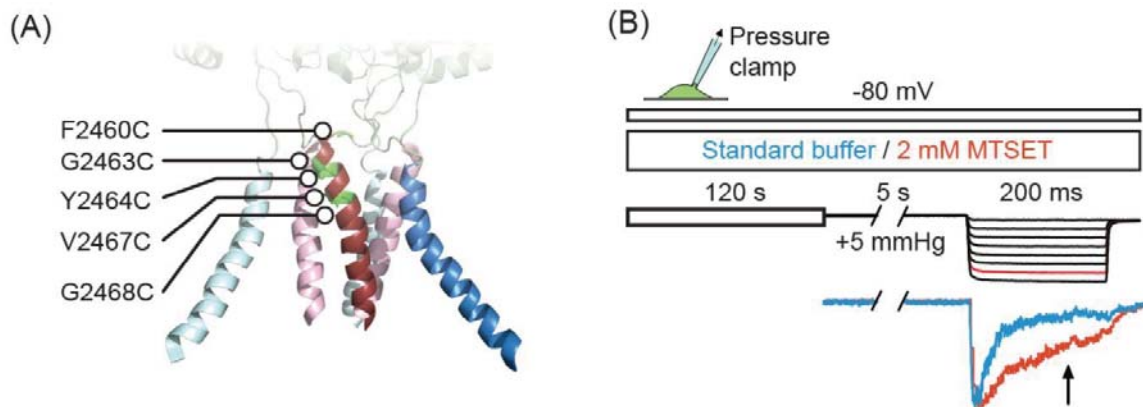


**Figure 39: Experimental setup for MTSET modification of inner pore helix. (A) Illustration of Piezo1 pore structure highlighting the outer pore helices (blue), inner pore helices (red), and five residues mutated individually to cysteines for MTSET accessibility experiments. (B) Pressure clamp stimulation and MTSET labeling protocol. Cells were held at a constant potential of -80mV, while allowing for 2 min incubation with standard buffer or 2mM MTSET before testing mechanical activation by a pressure-step protocol (5 s, +5 mmHg prepulse, followed by 200 ms pressure steps from 0 to -70 mmHg). Representative current traces from cell-attached patches of HEK293T-P1KO cells transiently transfected with cysteine point mutant V2467C at the -60 mmHg stimulus step with standard buffer (blue) or MTSET (red).**

Mechanically activated peak current amplitudes at -60 mmHg varied amongst constructs and for G2468C, were too small (< 30 pA) to reliably quantify the degree of inactivation, so that it was excluded from further analysis (Figure 40A). Interestingly, the degree of inactivation for construct V2467C was markedly affected by MTSET application ( $40.4 \pm 8.4\%$  with 2mM MTSET vs.  $68.6 \pm 3.3\%$  with buffer alone), whereas inactivation was not significantly changed for constructs F2460C, G2463C, and Y2464C, nor for wild-type Piezo1 (Figure 40B). Importantly, when we repeated this experiment at a 10-fold lower concentration of MTSET, the extent of inactivation for construct V2467C

was reversed to levels observed with buffer alone ( $69.6 \pm 4.7\%$  with  $200 \mu\text{M}$  MTSET,  $n = 6$  cells) (Figure 40C).

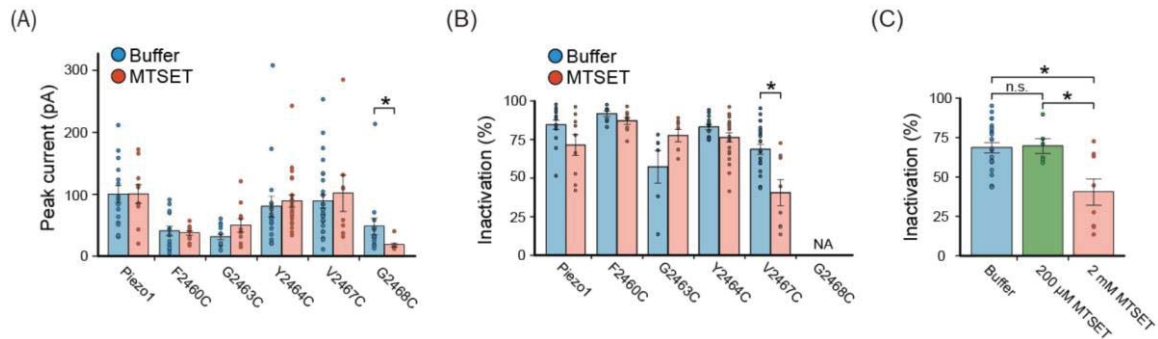


**Figure 40: Effect of MTSET modification on inner pore helix. (A) Mean peak currents and (B) mean degree of inactivation of currents from cells stimulated with protocol in 'B' upon application of 2 mM MTSET or buffer alone ( $n = 8 - 27$  cells,  $* p \leq 0.05$ , unpaired Student's  $t$ -test; NA, omitted from analysis). (C) Degree of inactivation for currents recorded from HEK293T-P1KO cells transiently transfected with cysteine point mutant V2467C stimulated by protocol in 'B' in the presence of standard buffer ( $n = 20$  cells),  $200 \mu\text{M}$  MTSET ( $n = 6$  cells), and 2 mM MTSET ( $n = 8$  cells) (n.s., no significance,  $p \geq 0.05$ ,  $* p \leq 0.05$ , unpaired Student's  $t$ -test). Error bars are SEM. Data collected and analyzed with M. Young.**

We concluded that residue V2467 can be modified by high concentration and long exposure of MTSET and asked next if its accessibility was dependent on voltage, which could be driven by a voltage-induced conformational change of the inner pore helix. To test this, we designed a second protocol, where two test pulses (5 s prepulse at +5mmHg, followed by 200 ms steps to -60 mmHg held at -80 mV) framed a 5 minute period of incubation with 2 mM MTSET or buffer alone as control, with the membrane potential during the incubation period held either at -80 mV or +60 mV (Figure 41A).

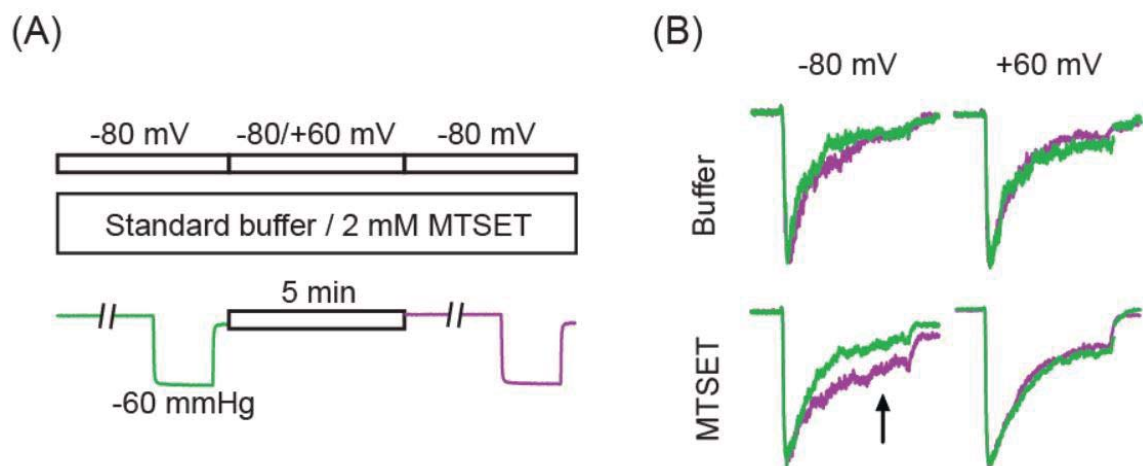


**Figure 41: Testing the voltage dependency of MTSET modification. (A) Pressure-clamp stimulation and MTSET labeling protocol. Cells were recorded either in standard buffer or 2 mM MTSET by first stimulating with a -60 mmHg pressure stimulus, allowing for MTSET labeling for 5 min at a holding potential of either -80 mV or +60 mV, and immediately following with a second -60 mmHg pressure stimulus. (B) Representative current traces from cell-attached patches of HEK293T-P1KO cells transiently transfected with cysteine point mutant V2467C depicting the first pulse (green) and second pulse (magenta) under indicated MTSET labeling conditions. Data collected and analyzed with M. Young.**

Peak current amplitudes of construct V2467 were not affected by voltage during labeling with MTSET (Figure 42A). Consistent with our previous finding, when applied during a negative holding potential, MTSET reduced the degree of inactivation ( $56.5 \pm 3.6\%$  after MTSET labeling,  $69.3 \pm 3.7\%$  before MTSET labeling). Strikingly, MTSET failed to induce such an effect on construct V2467 at positive holding potential during the incubation time, as the degree of inactivation was unchanged under this condition ( $65.7 \pm 2.7\%$  after MTSET labeling,  $66.7 \pm 2.6\%$  before MTSET labeling) (Figures 41B and 42B). Altogether, these data suggest that residue V2467 in the upper part of the inner pore helix is accessible to MTSET specifically at negative potentials, but not at positive potentials.

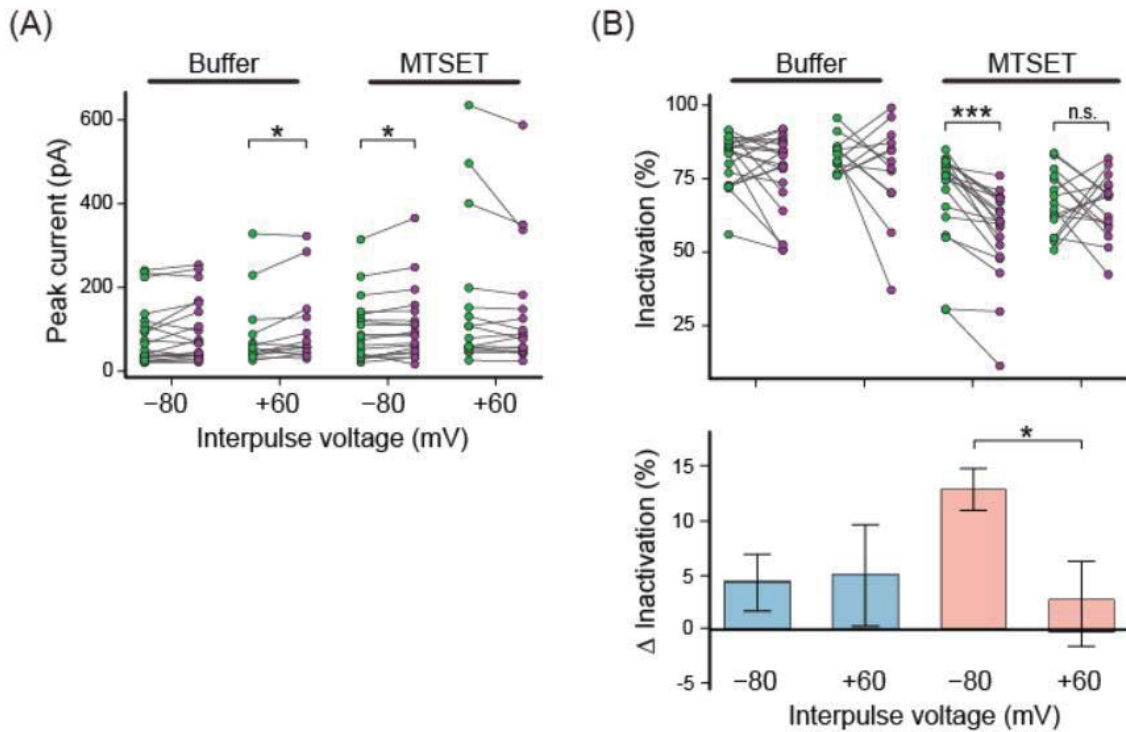


**Figure 42: MTSET modification of inactivation is voltage dependent. (A)** Individual peak currents from recordings with two pulse stimulation protocol of mutant V2467C with indicated MTSET labeling conditions (n = 13 – 20 cells, \*  $p \leq 0.05$ , paired Student's t-test). **(B)** Individual measures of degree of inactivation (top) and mean change in inactivation (below) for recordings of mutant V2467C from 'A' (n.s., no significance,  $p \geq 0.05$ , \*\*\*  $p \leq 0.0005$ , paired Student's t-test; \*  $p \leq 0.05$  unpaired Student's t-test). Error bars are SEM. Data collected and analyzed with M. Young.

### 3.7 Discussion

The mechanisms for inactivation and desensitization are very well understood for virtually all major ion channel families, which has provided a handle to manipulate countless biological processes. Our long term goal is to achieve the same depth of understanding for Piezo ion channels, and the first step towards it must be the identification of structures important for inactivation.

We combined previous observations and novel detailed analysis of Piezo1 function to narrow down and ultimately identify structural correlates of inactivation and its voltage dependence. The two pertinent structures we identified are located proximal to the ion permeation pathway and within the pore itself, bringing to mind known mechanisms for inactivation in other ion channels where inactivation is mediated by direct interactions with or conformational changes of the pore domain.

For example, N-type inactivation, otherwise known as the ‘ball-and-chain’ mechanism, has been most prominently studied in Kv and Nav channels and is described whereby an inactivation domain obstructs the pore and thus blocks ion permeation (Goldin, 2003; Hoshi et al., 1991). The facts that the CED domain is a globular structure, is located at the entry to the ion permeation pathway, and confers the characteristic time course of inactivation between Piezo1 and Piezo2 certainly resonates with an N-type mechanism. However, in our hands Piezo1 was not amenable to the most stringent test of an N-type mechanism, which is the removal and restoration of the inactivation particle leading to a complete loss and rescue of inactivation, respectively. The CED likely provides other functionalities to Piezo1 as well, and our results that CED deletion constructs are non-functional and that at least one of them fails to target to the membrane support this possibility. In addition, the cryo-EM structural analysis of Piezo1 did not capture the CED in any obviously pore-blocking positions, calling into question whether this distinct and unusual structural fold can act as a blocking particle.

Certainly, our chimeric constructs suggest that the CED can at least allosterically modulate inactivation kinetics.

Another prominent mechanism for channel inactivation is C-type inactivation, which involves structural changes within and around the selectivity filter and the pore entrance (Kurata & Fedida, 2006). The residues we identify to be important for voltage dependence of inactivation are also located within the pore and in tertiary structure, proximal to a residue that influences unitary conductance and reversal potential (E2133), (Coste et al., 2015). By neutralizing or reversing the charge of the residue K2479 in the inner pore helix, we were able to abolish voltage sensitivity of inactivation and set inactivation times at different values, suggesting that we have biased the channel towards distinct conformational states that transition to the inactivated state with different lifetimes. In addition, we find that MTSET has restricted access to residue V2467C, which is located in the upper pore domain, specifically at positive holding potentials. This specific result could be a consequence of electrostatic repulsion of MTSET from the membrane potential or alternatively from structural changes within the pore, the latter of which would be characteristic of a C-type mechanism. On the contrary, we do not find a strong dependence of inactivation on ion occupancy, another hallmark of C-type inactivation. Clearly, the exact conformational changes that occur in the pore helix remain to be studied in greater detail.

The mechanism of inactivation in Piezos may involve aspects from both N-type and C-type as well as novel forms of inactivation. Previously we have shown that Piezo1 can adopt two inactivated states that are kinetically distinct, raising the intriguing possibility that Piezos possess two inactivation mechanisms, perhaps mediated through distinct structures (Lewis et al., 2017).

Such a dual mechanism would not be unprecedented as Shaker channels are known to undergo both N-type and C-type inactivation (Hoshi et al., 1991). It is striking however that in a mechanically activated ion channel, mechanical energy provided by membrane tension does not seem to influence the mechanism of inactivation. This result directly argues that mechanical activation and voltage-dependent inactivation are mechanistically and perhaps also structurally distinct.

Alternatively, it also seems possible that the CED and inner pore helix may act in conjunction to mediate one common mechanism of inactivation. While we provide some evidence that the CED may not form part of the permeation pathway itself, we can speculate that highly conserved linkers may provide allosteric coupling to the pore helices, which in turn promote structural restriction of the permeation pathway.

Finally, perhaps endogenous modulators of inactivation, such as pH, affect inactivation by acting on either the CED or pore helices. Our results provide rationale for future studies to test whether the CED can be efficiently targeted by small molecules

to change overall channel function and mechanotransduction, ultimately having clear implications in addressing disease related mutations of Piezo.

## **4. Concluding Remarks and Future Directions**

### ***4.1 Major results and interpretations***

In this dissertation, I aimed to study the molecular mechanisms of mechanosensing in Piezo ion channels. Piezos are modulated by a broad collection of different molecular and physical mediators, and they respond to various modes and magnitudes of physical force within the contexts of the many organ systems where they are found (Wu, Lewis, & Grandl, 2017). Along with their unusually large structure and lack of sequence homology or structural similarity to other channels, these characteristics make understanding the mechanosensing mechanism of Piezos a remarkably complex question. One of the first steps to addressing this question is to identify the relevant structural domains within the protein that correspond to channel function. For this aim, I developed a semi-unbiased screen to mechanically stimulate distinct protein domains and tested how such perturbation affected mechanosensitivity. Next, I used molecular cloning strategies to test how precise alterations to those domains affected specific channel functions. Finally, I combined what we had learned about mechanosensitive structures and how they affect channel properties in response to stimulus to make and test hypotheses about how these domains move and mediate a mechanosensing mechanism.

### **4.1.1 Identification of mechanosensitive domains**

In Chapter 2, I developed a method to attach magnetic nanoparticles to different extracellular domains of Piezo1 in order to physically pull on those domains with a magnetic field and record how this affected mechanosensitivity of the channel. Initially, we had expected that pulling on a 'mechanosensor' would itself be sufficient to induce channel opening. However instead, we observed an unexpected result in which pulling on certain domains induced a dramatic slowing of inactivation, while none of the tested domains caused acute activation when pulled with a magnetic field. Regarding channel activation, a number of possibilities could explain why we were unable to directly activate the channel. 1. Mechanosensing might not be mediated by a single domain, and multiple domains or the entire protein may be needed to act in unison for mechanical activation. 2. The mechanosensing domain may be intracellular or in another region inaccessible to nanoparticle labeling. 3. The force with which we pulled was not sufficient for activation. 4. The direction of pulling was not optimal for perturbing a mechanosensor in a way similar to its natural movement 5. The geometries of nanoparticle labeling may have only allowed one subunit out of a trimer to be labeled, or all three subunits in a channel may have been labeled by the same nanoparticle which could have prevented an optimal activating condition.

The two domains we identified to affect inactivation were the peripheral blade domains and the CED. While we did observe a modest change in activation kinetics

when the CED was pulled, the most noticeable change was in the kinetics of inactivation, and this effect was more prominent for the CED than compared to the blade domains. Both activation and inactivation are critical channel functions that both contribute to the channel's overall mechanosensitivity. In Chapter 3, we demonstrate that the kinetics of inactivation are not directly dependent on membrane tension and therefore not inherently mechanosensitive. However, the properties of inactivation and the transition of Piezo1 into an inactivated state both affect subsequent response to mechanical stimulus (Lewis et al., 2017). With this result implicating the CED in inactivation, we thus turned our attention to understanding the mechanism of inactivation. The specific role of the blade domains was not further investigated in this dissertation due to the fact that the available structural model had not been resolved to a high enough resolution to map specific residues onto the blades.

#### **4.1.2 Structure-function relationships of the CED and inner pore helix**

The CED is immediately flanked by the highly conserved pore helices, and therefore it seemed possible that pulling on the CED with a magnetic field may have pulled on the pore helices as well, making both of these domains candidates for structural correlates of inactivation. In Chapter 3, I investigated the specific role of the CED and pore helices in inactivation. With the hypothesis that the CED mediated the kinetics of inactivation, I made chimeric constructs to interchange the CED of Piezo1 and Piezo2 and found that the chimeric channels took on the inactivation kinetics of the CED

origin. In the previous study, Piezo2 was not tested due to its unreliable response to pressure clamp stimulation. This experiment however was performed with force probe stimulation and revealed not only that the CED was able to confer the kinetics of inactivation, but that this property was conserved between the two mammalian homologs as well.

Chimeric constructs were not made to investigate the pore helices because Piezo1 and Piezo2 share almost identical sequence homology for these regions (Figure 43). Therefore I decided to investigate a specific property of inactivation that is found in both homologs- voltage dependency. The kinetics of inactivation for both Piezo1 and Piezo2 become slower as the membrane voltage becomes more depolarized, in a continuous but non-linear manner. In Chapter 3 I identified one positively charged residue in the inner pore helix that when neutralized, completely abolished this voltage dependency for Piezo1 and clamped inactivation kinetics to that observed at very negative voltages for wild-type channels. In contrast, reversing the charge of this residue clamped its inactivation kinetics to that observed at very positive voltages for wild-type channels. These results imply that the dynamics of the inner pore helix govern the kinetics of inactivation in a voltage dependent manner.



that effects on voltage dependency in Piezo2 may be masked by the margin of error. An adjacent charged residue in the inner pore helix of Piezo1 also had some attenuating effect on the voltage dependency of inactivation, though not as strongly, and future studies will need to test whether this same experiment yields a similar effect in Piezo2. Future studies will also be necessary to understand how charged residues influence voltage dependency on a mechanistic level.

#### **4.1.3 Hypotheses for the mechanism of Piezo inactivation**

In the second half of Chapter 3, we investigated the hypothesis that voltage induces a conformational change in the inner pore helix that leads to inactivation. In the context of a canonical voltage sensor, a transmembrane charge will translocate within the membrane in response to the electrostatic forces of membrane depolarization (Long et al., 2005). To test whether this occurred in Piezo1, we mutated residues near the membrane interface of the inner pore helix to cysteine, with the reasoning that these residues were most likely to change in solvent accessibility as a result of conformational changes of the pore helix. We identified one residue that was strongly modified by the covalent binding of the cysteine modifier MTSET at a negative voltage, and this effect was not observed at a positive voltage. This was evidence that the inner pore helix changes in conformation as a result to voltage.

There is however a disconnect with the model of a canonical voltage sensor. If depolarization causes positively charged residues to translocate in the membrane

towards the extracellular side, then we would have expected to see increased solvent accessibility at positive voltages and less at negative voltages. Although our results are opposing this expectation, it is still possible that a different conformational change such as a rotation of a helix could bury a residue upon depolarization. Alternatively, another group has proposed a mechanism for non-canonical voltage sensing in K2P channels that is mediated by the movement of ions in the selectivity filter (Schewe et al., 2016). It is certainly possible that charged residues within the inner pore helix influence ion permeation and selectivity, and voltage dependent inactivation is mediated through a non-canonical mechanism instead. Future studies will be necessary to test whether the pore helix charge corresponds with conformation change of the pore helix or if voltage dependent inactivation is dependent on ion permeation or selectivity instead.

In Chapter 3 we also demonstrate that the CED itself probably does not act as part of the permeation pathway, which prompts the question- How does the CED mediate the time course of inactivation? The CED and inner pore helix are connected in sequence through a short linker sequence of only 8-10 amino acids (Figure 43), so the two structural domains are likely tightly coupled. One possibility for the CED mechanism could be determined by the affinity at which CED subunits interact. As the CED is pulled apart during tension mediated channel opening, the strength of this affinity determines the rate at which it reassembles, and allosteric coupling to the pore domain transfer this rate to pore closure. The strength of this affinity may then differ

depending on the specific sequence characteristics of Piezo1 versus Piezo2 or other orthologs and mutants. In the same mechanism, as voltage changes the conformation of the inner pore helices, allosteric coupling to the CED may change the nature of intersubunit interactions and thus modulate inactivation in a voltage dependent manner. Further experiments including chimeras of subdomains within the CED, investigation of the strength of allosteric coupling, and structural models capturing different conformations between Piezo variants and states will be necessary to test these hypotheses.

## ***4.2 Potentials for Piezo in tool development***

### **4.2.1 The advent of magnetogenetics**

Ion channels are frequently employed as research tools in neuroscience and chemical biology (Mayer & Yang, 2013). Perhaps the most notable example is the tool of optogenetics, in which electrical activity of cells and downstream processes are controlled through the activation of genetically encoded light-gated ion channels (Deisseroth, 2015). In our development of the magnetic pulling assay in Chapter 2, one of our initial expectations was that directly perturbing a mechanosensing domain of a mechanically activated ion channel would be sufficient to activate the ion channel. This result would have introduced a new experimental method to remotely activate cells with a magnetic force, a concept which has since been referred to as ‘magnetogenetics’.

Magnetogenetics has several distinct advantages over existing methods such as optogenetics. A magnetic field can remotely penetrate deep into organic tissue, obviating the need for intrusive optic fibers implanted directly into the studied tissue as needed for optogenetics. Additionally, a magnetic field can be precisely targeted and tuned in strength, and it can achieve uniform stimulation for all cells in the targeted area, whereas light based methods are limited by the diffusion of light through tissue and the decrease in signal further away from the light source. Finally, magnetic nanoparticles could be conjugated with peptides made to recognize specific protein epitopes, thus making it unnecessary for costly and time consuming genetic intervention through mice models or viral transfection.

In the past several years a handful of groups have taken on the task of engineering a magnetically activated ion channel. In 2010, one group used magnetic nanoparticles targeted to the cell membrane to activate the temperature activated channel TRPV1 through radio-frequency magnetic field heating, which was shown to induce action potential firing and behavioral effects in *C. elegans* (Huang et al., 2010). A similar study activated exogenously expressed TRPV1 with magnetic field-induced hysteresis of injected magnetic nanoparticles, leading to neuronal excitation in mice (Chen et al., 2015). Both of these studies require the injection of nanoparticles and channel activation through nanoparticle heating. Two other groups developed techniques to fuse endogenously expressed ferritin particles to ion channels and activate

channels with mechanical force. In one study, endogenous ferritin particles were engineered to bind to TRPV1, and magnetic stimulation of this pairing expressed in mesenchymal stem cells induced channel activity and calcium-dependent insulin transgene expression (Stanley et al., 2014). Most recently, a separate group fused endogenous ferritin particles to the mechanically sensitive channel TRPV4 and with magnetic stimulation were able to elicit neuronal activity in freely behaving mice (Wheeler et al., 2016). While these are prominent and important studies in the development of magnetogenetics, they have been met with skepticism as calculations of the amount of temperature or mechanical force generated by magnetic nanoparticles under these stimulations differs from that needed to activate a channel by up to 10 orders of magnitude (Meister, 2016). Therefore a clear mechanism for how magnetic force activates ion channels in these studies is still missing.

#### **4.2.2 Directions for Piezo and ion channels in magnetogenetics**

While in our work, we did not directly activate Piezo channels, it remains possible that finer understanding of the mechanisms for activation in Piezo channels may provide more insight as to how to make this possibility a reality. Our results provide some evidence that Piezo channels may be a good candidate for the development of this technique: First, we show that Piezos have numerous structural domains that can be genetically modified with minimal or no impact on basal channel function. Second, as a mechanically activated channel, Piezo is more likely to be

sensitive to the mechanical forces that are imposed by a magnetic field on conjugated magnetic nanoparticles. Finally, in our study we show that pulling on attached magnetic nanoparticles with a magnetic field can already alter another function in Piezo1. Together these data support the notion that Piezo ion channels may be prime candidates for tools in the development of magnetogenetics.

One advantage to the technique that we have developed is that the nanoparticles we use, which are ~75 nm in diameter, are much larger in volume than particles used in the above studies which are ~10 nm in diameter. Because the force a magnetic field imposes on an object scales with the volume of that object, we have reached a range of force that is on the same order of magnitude experienced by molecules in a cellular environment. This gives us the ability to apply a defined amount of force on a molecule, and with an understanding of how much force is necessary to activate an ion channel, we should be able to generate a magnetically activated channel.

In preliminary experiments, we have selected a small library of candidate channels that have more established activation mechanisms to conjugate with nanoparticles and stimulate with a magnetic field (Appendix Table 4). In line with the reasoning that a mechanically activated channel may be optimal for a magnetogenetic application, we first selected smaller, better understood mechanochannels to test. Bungarotoxin binding sites (BBS) were cloned into the extracellular loops of MscL, TREK1, and TRAAK and tested for labeling specificity by  $\alpha$ -bungarotoxin as well as for

functionality by pressure clamp stimulation. However, the relatively short length of these channels made it difficult to insert binding sites without disrupting channel function, as several were either non-functional or poorly labeled. Select constructs remain to be tested thoroughly, and may be promising candidates for following experiments with magnetic field stimulation.

In Chapter 2, we introduced a non-functional Kir channel, and in fact multiple attempts were made to insert a BBS into this channel, but none yielded functional constructs. We also presented the same experiment for Kv1.2, and while two constructs were both accessible by nanoparticle labeling and functional, neither was directly activated by a magnetic field. One potential explanation for why this was unsuccessful was that it was likely that only one subunit out of the tetramer was bound to the nanoparticle and mechanically perturbed; perhaps all four subunits needed to be manipulated simultaneously in order to induce channel opening. To address this, we obtained a concatemeric Shaker construct in which three of the subunits were mutated to be in a constitutively active state with one remaining in the inactive state (Gagnon & Bezanilla, 2009). We inserted a binding site in two extracellular loops that made up the voltage sensing domain of the inactive subunit with the hopes that pulling on only this one subunit with a magnetic field would be sufficient to activate the channel. However, like previously tested channels, these constructs were not accessible to bungarotoxin labeling.

With the thought in mind that subunit cooperativity was a necessary aspect of channel activation, we selected the Nav1.2 channel to test with this experiment. Na<sup>+</sup> channels are known for having an inactivation domain in the DIV-S4 structural domain, where it is involved in voltage modulation of the blocking particle binding site (Raman & Bean, 2001). Considering this subunit specificity of function, we inserted a BBS into the extracellular loop adjacent to this site to test whether a local pulling force by a magnetic field could affect inactivation (or attenuate activation). Once again, these constructs were inaccessible by bungarotoxin labeling. The Cav1.2 channel which shares a similar topology with Na<sup>+</sup> channels, was already available with a BBS inserted as presented by the Colecraft lab, however further optimization with the co-expression of  $\beta$ -subunits is necessary to achieve sufficient membrane expression (Subramanyam et al., 2013).

Finally, we have also inserted a BBS into *Drosophila* Piezo, which has yet to be characterized, as well as Piezo2 which remains to be tested under a different stimulation protocol due to its unresponsiveness to pressure clamp stimulation. Clearly, many more channels remain as potential candidates and future studies will perhaps reveal one that is ideal for the application of magnetogenetics.

Another possible avenue with which to continue towards the aim of activating Piezos with a magnetic force is to consider whether the precise direction of force can be controlled to optimize activation. In preliminary experiments I have constructed an

apparatus to impose magnetic torque on a magnetic nanoparticle bound to Piezo. In this apparatus, two permanent neodymium magnets are arranged in parallel and attached to a rotating motor. The axis of rotation is centered on the coverslip with Piezo expressing cells, and the speed and direction of rotation can be controlled directly through an amplifier. In theory, this is one method in which a specific direction of force stimulus can be applied. However, by measuring Piezo activity through calcium imaging, this technique was still insufficient to induce Piezo activation. Numerous other geometrical configurations can and should be tested to achieve this aim, but a thorough understanding of the activating mechanism of Piezo will be a critical piece of information in expediting this effort.

### ***4.3 The question of Piezo activation***

The results of this dissertation provide significant insight into the structural correlates and mechanisms for Piezo inactivation, however it remains to be seen what structural features are involved in transducing membrane tension into channel opening for activation. In Chapter 1, various potential models for Piezo channel activation were proposed, falling into the broad categories of the 'bilayer model' and 'tether model'. A number of experiments are possible to more precisely test these models.

#### **4.3.1 Activation through the tether model**

In Chapter 2, our unbiased assay to physically pull on different extracellular domains was a first test of whether the tether model could be a plausible mechanism.

Because we did not see any channel activation from this assay, in addition to the fact that Piezos can be reliably activated in systems devoid of an extracellular matrix, it seems unlikely that Piezo is gated through extracellular tethers. However we did not test the possibility of intracellular tethers, so it remains possible that cytoskeletal attachments are responsible for gating Piezo channels. Once again, studies have shown that Piezo1 can be activated in artificial bilayers devoid of cytoskeleton, suggesting that this may not be a plausible mechanism (Syeda et al., 2016). However under these systems, Piezo1 at least is not activated by pressure clamp stimulation which is a reliable method for activation when expressed in live cells (Coste et al., 2012). One of the first steps towards further testing this mechanism will be to study molecular interactions between Piezo1 (and Piezo2) and cytoskeletal elements in different cell types to see whether this interaction is possible under various conditions. This hypothesis may also be indirectly tested by using high resolution microscopy to find patterns of interactions between Piezos and the cytoskeleton. Ultimately, to prove that Piezo activates with this mechanism, a method must be developed to activate Piezo through a tether in the absence of membrane tension.

#### **4.3.2 Activation through the bilayer model**

Because Piezos are directly gated by membrane tension, it seems likely that some variant of the bilayer model may be at play (Lewis et al., 2017). As introduced in Chapter 1, the bilayer model describes the process by which lateral membrane tension causes

hydrophobic mismatch of protein structures buried in the cell membrane, and as these structures shift back into energetically favorable positions, allosteric coupling transitions the channel into an open state. One study demonstrated that introducing hydrophobic mismatch by changing the length of the lipid hydrocarbon chains in the bilayer could change the gating energy of MscL (Perozo et al., 2002). It would be interesting to perform this experiment for Piezo channels to test if they are likewise sensitive to hydrophobic mismatch. In a separate study, authors demonstrate the TREK1 is sensitive to membrane curvature, as bilayer crenators activate the channel and cup formers inhibit it (Anishkin et al., 2014). These agents introduce local curvatures throughout the membrane, generating microdomains in which Piezos would encounter hydrophobic mismatch. Therefore altering Piezo activity with the introduction of curvature inducing lipids such as crenators and cup formers and other amphipathic molecules would also be evidence in support of a bilayer model mechanism. It would also be interesting to investigate whether Piezos have any pattern of localization in regard to lipid rafts, which are tightly packed domains in the membrane made of cholesterol and glycolipids, to test whether and how lipid concentrations and species influence Piezo activation. All of these directions would provide evidence to help prove or disprove an activation mechanism by hydrophobic mismatch.

One interesting feature in the structural model of Piezo1 is the blade domain that, in a trimeric complex, forms the periphery of the channel (Ge et al., 2015). The

blade domains are a unique structures making up more than 70% of the entire channel architecture, yet it is still unclear what the precise function is of these domains.

Although this domain is not resolved to a resolution where we can be certain of its precise architecture, preliminary observations suggest the blades confer a particular conformation that does not rest in a flat plane. This raises the possibility that either the channel is at rest in a structurally curved architecture, or that it can take on this conformation under some stimulus, both implying that the channel is sensitive to membrane geometry through its blade structures. In order to test whether this can be an activating stimulus, future studies will be necessary to precisely measure how a resting and active channel is situated within a lipid membrane, perhaps by purification and cryo-EM in different lipid contexts.

One might also hypothesize that the blade domains confer tension to the channel not through inducing local curvature, but by securing the channel in an optimal position to sense membrane stretch. The large size of the blades may provide a maximal surface area contact with the lipid bilayer and thus allow them to be highly sensitive to smaller changes in membrane tension. Older Piezo channels found in unicellular organisms however, have shorter sequences than their vertebrate orthologs, implying that a large blade domain might not be essential for tension sensing (Prole & Taylor, 2013). Granted, these channels have not yet been functionally characterized. Nevertheless, it seems unlikely that such a large protein domain would have persisted through evolution if it

did not offer an indispensable function. It will be of great interest to measure the mechanosensitivity of protozoan Piezo channels and observe if these differ from those in vertebrates. Additionally, either truncation of the vertebrate blades or chimeric constructs interchanging the blade domains between vertebrates and protozoa will also be useful in understanding their function and whether there is an advantage for sensing tension over a larger area. Higher resolution of structural models will again be necessary to fully understand the organization and interactions of the transmembrane domains that make up the blades, and these potential experiments combined with alterations in lipid compositions may be telling of how the blade domains respond to hydrophobic mismatch.

#### **4.3.3 Transduction of tension sensing to pore opening**

Finally, the question remains of how tension sensing is translated to pore opening. Unlike MscL channels which have two transmembrane domains and TREK1 channels that have four, Piezos have more than fourteen, suggesting that the transduction mechanism between tension sensing and pore opening may involve more complex allosteric interactions. In the current cryo-EM model, one interesting structure that stands out in the context of allosteric connections between the pore and the rest of the channel body is the 'beam'. The beam is a coiled coil domain that spans the intracellular surface of the channel from the inner region of the pore module to the peripheral transmembrane helices (Ge et al., 2015). It seems possible that this may serve

as a form of allosteric linker that allows tension-induced changes in the blades to be transduced to the pore for activation. Because this domain is not resolved enough to assign amino acid residues, it is difficult to confirm what domains it is connecting, if any. It remains to be seen whether the beam itself is a dynamic structure, as proposed in Chapter 2, or if it simply serves as a rigid backbone for the rest of the channel. Additionally, without knowledge of its amino acid sequence, it is currently impossible to accurately generate mutants and chimeras to study its function. Once again, the establishment of high resolution models will be necessary for this aim.

By analyzing the sequence and predicted hydrophathy profiles of Piezo however, I have identified one intracellular domain is distinctly longer than all other intracellular domains that may form the beam. Preliminary experiments in which I have deleted this domain have yielded channels that do not activate under pressure clamp stimulation. This could of course occur be due to a number of reasons, including failure to transport or fold properly. When it becomes possible to make such deletion constructs in a more informed manner, it will be necessary to demonstrate that deleting an allosteric linker eliminates the channels ability to activate in response to tension, but that it retains the ability to form a conducting pore. This requires a method for tension-independent channel activation, perhaps with the partial agonist Yoda1, though the activating mechanism of Yoda1 is currently unknown as well. It will also be interesting to study whether specific mechanisms of mechanical activation, such as that which makes Piezo1

but not Piezo2 sensitive to pressure clamp stimulation, are mediated by specific structures that can be interchanged with chimeric studies. Ultimately, complete structural models, the conformational changes induced by tension sensing, and the pathway of allosteric coupling to the pore will each be necessary to resolve the mechanism of activation.

#### ***4.4 Solving the mechanism of inactivation***

Understanding the many aspects of inactivation in Piezo ion channels is still in its most early stages, and a number of overarching questions remain to be answered. Why do Piezos inactivate? What roles does Piezo inactivation play in biology? Why does inactivation in Piezo have and/or need the ability to be modulated? Why and how is inactivation modulated by so many different factors? Why is voltage dependency a necessary element of inactivation in Piezo channels? What other structures might influence channel inactivation? How do the structures that influence inactivation mediate conformational change and/or changes in ion permeation? And finally can, and if so, how can inactivation be modulated by therapeutic measures in human disease?

In this dissertation a number of physiological roles and diseases are introduced as being influenced if not entirely caused by properties of Piezo inactivation. In diseases such as distal arthrogyriposis and hereditary xerocytosis, slowing of inactivation leads to toxicity caused by increased and unregulated calcium influx. Additional studies are necessary to show whether Piezo inactivation is simply a mechanism to regulate calcium

influx in non-excitabile cells, or if it plays other roles such as adapting cells to changing environments and developmental processes. In excitable cells, the role of inactivation is even less clear. Future studies will be necessary to investigate how the inactivation properties of Piezos affect the overall excitability of neurons and cardiac tissue. Additionally the added element of voltage sensitivity in inactivation calls to question how Piezo channels function in constantly changing membrane voltages, especially during an action potential. Studies focusing on how modulating factors of Piezo inactivation affect the firing properties of neurons may ultimately help to gain insight into how different mechanical signals are transduced into sensation.

Identifying structural correlates that mediate the kinetics and voltage dependence of inactivation in Piezos was a key step in understanding an overall mechanism for inactivation. While we also provide evidence that one of these domains, the inner pore helix, shifts in conformation in a voltage dependent manner, further experiments will need to address if and how this affects conformations of the CED as well as the pore. Likewise, complementary studies must also answer the question of if and how the CED changes in conformation during inactivation. High resolution models for the chimeric constructs introduced in this dissertation as well as for Piezo2, slowly inactivating mutants, or Piezos in the presence of modulating agents will reveal a vast amount of information to answer these questions. Other experiments such as measuring

inactivation after crosslinking the CED subunits or altering the connections between the CED and pore helices may also provide indirect evidence for a conformational change.

Another study from our laboratory has shown that two inactivation states are present in Piezo1 (Lewis et al., 2017). This result raises the possibility that two different mechanisms for inactivation are present in Piezo channels. In fact, this is not an uncommon characteristic of ion channels, as K<sup>+</sup> channels have been shown to employ properties of both N-type and C-type inactivation (Hoshi et al., 1991). In this dissertation, identifying two distinct structural correlates certainly supports this as a possibility for Piezos as well. In K<sup>+</sup> channels, C-type inactivation was revealed after the blocking particle responsible for N-type inactivation was removed. Likewise, one of the best ways to demonstrate two inactivation mechanisms in Piezo is to also remove the structural mediator of one mode. As we presented in Chapter 3, removing the CED has proven to be difficult without impacting channel functionality, and removing the inner pore helix is certainly impossible due to its obvious role in pore formation. One possibility however, may be to render one domain non-functional or severely modulate it without a structural removal to decouple two mechanisms. This may already be possible with the experiments that we have presented. For example, if neutralization of a lysine residue eliminates voltage sensitivity that is specific to one mechanism, then the remaining inactivation kinetic may be entirely mediated by the CED. Additional alterations to the CED in this charge neutralized state may then be used to observe CED

mediated inactivation kinetics. Furthermore, preliminary analysis of the chimeras presented in Chapter 3 also reveal an incomplete changeover of inactivation kinetics at more positive potentials for P1-P2CED, suggesting that perhaps the inactivation mechanisms carried by one domain of Piezo1 and another domain of Piezo2 might both be present and decoupled under these voltages.

The studies presented in this dissertation aimed to gain a greater understanding of mechanosensation through Piezo ion channels. The identification of the CED and inner pore helix as structural correlates of inactivation, as well as the development of a new method to study their functions, are novel findings towards this aim. Ultimately these results help to work towards the long term goals of developing possible therapies in Piezo-related diseases in both sensory and non-sensory organs, as well as understanding the basic science of how the great diversity of somatosensory stimuli is encoded on a molecular level.

## Appendix: Supporting data

The following table is drawn from (Wu, Lewis, & Grandl, 2017).

**Table 2: List of mutations in Piezo1 and Piezo2 associated with human diseases. a, colorectal adenomatous polyposis; b, dehydrated hereditary stomatocytosis; c, premature stop codon; d, generalized lymphatic dysplasia; e, splice variant encoding truncated product at S1153; f, outer helix; g, deletion of 4 indicated residues; h, c-terminal extracellular domain; i, inner helix; j, c-terminal domain; k, insertion of two residues (LE); l, hemolytic anemia; m, distal arthrogyriposis subtype 5; n, Gordon syndrome; o, Marden-Walker syndrome; p, single base pair deletion leading to premature stop codon. Table by A. Lewis.**

Piezo1	Channel Domain	Mutation	Disease	Effect on channel	Citation
		H702Y	CAP <sup>a</sup>	unknown	(Spier et al., 2016)
		G718S	DHS <sup>b</sup>	unknown	(Andolfo et al., 2013)
		E755X <sup>c</sup>	GLD <sup>d</sup>	unknown	(Fotiou et al., 2015)
		G782S	DHS	unknown	(Andolfo et al., 2013)
		R808Q	DHS	unknown	(Andolfo et al., 2013)
		L939M	GLD	unknown	(Fotiou et al., 2015)
		I1007M	CAP	unknown	(Spier et al., 2016)
		S1117L	DHS	unknown	(Andolfo et al., 2013)
		S1153Trpfs*21 <sup>e</sup>	GLD	unknown	(Lukacs et al., 2015)
		R1358P	DHS	slowed inactivation	(Albuisson et al., 2013)
		E1630X	GLD	reduced expression	(Fotiou et al., 2015)
		V1712M	CAP	unknown	(Spier et al., 2016)
		Y1763X	CAP	unknown	(Spier et al., 2016)
		R1955C	CAP	unknown	(Spier et al., 2016)
		A2003D	DHS	unknown	(Andolfo et al., 2013)
		A2020T	DHS	slowed inactivation	(Albuisson et al., 2013)
		A2020V	DHS	unknown	(Andolfo et al., 2013)
		G2029R	GLD	reduced expression	(Lukacs et al., 2015)
	anchor	T2127M	DHS	slowed inactivation	(Albuisson et al., 2013; Andolfo et al., 2013)
	OH <sup>f</sup>	K2166-2169 del <sup>g</sup>	DHS	unknown	(Andolfo et al., 2013)
	OH	V2171F	GLD	reduced expression	(Fotiou et al., 2015)
	CED <sup>h</sup>	M2225R	DHS	slowed inactivation	(Zarychanski et al., 2012)
	CED	Q22Andolfo, 2013X	GLD	reduced expression	(Fotiou et al., 2015)
	CED-IH <sup>i</sup> linker	P2430L	GLD	unknown	(Fotiou et al., 2015)
	IH	R2456H	DHS	slowed inactivation	(Andolfo et al., 2013; Zarychanski et al., 2012)

	IH	R2456C	GLD	unknown	(Fotiou et al., 2015)
	IH	F2458L	GLD	unknown	(Fotiou et al., 2015)
	CTD <sup>i</sup>	R2488Q	DHS	unknown	(Andolfo et al., 2013)
	CTD	E2496ELE <sup>k</sup>	DHS/HA <sup>l</sup>	slowed inactivation	(Albuisson et al., 2013)
<b>Piezo2</b>	<b>Channel Domain</b>	<b>Mutation</b>	<b>Disease</b>	<b>Effect on channel</b>	<b>Citation</b>
		M712V	DA5 <sup>m</sup>	unknown	(McMillin et al., 2014)
		I802F	DA5	faster recovery from inactivation	(B. Coste et al., 2013)
		M998T	DA5	unknown	(McMillin et al., 2014)
		A1486P	DA5	unknown	(Okubo et al., 2015)
		T2221I	DA5	unknown	(McMillin et al., 2014)
		S2223L	DA5	unk	(McMillin et al., 2014)
	anchor	T2356M	DA5	unknown	(McMillin et al., 2014)
	IH	R2686H	GS <sup>n</sup> /DA5	unknown	(McMillin et al., 2014)
	IH	R2686C	MWS <sup>o</sup>	unknown	(McMillin et al., 2014)
	CTD	R2718L	DA5	unknown	(McMillin et al., 2014)
	CTD	R2718P	DA5	unknown	(McMillin et al., 2014)
	CTD	E2727del	DA5	slower onset, faster recovery from inactivation	(B. Coste et al., 2013; McMillin et al., 2014)
	CTD	Y2737Ilefs*7 <sup>p</sup>	DA5	unknown	(McMillin et al., 2014)
	CTD	S2739P	DA5	unknown	(McMillin et al., 2014)
CTD	W2746X	GS	unknown	(McMillin et al., 2014)	

The following figures supplement data referenced in Chapter 2 and are adapted from Wu et al. 2016.

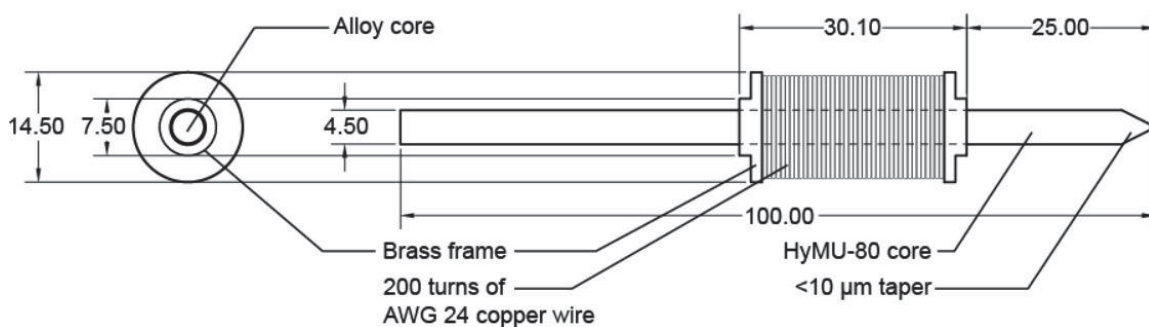


**Figure 44: Design of electromagnetic needle. Design specifications for electromagnetic needle (units in mm).**

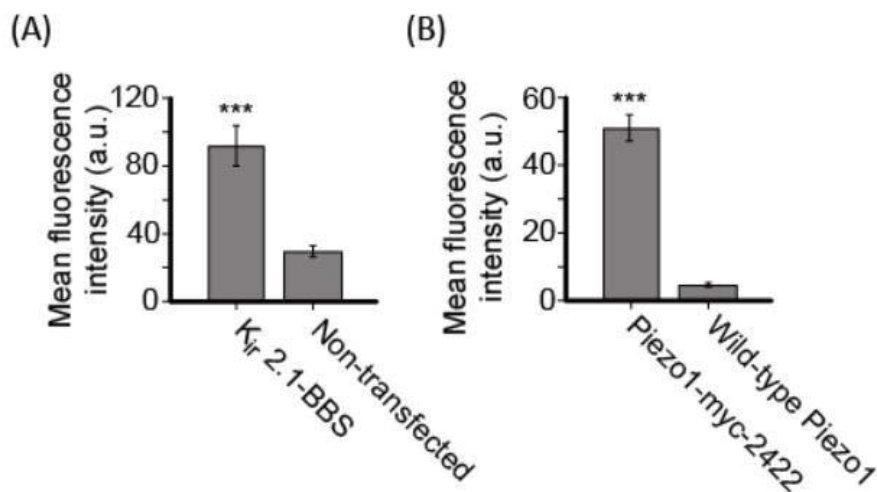


Figure 45: Labeling specificity of tagged constructs. (A) Quantification of mean membrane fluorescence intensity of Kir 2.1-BBS vs non-transfected cells (n = 12 cells each, \*\*\*p < 0.0001, unpaired t-test), (B) Piezo1-myc-2422 transfected cells vs wild-type Piezo1 (n = 13 cells each, \*\*\*p < 0.0001, unpaired t-test). Error bars are SEM.

Table 3: Primer list. Complementary primer sets used to insert bungarotoxin binding sequence or myc tag (underlined).

Construct	Forward primers	Reverse primers
Piezo1-BBS-86	GCCTACACACCGTGCCTCACT <u>TGGA</u> <u>GATACTACGAGAGCTCCCTGGAG</u> <u>CCCTACCCTGACCTGGACCAGTTT</u> CTGGGAC	GTCCCAGAAACTGGTCCAGGTCAG <u>GGTAGGGCTCCAGGGAGCTCTCGT</u> <u>AGTATCTCCAGTGAGGCACGGTGT</u> GTAGGC
Piezo1-BBS-300	TCAAGAACTTCGTAGACCTCT <u>TGGA</u> <u>GATACTACGAGAGCTCCCTGGAG</u> <u>CCCTACCCTGACCCTAACTACTCC</u> AGCCCCAA	TTGGGGCTGGAGTAGTTAGGGTCA <u>GGGTAGGGCTCCAGGGAGCTCTCG</u> <u>TAGTATCTCCAGAGGTCTACGAAG</u> TTCTTGA
Piezo1-BBS-508	TGGGCCCTGTCAGCCTGCACT <u>TGGA</u> <u>GATACTACGAGAGCTCCCTGGAG</u> <u>CCCTACCCTGACCAGTTGGGACTG</u> GAACACACA	TGTGTGTTCCAGTCCCAACTGGTCA <u>GGGTAGGGCTCCAGGGAGCTCTCG</u> <u>TAGTATCTCCAGTGCAGGCTGACA</u> GGGCCA

Piezo1-BBS-659	<u>CTTCCAGTTCCAGGACTTCCCCTG</u> <u>GAGATACTACGAGAGCTCCCTGG</u> <u>AGCCCTACCCTGACACCTATTGGC</u> GCAACCTCACG	<u>CGTGAGGTTGCGCCAATAGGTGTC</u> <u>AGGGTAGGGCTCCAGGGAGCTCTC</u> <u>GTAGTATCTCCAAGGGAAGTCCTG</u> GAACTGGAAG
Piezo1-BBS-893	<u>CAACAATACCAACTTGCAGCCTTG</u> <u>GAGATACTACGAGAGCTCCCTGG</u> <u>AGCCCTACCCTGACTTGGAGATCA</u> ACCAGTCTTG	<u>CAAAGACTGGTTGATCTCCAAGTC</u> <u>AGGGTAGGGCTCCAGGGAGCTCTC</u> <u>GTAGTATCTCCAAGGCTGCAAGTT</u> GGTATTGTTG
Piezo1-BBS-1070	<u>TGGCGCTGGAGCAAGGCCATCTG</u> <u>GAGATACTACGAGAGCTCCCTGG</u> <u>AGCCCTACCCTGACCCCATGAATT</u> CCGCCCTCAT	<u>ATGAGGGCGGAATTCATGGGGTCA</u> <u>GGGTAGGGCTCCAGGGAGCTCTCG</u> <u>TAGTATCTCCAGATGGCCTTGCTCC</u> AGCGCCA
Piezo1-BBS-1201	<u>CACTACCCTGCTGCAGAAGTGGA</u> <u>GATACTACGAGAGCTCCCTGGAG</u> <u>CCCTACCCTGACGACACGCGAGC</u> CCAGCTCGTGC	<u>GCACGAGCTGGGCTCGCGTGTCGT</u> <u>CAGGGTAGGGCTCCAGGGAGCTCT</u> <u>CGTAGTATCTCCAATTCTGCAGCAG</u> GGTAGTG
Piezo1-BBS-1758	<u>CCCCTGGAACAGCTACGTTTGGAG</u> <u>ATACTACGAGAGCTCCCTGGAGC</u> <u>CCTACCCTGACGTGCTGCGGCGCT</u> ATGAGAAC	<u>GTTTCATAGCGCCGCAGCACGTC</u> <u>AGGGTAGGGCTCCAGGGAGCTCTC</u> <u>GTAGTATCTCCAACGTAGCTGTTC</u> CAGGGG
Piezo1-BBS-2075	<u>CTGAGAGGATGTTTCAGCCAGTGG</u> <u>AGATACTACGAGAGCTCCCTGGA</u> <u>GCCCTACCCTGACAATGCGGTGGC</u> ACAGCTGTG	<u>CACAGCTGTGCCACCGCATTGTCA</u> <u>GGGTAGGGCTCCAGGGAGCTCTCG</u> <u>TAGTATCTCCAAGTGAACATCC</u> TCTCAG
Piezo1-BBS-2329	<u>CCAAAGGGACCTGGCCAAGTGGA</u> <u>GATACTACGAGAGCTCCCTGGAG</u> <u>CCCTACCCTGACGGTGGCACTGTG</u> GAGTATAC	<u>GTATACTCCACAGTGCCACCGTCA</u> <u>GGGTAGGGCTCCAGGGAGCTCTCG</u> <u>TAGTATCTCCAATTGGCCAGTCCC</u> TTTGG
Piezo1-BBS-2343	<u>ATGAGAAGCACACCTTGGAGTGG</u> <u>AGATACTACGAGAGCTCCCTGGA</u> <u>GCCCTACCCTGACCTGGCCCCAA</u> CAGTACGGC	<u>GCCGTAAGTGTGGGGCCAGGTCA</u> <u>GGGTAGGGCTCCAGGGAGCTCTCG</u> <u>TAGTATCTCCAAGTGAACATCC</u> TCTCAT
Piezo1-BBS-2356	<u>GCACGAAGGCAGCTGGCCCAATG</u> <u>GAGATACTACGAGAGCTCCCTGG</u> <u>AGCCCTACCCTGACCTGCTCGAGG</u> GCAGACCTGAC	<u>GTCAGGTCTGCCCTCGAGCAGGTC</u> <u>AGGGTAGGGCTCCAGGGAGCTCTC</u> <u>GTAGTATCTCCAATTGGGCCAGCTGC</u> CTTCGTGC
Piezo1-BBS-2409	<u>CAGCTGCGGAGGGAGCAATGGAG</u> <u>ATACTACGAGAGCTCCCTGGAGC</u> <u>CCTACCCTGACGTGGGCACAGGG</u> GCCTCTG	<u>CAGAGCCCCCTGTGCCACGTCAG</u> <u>GGTAGGGCTCCAGGGAGCTCTCGT</u> <u>AGTATCTCCAATTGCTCCCTCCGAG</u> CTG

Piezo1-BBS-2422	<u>GGAGCAAGCGGGCACCAAGTGGAG</u> <u>GATACTACGAGAGCTCCCTGGAG</u> <u>CCCTACCCTGACGCCTCCGACTTC</u> CTCGAGTGG	<u>CCACTCGAGGAAGTCGGAGGCGTC</u> <u>AGGGTAGGGCTCCAGGGAGCTCTC</u> <u>GTAGTATCTCCA</u> CTTGGTGCCCGCT TGCTCC
Piezo1-BBS-2425	GGCACCAAGGCCTCCGACTGGAG ATACTACGAGAGCTCCCTGGAG <u>CCTACCCTGACTTCCTCGAGTGGT</u> GGGTCATC	<u>GATGACCCACCACTCGAGGAAGTC</u> <u>AGGGTAGGGCTCCAGGGAGCTCTC</u> <u>GTAGTATCTCCA</u> TCGGAGGCCTTG GTGCC
K <sub>ir</sub> 2.1-BBS	<u>GATACTTCTAAAGTGAGCAAATG</u> <u>GAGATACTACGAGAGCTCCCTGG</u> <u>AGCCCTACCCTGACGCATGCGTGT</u> CGGAGGTCAAC	<u>GTTGACCTCCGACACGCATGCGTC</u> <u>AGGGTAGGGCTCCAGGGAGCTCTC</u> <u>GTAGTATCTCCA</u> TTTGCTCACTTTA GAAGTATC
K <sub>v</sub> 1.2-BBS-S1-S2	GAATGAAGACATGCATGGTTGGAG <u>GATACTACGAGAGCTCCCTGGAG</u> <u>CCCTACCCTGACAGTGGGGTGACC</u> TTCCAC	<u>GTGGAAGGTCACCCCACTGTCAGG</u> <u>GTAGGGCTCCAGGGAGCTCTCGTA</u> <u>GTATCTCCA</u> ACCATGCATGTCTTCA TTC
K <sub>v</sub> 1.2-BBS-S3-S4	GAGGACGCTCAGCAAGGCTGGAG <u>ATACTACGAGAGCTCCCTGGAGC</u> <u>CCTACCCTGACCAGCAGGCCATGT</u> CACTG	<u>CAGTGACATGGCCTGCTGGTCAGG</u> <u>GTAGGGCTCCAGGGAGCTCTCGTA</u> <u>GTATCTCCAGCCTTGCTGAGCGTCC</u> TC
K <sub>v</sub> 1.2-BBS-S5-PH	GCTGTGATTTTGCAGAGTGGAGA <u>TACTACGAGAGCTCCCTGGAGCC</u> <u>CTACCCTGACGCCGATGAGCGAG</u> AGTCC	<u>GGACTCTCGCTCATCGGCCTCAGG</u> <u>GTAGGGCTCCAGGGAGCTCTCGTA</u> <u>GTATCTCCA</u> CTCTGCAAAATACAC AGC
Piezo1-myc-2422	GGAGCAAGCGGGCACCAAGGAG <u>CAGAACTCATCTCTGAAGAGGA</u> <u>TCTGGCCTCCGACTTCCTCGAGTG</u> G	<u>CCACTCGAGGAAGTCGGAGGCCAG</u> <u>ATCCTCTTCAGAGATGAGTTTCTGC</u> <u>TCCTTGGTGCCCGCTTGCTCC</u>

The following figures supplement data referenced in Chapter 3.

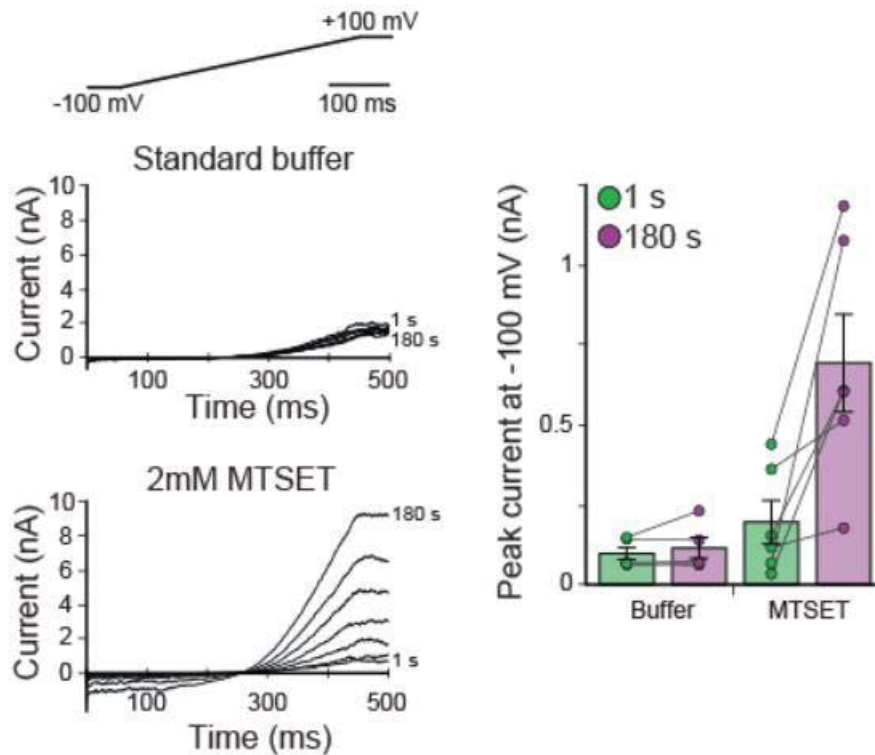


**Figure 46: Confirmation of MTSET functionality.** Voltage-ramp stimulation protocol and elicited currents recorded from HEK293T transiently transfected with wild-type mouse TRPA1 in standard buffer and 2 mM MTSET to demonstrate efficacy of MTSET reagent (left). Individual and mean current amplitudes of TRPA1 under indicated MTSET labeling conditions (right).

The following table supplements data discussed in Chapter 4.

**Table 4: Candidate ion channels for magnetogenetics.** Ion channels tested by inserting bungarotoxin binding site at indicated locations and tested for labeling accessibility with  $\alpha$ -bungarotoxin-AlexaFluor-555 and functionality with electrophysiology. 'Weak labeling' indicates faint fluorescent signal.

<b>Ion Channel</b>	<b>Species</b>	<b>BBS insertion</b>	<b>Structural location</b>	<b>Fluorescently labels</b>	<b>Functional</b>	<b>Reference</b>
MscL	E. coli	Q56	Single extra-cellular loop	Yes	No	--
MscL	E. coli	R62	Single extra-cellular loop	Yes	No	--
TREK1	M. musculus	A107	Cap domain, first extra-cellular loop	No	--	--
TREK1	M. musculus	S135	P1 loop, first extracellular loop	--	--	--
TREK1	M. musculus	L282	P2 loop, second extracellular loop	No	--	--
TRAAK	H. sapiens	D55	Cap domain, first extracellular loop	Yes, weak	--	--
TRAAK	H. sapiens	S83	P1 loop, first extracellular loop	Yes, weak	--	--
TRAAK	H. sapiens	Q226	P2 loop, second extracellular loop	Yes, weak	--	--
Kir2.1	M. musculus	K120	S1-Pore loop	Yes	No	(Wu et al., 2016)
Kir2.1	M. musculus	V150	Pore loop-S2	Yes	No	--
Kv1.2	H. sapiens	G197	S1-S2 loop	Yes	Yes	(Wu et al., 2016)
Kv1.2	H. sapiens	G284	S3-S4 loop (voltage sensor)	Yes	Yes	(Wu et al., 2016)
Kv1.2	H. sapiens	E350	S5-Pore loop	Yes	No	(Wu et al., 2016)
Shaker concatemeric	D. melanogaster	K215	DI-S1-S2 loop	No	--	(Gagnon & Bezanilla, 2009)
Shaker concatemeric	D. melanogaster	S311	DI-S3-S4 loop (voltage sensor)	No	--	(Gagnon & Bezanilla, 2009)
Nav1.2	H. sapiens	V1620	DIV-S3-S4 loop	No	--	--
Nav1.2	H. sapiens	T1623	DIV-S3-S4 loop	No	--	--
Cav1.2	H. sapiens	E713	DII-S5-S6 loop	No, optimize $\beta$ subunit		(Subramanyam et al., 2013)
dPiezo	D. melanogaster	C2397	CED (ortholog to mPiezo1 2422)	--	--	--
Piezo2	M. musculus	A86	First extracellular loop	No	--	--
Piezo2	M. musculus	K2695	CED (ortholog to mPiezo1 2422)	Yes, weak	--	--

## References

- Albuisson, J., Murthy, S. E., Bandell, M., Coste, B., Louis-dit-Picard, H., Mathur, J., ... Patapoutian, A. (2013). Dehydrated hereditary stomatocytosis linked to gain-of-function mutations in mechanically activated PIEZO1 ion channels. *Nature Communications*, 4(May). <https://doi.org/10.1038/ncomms2899>
- Alcaino, C., Farrugia, G., & Beyder, A. (2016). *Mechanosensitive Piezo Channels in the Gastrointestinal Tract. Current Topics in Membranes* (Vol. 79). Elsevier Ltd. <https://doi.org/10.1016/bs.ctm.2016.11.003>
- Alper, S. L. (2017). *Genetic Diseases of PIEZO1 and PIEZO2 Dysfunction. Current Topics in Membranes* (Vol. 79). Elsevier Ltd. <https://doi.org/10.1016/bs.ctm.2017.01.001>
- Andolfo, I., Alper, S. L., De Franceschi, L. D., Auriemma, C., Russo, R., De Falco, L. D., ... Iolascon, A. (2013). Multiple clinical forms of dehydrated hereditary stomatocytosis arise from mutations in PIEZO1. *Blood*, 121(19), 3925–3935. <https://doi.org/10.1182/blood-2013-02-482489>
- Anishkin, A., Loukin, S. H., Teng, J., & Kung, C. (2014). Feeling the hidden mechanical forces in lipid bilayer is an original sense. *Proceedings of the National Academy of Sciences*, 111(22), 7898–7905. <https://doi.org/10.1073/pnas.1313364111>
- Árnadóttir, J., & Chalfie, M. (2010). Eukaryotic Mechanosensitive Channels. *Annual Review of Biophysics*, 39(1), 111–137. <https://doi.org/10.1146/annurev.biophys.37.032807.125836>
- Arnadóttir, J., O'Hagan, R., Chen, Y., Goodman, M. B., & Chalfie, M. (2011). The DEG/ENaC Protein MEC-10 Regulates the Transduction Channel Complex in *Caenorhabditis elegans* Touch Receptor Neurons. *Journal of Neuroscience*, 31(35), 12695–12704. <https://doi.org/10.1523/JNEUROSCI.4580-10.2011>
- Bae, C., Gnanasambandam, R., Nicolai, C., Sachs, F., & Gottlieb, P. a. (2013). Xerocytosis is caused by mutations that alter the kinetics of the mechanosensitive channel PIEZO1. *Proceedings of the National Academy of Sciences of the United States of America*, 110(12), E1162-8. <https://doi.org/10.1073/pnas.1219777110>
- Bae, C., Sachs, F., & Gottlieb, P. A. (2015). Protonation of the human PIEZO1 ion channel stabilizes inactivation. *Journal of Biological Chemistry*, 290(8), 5167–5173. <https://doi.org/10.1074/jbc.M114.604033>

- Bagriantsev, S. N., Gracheva, E. O., & Gallagher, P. G. (2014). Piezo proteins: Regulators of mechanosensation and other cellular processes. *Journal of Biological Chemistry*, 289(46), 31673–31681. <https://doi.org/10.1074/jbc.R114.612697>
- Baukrowitz, T., & Yellen, G. (1995). Modulation of K<sup>+</sup> current by frequency and external [K<sup>+</sup>]: A tale of two inactivation mechanisms. *Neuron*, 15(4), 951–960. [https://doi.org/10.1016/0896-6273\(95\)90185-X](https://doi.org/10.1016/0896-6273(95)90185-X)
- Blumenthal, N. R., Hermanson, O., Heimrich, B., & Shastri, V. P. (2014). Stochastic nanoroughness modulates neuron–astrocyte interactions and function via mechanosensing cation channels. *Proceedings of the National Academy of Sciences*, 111(45), 16124–16129. <https://doi.org/10.1073/pnas.1412740111>
- Borbiro, I., Badheka, D., & Rohacs, T. (2015). Activation of TRPV1 channels inhibits mechanosensitive Piezo channel activity by depleting membrane phosphoinositides. *Science Signaling*, 8(363), ra15. <https://doi.org/10.1126/scisignal.2005667>
- Cahalan, S. M., Lukacs, V., Ranade, S. S., Chien, S., Bandell, M., & Patapoutian, A. (2015). Piezo1 links mechanical forces to red blood cell volume. *eLife*, 4(MAY), 1–12. <https://doi.org/10.7554/eLife.07370>
- Chaudhari, N., & Roper, S. D. (2010). The cell biology of taste. *Journal of Cell Biology*, 190(3), 285–296. <https://doi.org/10.1083/jcb.201003144>
- Chen, R., Romero, G., Christiansen, M. G., Mohr, A., & Anikeeva, P. (2015). Wireless magnetothermal deep brain stimulation. *Science*, 347(6229), 1477–1480. <https://doi.org/10.1126/science.1261821>
- Chesler, A. T., Szczot, M., Bharucha-Goebel, D., Čeko, M., Donkervoort, S., Laubacher, C., ... Bönnemann, C. G. (2016). The Role of *PIEZO2* in Human Mechanosensation. *New England Journal of Medicine*, 375(14), 1355–1364. <https://doi.org/10.1056/NEJMoa1602812>
- Choi, H. J., Sun, D., & Jakobs, T. C. (2015). Astrocytes in the optic nerve head express putative mechanosensitive channels. *Molecular Vision*, 21(January), 749–66. Retrieved from <http://www.pubmedcentral.nih.gov/articlerender.fcgi?artid=4502055&tool=pmcentrez&rendertype=abstract>
- Cinar, E., Zhou, S., DeCoursey, J., Wang, Y., Waugh, R. E., & Wan, J. (2015). Piezo1 regulates mechanotransductive release of ATP from human RBCs. *Proceedings of the*

*National Academy of Sciences*, 112(38), 11783–11788.  
<https://doi.org/10.1073/pnas.1507309112>

- Cormier, J. W., Rivolta, I., Tateyama, M., Yang, A. S., & Kass, R. S. (2002). Secondary structure of the human cardiac Na<sup>+</sup> channel C terminus. Evidence for a role of helical structures in modulation of channel inactivation. *Journal of Biological Chemistry*, 277(11), 9233–9241. <https://doi.org/10.1074/jbc.M110204200>
- Coste, B., Houge, G., Murray, M. F., Stitzel, N., Bandell, M., Giovanni, M. A., ... Patapoutian, A. (2013). Gain-of-function mutations in the mechanically activated ion channel PIEZO2 cause a subtype of Distal Arthrogyriposis. *Proceedings of the National Academy of Sciences*, 110(12), 4667–4672.  
<https://doi.org/10.1073/pnas.1221400110>
- Coste, B., Mathur, J., Schmidt, M., Earley, T. J., Ranade, S., Petrus, M. J., ... Patapoutian, A. (2010). Piezo1 and Piezo2 Are Essential Components of Distinct Mechanically Activated Cation Channels. *Science*, 330(October), 55–60.  
<https://doi.org/10.1126/science.1193270>
- Coste, B., Murthy, S. E., Mathur, J., Schmidt, M., Mechioukhi, Y., Delmas, P., & Patapoutian, A. (2015). Piezo1 ion channel pore properties are dictated by C-terminal region. *Nature Communications*, 6(May), 7223.  
<https://doi.org/10.1038/ncomms8223>
- Coste, B., Xiao, B., Santos, J. S., Syeda, R., Grandl, J., Spencer, K. S., ... Patapoutian, A. (2012). Piezo proteins are pore-forming subunits of mechanically activated channels. *Nature*, 483(7388), 176–181. <https://doi.org/10.1038/nature10812>
- Cox, C. D., Bae, C., Ziegler, L., Hartley, S., Nikolova-Krstevski, V., Rohde, P. R., ... Martinac, B. (2016). Removal of the mechanoprotective influence of the cytoskeleton reveals PIEZO1 is gated by bilayer tension. *Nature Communications*, 7, 10366.  
<https://doi.org/10.1038/ncomms10366>
- Cox, R. H. (2005). Molecular determinants of voltage-gated potassium currents in vascular smooth muscle. *Cell Biochemistry and Biophysics*, 42(2), 167–95.  
<https://doi.org/10.1385/CBB:42:2:167>
- Deisseroth, K. (2015). Optogenetics: 10 years of microbial opsins in neuroscience. *Nature Neuroscience*, 18(9), 1213–1225. <https://doi.org/10.1038/nn.4091>
- Dubin, A. E., Murthy, S., Lewis, A. H., Brosse, L., Cahalan, S. M., Grandl, J., ... Patapoutian, A. (2017). Endogenous Piezo1 Can Confound Mechanically Activated

- Channel Identification and Characterization. *Neuron*, 94(2), 266–270.e3.  
<https://doi.org/10.1016/j.neuron.2017.03.039>
- Dubin, A. E., Schmidt, M., Mathur, J., Petrus, M. J., Xiao, B., Coste, B., & Patapoutian, A. (2012). Inflammatory Signals Enhance Piezo2-Mediated Mechanosensitive Currents. *Cell Reports*, 2(3), 511–517. <https://doi.org/10.1016/j.celrep.2012.07.014>
- Dupont, S., Morsut, L., Aragona, M., Enzo, E., Giulitti, S., Cordenonsi, M., ... Piccolo, S. (2011). Role of YAP/TAZ in mechanotransduction. *Nature*, 474(7350), 179–183.  
<https://doi.org/10.1038/nature10137>
- Eijkelkamp, N., Linley, J. E., Torres, J. M., Bee, L., Dickenson, A. H., Gringhuis, M., ... Wood, J. N. (2013). A role for Piezo2 in EPAC1-dependent mechanical allodynia. *Nature Communications*, 4, 1682. <https://doi.org/10.1038/ncomms2673>
- Elosegui-Artola, A., Oria, R., Chen, Y., Kosmalska, A., Pérez-González, C., Castro, N., ... Roca-Cusachs, P. (2016). Mechanical regulation of a molecular clutch defines force transmission and transduction in response to matrix rigidity. *Nature Cell Biology*, 18(5), 540–548. <https://doi.org/10.1038/ncb3336>
- Ferrari, L. F., Bogen, O., Green, P., & Levine, J. D. (2015). Contribution of Piezo2 to Endothelium-Dependent Pain. *Molecular Pain*, 11. <https://doi.org/10.1186/s12990-015-0068-4>
- Fleischer, J. (2009). Mammalian olfactory receptors. *Frontiers in Cellular Neuroscience*, 3(August), 1–10. <https://doi.org/10.3389/neuro.03.009.2009>
- Fotiou, E., Martin-Almedina, S., Simpson, M. A., Lin, S., Gordon, K., Brice, G., ... Ostergaard, P. (2015). Novel mutations in PIEZO1 cause an autosomal recessive generalized lymphatic dysplasia with non-immune hydrops fetalis. *Nature Communications*, 6, 8085. <https://doi.org/10.1038/ncomms9085>
- Gagnon, D. G., & Bezanilla, F. (2009). A single charged voltage sensor is capable of gating the Shaker K<sup>+</sup> channel. *The Journal of General Physiology*, 133(5), 467–483.  
<https://doi.org/10.1085/jgp.200810082>
- Ge, J., Li, W., Zhao, Q., Li, N., Chen, M., Zhi, P., ... Yang, M. (2015). Architecture of the mammalian mechanosensitive Piezo1 channel. *Nature*, 527(7576), 64–69.  
<https://doi.org/10.1038/nature15247>
- Gerhold, K. A., Pellegrino, M., Tsunozaki, M., Morita, T., Leitch, D. B., Tsuruda, P. R., ... Bautista, D. M. (2013). The Star-Nosed Mole Reveals Clues to the Molecular Basis of

- Mammalian Touch. *PLoS ONE*, 8(1). <https://doi.org/10.1371/journal.pone.0055001>
- Goldin, A. L. (2003). Mechanisms of sodium channel inactivation. *Current Opinion in Neurobiology*, 13(3), 284–290. [https://doi.org/10.1016/S0959-4388\(03\)00065-5](https://doi.org/10.1016/S0959-4388(03)00065-5)
- Goldmann, W. H. (2012). Mechanotransduction and focal adhesions. *Cell Biology International*, 36(7), 649–652. <https://doi.org/10.1042/CBI20120184>
- Gottlieb, P. A., Bae, C., & Sachs, F. (2012). Gating the mechanical channel Piezo1: a comparison between whole-cell and patch recording. *Channels*, 6(4), 282–289. <https://doi.org/10.4161/chan.21064>
- Gudipaty, S. A., Lindblom, J., Loftus, P. D., Redd, M. J., Edes, K., Davey, C. F., ... Rosenblatt, J. (2017). Mechanical stretch triggers rapid epithelial cell division through Piezo1. *Nature*, 543(7643), 118–121. <https://doi.org/10.1038/nature21407>
- Guillot, C., & Lecuit, T. (2013). Mechanics of Epithelial Tissue Homeostasis and Morphogenesis. *Science*, 340(6137), 1185–1189. <https://doi.org/10.1126/science.1235249>
- Haliloglu, G., Becker, K., Temucin, C., Talim, B., Küçükşahin, N., Pergande, M., ... Cirak, S. (2016). Recessive PIEZO2 stop mutation causes distal arthrogyrosis with distal muscle weakness, scoliosis and proprioception defects. *Journal of Human Genetics*, 62(August), 497–501. <https://doi.org/10.1038/jhg.2016.153>
- Hao, J., Padilla, F., Dandonneau, M., Lavebratt, C., Lesage, F., Noël, J., & Delmas, P. (2013). Kv1.1 channels act as mechanical brake in the senses of touch and pain. *Neuron*, 77(5), 899–914. <https://doi.org/10.1016/j.neuron.2012.12.035>
- Hodgkin, A. L., & Huxley, A. F. (1952). The dual effect of membrane potential on sodium conductance in the giant axon of Loligo. *The Journal of Physiology*, 116, 497–506. <https://doi.org/10.1016/j.phrs.2011.05.021>
- Hoffmann, T., Tych, K. M., Hughes, M. L., Brockwell, D. J., & Dougan, L. (2013). Towards design principles for determining the mechanical stability of proteins. *Physical Chemistry Chemical Physics*, 15(38), 15767–15780. <https://doi.org/10.1039/c3cp52142g>
- Honoré, E. (2007). The neuronal background K2P channels: focus on TREK1. *Nature Reviews Neuroscience*, 8(4), 251–261. <https://doi.org/10.1038/nrn2117>
- Hoshi, T., Zagotta, W. N., & Aldrich, R. W. (1991). Two types of inactivation in Shaker

- K<sup>+</sup> channels: Effects of alterations in the carboxy-terminal region. *Neuron*, 7(4), 547–556. [https://doi.org/10.1016/0896-6273\(91\)90367-9](https://doi.org/10.1016/0896-6273(91)90367-9)
- Huang, H., Delikanli, S., Zeng, H., Ferkey, D. M., & Pralle, A. (2010). Remote control of ion channels and neurons through magnetic-field heating of nanoparticles. *Nature Nanotechnology*, 5(8), 602–606. <https://doi.org/10.1038/nnano.2010.125>
- Hung, W. C., Yang, J. R., Yankaskas, C. L., Wong, B. S., Wu, P. H., Pardo-Pastor, C., ... Konstantopoulos, K. (2016). Confinement Sensing and Signal Optimization via Piezo1/PKA and Myosin II Pathways. *Cell Reports*, 15(7), 1430–1441. <https://doi.org/10.1016/j.celrep.2016.04.035>
- Ikeda, R., Cha, M., Ling, J., Jia, Z., Coyle, D., & Gu, J. G. (2014). Merkel cells transduce and encode tactile stimuli to drive  $\alpha\beta$ -Afferent impulses. *Cell*, 157(3), 664–675. <https://doi.org/10.1016/j.cell.2014.02.026>
- Iscla, I., & Blount, P. (2012). Sensing and responding to membrane tension: The bacterial MscL channel as a model system. *Biophysical Journal*, 103(2), 169–174. <https://doi.org/10.1016/j.bpj.2012.06.021>
- Jia, Z., Ikeda, R., Ling, J., & Gu, J. G. (2013). GTP-dependent run-up of Piezo2-type mechanically activated currents in rat dorsal root ganglion neurons. *Molecular Brain*, 6, 57. <https://doi.org/10.1186/1756-6606-6-57>
- Jin, Y., Li, J., Wang, Y., Ye, R., Feng, X., Jing, Z., & Zhao, Z. (2015). Functional role of mechanosensitive ion channel Piezo1 in human periodontal ligament cells. *The Angle Orthodontist*, 85(1), 87–94. <https://doi.org/10.2319/123113-955.1>
- Kamajaya, A., Kaiser, J. T., Lee, J., Reid, M., & Rees, D. C. (2014). The structure of a conserved piezo channel domain reveals a topologically distinct ?? sandwich fold. *Structure*, 22(10), 1520–1527. <https://doi.org/10.1016/j.str.2014.08.009>
- Kehl, S. J., Eduljee, C., Kwan, D. C., Zhang, S., & Fedida, D. (2002). Molecular determinants of the inhibition of human Kv1.5 potassium currents by external protons and Zn(2+). *The Journal of Physiology*, 54(1), 9–24. [https://doi.org/PHY\\_14456](https://doi.org/PHY_14456) [pii]
- Kernan, M., Cowan, D., & Zuker, C. (1994). Genetic dissection of mechanosensory transduction: Mechanoreception-defective mutations of drosophila. *Neuron*, 12(6), 1195–1206. [https://doi.org/10.1016/0896-6273\(94\)90437-5](https://doi.org/10.1016/0896-6273(94)90437-5)
- Kim, S. E., Coste, B., Chadha, A., Cook, B., & Patapoutian, A. (2012). The role of

- Drosophila Piezo in mechanical nociception. *Nature*, 483(7388), 209–212.  
<https://doi.org/10.1038/nature10801>
- Kollmannsberger, P., & Fabry, B. (2007). High-force magnetic tweezers with force feedback for biological applications. *Review of Scientific Instruments*, 78(11).  
<https://doi.org/10.1063/1.2804771>
- Kurata, H. T., & Fedida, D. (2006). A structural interpretation of voltage-gated potassium channel inactivation. *Progress in Biophysics and Molecular Biology*, 92(2), 185–208.  
<https://doi.org/10.1016/j.pbiomolbio.2005.10.001>
- Lamb, T. D., Collin, S. P., & Pugh, E. N. (2007). Evolution of the vertebrate eye: opsins, photoreceptors, retina and eye cup. *Nature Reviews Neuroscience*, 8(12), 960–976.  
<https://doi.org/10.1038/nrn2283>
- Larsson, H. P., & Elinder, F. (2000). A conserved glutamate is important for slow inactivation in K<sup>+</sup> channels. *Neuron*, 27(3), 573–583. [https://doi.org/10.1016/S0896-6273\(00\)00067-2](https://doi.org/10.1016/S0896-6273(00)00067-2)
- Lee, W., Leddy, H. A., Chen, Y., Lee, S. H., Zelenski, N. A., McNulty, A. L., ... Liedtke, W. B. (2014). Synergy between Piezo1 and Piezo2 channels confers high-strain mechanosensitivity to articular cartilage. *Proceedings of the National Academy of Sciences*, 111(47), E5114–E5122. <https://doi.org/10.1073/pnas.1414298111>
- Lewis, A. H., Cui, A. F., McDonald, M. F., & Grandl, J. (2017). Transduction of Repetitive Mechanical Stimuli by Piezo1 and Piezo2 Ion Channels. *Cell Reports*, 19(12), 2572–2585. <https://doi.org/10.1016/j.celrep.2017.05.079>
- Lewis, A. H., & Grandl, J. (2015). Mechanical sensitivity of Piezo1 ion channels can be tuned by cellular membrane tension. *eLife*, 4(December2015), 1–17.  
<https://doi.org/10.7554/eLife.12088>
- Li, C., Rezaia, S., Kammerer, S., Sokolowski, A., Devaney, T., Gorischek, A., ... Schreibmayer, W. (2015). Piezo1 forms mechanosensitive ion channels in the human MCF-7 breast cancer cell line. *Scientific Reports*, 5(1), 8364.  
<https://doi.org/10.1038/srep08364>
- Li, J., Hou, B., Tumova, S., Muraki, K., Bruns, A., Ludlow, M. J., ... Beech, D. J. (2014). Piezo1 integration of vascular architecture with physiological force. *Nature*, 515(7526), 279–282. <https://doi.org/10.1038/nature13701>
- Long, S. B., Campbell, E. B., & Mackinnon, R. (2005). Crystal structure of a mammalian

- voltage-dependent Shaker family K<sup>+</sup> channel. *Science*, 309, 897–904.  
<https://doi.org/10.1126/science.1116269>
- Lukacs, V., Mathur, J., Mao, R., Bayrak-Toydemir, P., Procter, M., Cahalan, S. M., ... Krock, B. L. (2015). Impaired PIEZO1 function in patients with a novel autosomal recessive congenital lymphatic dysplasia. *Nature Communications*, 6, 8329.  
<https://doi.org/10.1038/ncomms9329>
- Mahmud, A. A., Nahid, N. A., Nassif, C., Sayeed, M. S. B., Ahmed, M. U., Parveen, M., ... Michaud, J. L. (2017). Loss of the proprioception and touch sensation channel PIEZO2 in siblings with a progressive form of contractures. *Clinical Genetics*, 91(3), 470–475. <https://doi.org/10.1111/cge.12850>
- Maksimovic, S., Nakatani, M., Baba, Y., Nelson, A. M., Marshall, K. L., Wellnitz, S. A., ... Lumpkin, E. A. (2014). Epidermal Merkel cells are mechanosensory cells that tune mammalian touch receptors. *Nature*, 509(7502), 617–621.  
<https://doi.org/10.1038/nature13250>
- Martins, J. R., Penton, D., Peyronnet, R., Arhatte, M., Moro, C., Picard, N., ... Demolombe, S. (2016). Piezo1-dependent regulation of urinary osmolarity. *Pflügers Archiv European Journal of Physiology*, 468(7), 1197–1206.  
<https://doi.org/10.1007/s00424-016-1811-z>
- Mauthner, S. E., Hwang, R. Y., Lewis, A. H., Xiao, Q., Tsubouchi, A., Wang, Y., ... Tracey, W. D. (2014). Balboa binds to pickpocket in vivo and is required for mechanical nociception in drosophila larvae. *Current Biology*, 24(24), 2920–2925.  
<https://doi.org/10.1016/j.cub.2014.10.038>
- Mayer, M., & Yang, J. (2013). Engineered ion channels as emerging tools for chemical biology. *Accounts of Chemical Research*, 46(12), 2998–3008.  
<https://doi.org/10.1021/ar400129t>
- McMillin, M. J., Beck, A. E., Chong, J. X., Shively, K. M., Buckingham, K. J., Gildersleeve, H. I. S., ... Bamshad, M. J. (2014). Mutations in PIEZO2 cause Gordon syndrome, Marden-Walker Syndrome, and distal arthrogryposis type 5. *American Journal of Human Genetics*, 94(5), 734–744. <https://doi.org/10.1016/j.ajhg.2014.03.015>
- Meister, M. (2016). Physical limits to magnetogenetics. *eLife*, 5(AUGUST), 1–14.  
<https://doi.org/10.7554/eLife.17210>
- Müller, D. J., Helenius, J., Alsteens, D., & Dufrêne, Y. F. (2009). Force probing surfaces of living cells to molecular resolution. *Nature Chemical Biology*, 5(6), 383–390.

<https://doi.org/10.1038/nchembio.181>

- Nilius, B., & Honoré, E. (2012). Sensing pressure with ion channels. *Trends in Neurosciences*, 35(8), 477–486. <https://doi.org/10.1016/j.tins.2012.04.002>
- Nourse, J. L., & Pathak, M. M. (2017). How cells channel their stress: Interplay between Piezo1 and the cytoskeleton. *Seminars in Cell and Developmental Biology*, *In Press*. <https://doi.org/10.1016/j.semcdb.2017.06.018>
- O'Hagan, R., Chalfie, M., & Goodman, M. B. (2005). The MEC-4 DEG/ENaC channel of *Caenorhabditis elegans* touch receptor neurons transduces mechanical signals. *Nature Neuroscience*, 8(1), 43–50. <https://doi.org/10.1038/nn1362>
- Okubo, M., Fujita, A., Saito, Y., Komaki, H., Ishiyama, A., Takeshita, E., ... Sasaki, M. (2015). A family of distal arthrogyrosis type 5 due to a novel PIEZO2 mutation. *American Journal of Medical Genetics*, 167(5), 1100–1106. <https://doi.org/10.1002/ajmg.a.36881>
- Oliver, D., Lien, C.-C., Soom, M., Baukrowitz, T., Jonas, P., & Fakler, B. (2004). Functional Conversion Between A-Type and Delayed Rectifier K<sup>+</sup> Channels by Membrane Lipids. *Science*, 304(5668), 265–270. <https://doi.org/10.1126/science.1094113>
- Paluch, E. K., Nelson, C. M., Biais, N., Fabry, B., Moeller, J., Pruitt, B. L., ... Federle, W. (2015). Mechanotransduction: use the force(s). *BMC Biology*, 13(1), 47. <https://doi.org/10.1186/s12915-015-0150-4>
- Pan, B., & Holt, J. R. (2015). The molecules that mediate sensory transduction in the mammalian inner ear. *Current Opinion in Neurobiology*, 34, 165–171. <https://doi.org/10.1016/j.conb.2015.06.013>
- Pathak, M. M., Nourse, J. L., Tran, T., Hwe, J., Arulmoli, J., Le, D. T. T., ... Tombola, F. (2014). Stretch-activated ion channel Piezo1 directs lineage choice in human neural stem cells. *Proceedings of the National Academy of Sciences*, 111(45), 16148–16153. <https://doi.org/10.1073/pnas.1409802111>
- Perozo, E., Kloda, A., Cortes, D. M., & Martinac, B. (2002). Physical principles underlying the transduction of bilayer deformation forces during mechanosensitive channel gating. *Nature Structural Biology*, 9(9), 696–703. <https://doi.org/10.1038/nsb827>
- Peyronnet, R., Martins, J. R., Duprat, F., Demolombe, S., Arhatte, M., Jodar, M., ... Patel,

- A. (2013). Piezo1-dependent stretch-activated channels are inhibited by Polycystin-2 in renal tubular epithelial cells. *EMBO Reports*, 14(12), 1143–1148. <https://doi.org/10.1038/embor.2013.170>
- Poole, K., Herget, R., Lapatsina, L., Ngo, H.-D., & Lewin, G. R. (2014). Tuning Piezo ion channels to detect molecular-scale movements relevant for fine touch. *Nature Communications*, 5, 1–14. <https://doi.org/10.1038/ncomms4520>
- Prole, D. L., & Taylor, C. W. (2013). Identification and Analysis of Putative Homologues of Mechanosensitive Channels in Pathogenic Protozoa. *PLoS ONE*, 8(6). <https://doi.org/10.1371/journal.pone.0066068>
- Qiu, Z., Dubin, A. E., Mathur, J., Tu, B., Reddy, K., Miraglia, L. J., ... Patapoutian, A. (2014). SWELL1, a plasma membrane protein, is an essential component of volume-regulated anion channel. *Cell*, 157(2), 447–458. <https://doi.org/10.1016/j.cell.2014.03.024>
- Qu, Y., Curtis, R., Lawson, D., Gilbride, K., Ge, P., DiStefano, P. S., ... Scheuer, T. (2001). Differential modulation of sodium channel gating and persistent sodium currents by the beta1, beta2, and beta3 subunits. *Molecular and Cellular Neurosciences*, 18(5), 570–80. <https://doi.org/10.1006/mcne.2001.1039>
- Raman, I. M., & Bean, B. P. (2001). Inactivation and Recovery of Sodium Currents in Cerebellar Purkinje Neurons: Evidence for Two Mechanisms. *Biophysical Journal*, 80(2), 729–737. [https://doi.org/10.1016/S0006-3495\(01\)76052-3](https://doi.org/10.1016/S0006-3495(01)76052-3)
- Ranade, S. S., Qiu, Z., Woo, S.-H., Hur, S. S., Murthy, S. E., Cahalan, S. M., ... Patapoutian, A. (2014). Piezo1, a mechanically activated ion channel, is required for vascular development in mice. *Proceedings of the National Academy of Sciences*, 111(28), 10347–10352. <https://doi.org/10.1073/pnas.1409233111>
- Ranade, S. S., Woo, S.-H., Dubin, A. E., Moshourab, R. A., Wetzel, C., Petrus, M., ... Patapoutian, A. (2014). Piezo2 is the major transducer of mechanical forces for touch sensation in mice. *Nature*, 516(7529), 121–125. <https://doi.org/10.1038/nature13980>
- Retailleau, K., Duprat, F., Arhatte, M., Ranade, S. S., Peyronnet, R., Martins, J. R., ... Honoré, E. (2015). Piezo1 in Smooth Muscle Cells Is Involved in Hypertension-Dependent Arterial Remodeling. *Cell Reports*, 13(6), 1161–1171. <https://doi.org/10.1016/j.celrep.2015.09.072>
- Rode, B., Shi, J., Endesh, N., Drinkhill, M.J., Webster, P.J., Lotteau, S.J., Bailey, M.A.,

- Yuldasheva, N.Y., Ludlow, M.J., Cubbon, R.M., Li, J., Futers, S., Morley, L., Gaunt, H.J., Marszalek, K., Viswambharan, H., Cuthbertson, K., Baxter, P.D., Foster, D. . (2017). Piezo1 channels sense whole body physical activity to reset cardiovascular homeostasis and enhance performance. *Nature Communications*, *In press*.  
<https://doi.org/10.1038/s41467-017-00429-3>
- Scherf, T., Kasher, R., Balass, M., Fridkin, M., Fuchs, S., & Katchalski-Katzir, E. (2001). A beta -hairpin structure in a 13-mer peptide that binds alpha -bungarotoxin with high affinity and neutralizes its toxicity. *Proceedings of the National Academy of Sciences of the United States of America*, *98*(12), 6629–6634.  
<https://doi.org/10.1073/pnas.111164298>
- Schewe, M., Nematian-Ardestani, E., Sun, H., Musinszki, M., Cordeiro, S., Bucci, G., ... Baukrowitz, T. (2016). A Non-canonical Voltage-Sensing Mechanism Controls Gating in K2P K+ Channels. *Cell*, *164*(5), 937–949.  
<https://doi.org/10.1016/j.cell.2016.02.002>
- Schneider, E. R., Mastrotto, M., Laursen, W. J., Schulz, V. P., Goodman, J. B., Funk, O. H., ... Bagriantsev, S. N. (2014). Neuronal mechanism for acute mechanosensitivity in tactile-foraging waterfowl. *Proceedings of the National Academy of Sciences*, *111*(41), 14941–14946. <https://doi.org/10.1073/pnas.1413656111>
- Smith, M. R., Yu, E. J., & Goldin, A. L. (1997). Interaction between the putative sodium channel inactivation particle and domain III S4-S5. *Biophysical Journal*, *72*(2), A261.  
[https://doi.org/10.1016/S0006-3495\(97\)78219-5](https://doi.org/10.1016/S0006-3495(97)78219-5)
- Spier, I., Kerick, M., Drichel, D., Horpaopan, S., Altmüller, J., Laner, A., ... Aretz, S. (2016). Exome sequencing identifies potential novel candidate genes in patients with unexplained colorectal adenomatous polyposis. *Familial Cancer*, *15*(2), 281–288.  
<https://doi.org/10.1007/s10689-016-9870-z>
- Stanley, S. A., Sauer, J., Kane, R. S., Dordick, J. S., & Friedman, J. M. (2014). Remote regulation of glucose homeostasis in mice using genetically encoded nanoparticles. *Nature Medicine*, *21*(1), 92–98. <https://doi.org/10.1038/nm.3730>
- Starkus, J. G., Kuschel, L., Rayner, M. D., & Heinemann, S. H. (1997). Ion conduction through C-type inactivated Shaker channels. *Journal of General Physiology*, *110*(5), 539–550. <https://doi.org/10.1085/jgp.110.5.539>
- Subramanyam, P., Chang, D. D., Fang, K., Xie, W., Marks, A. R., & Colecraft, H. M. (2013). Manipulating L-type calcium channels in cardiomyocytes using split-intein protein transsplicing. *Proceedings of the National Academy of Sciences of the United*

- States of America*, 110(38), 15461–6. <https://doi.org/10.1073/pnas.1308161110>
- Sukharev, S., & Corey, D. P. (2004). Mechanosensitive channels: multiplicity of families and gating paradigms. *Science's STKE : Signal Transduction Knowledge Environment*, 219. <https://doi.org/10.1126/stke.2192004re4>
- Sukharev, S., & Sachs, F. (2012). Molecular force transduction by ion channels – diversity and unifying principles. *Journal of Cell Science*, 125(13), 3075–3083. <https://doi.org/10.1242/jcs.092353>
- Suzuki, M., Mizuno, A., Kodaira, K., & Imai, M. (2003). Impaired pressure sensation in mice lacking TRPV4. *Journal of Biological Chemistry*, 278(25), 22664–22668. <https://doi.org/10.1074/jbc.M302561200>
- Syeda, R., Florendo, M. N., Cox, C. D., Kefauver, J. M., Santos, J. S., Martinac, B., & Patapoutian, A. (2016). Piezo1 Channels Are Inherently Mechanosensitive. *Cell Reports*, 17(7), 1739–1746. <https://doi.org/10.1016/j.celrep.2016.10.033>
- Syeda, R., Xu, J., Dubin, A. E., Coste, B., Mathur, J., Huynh, T., ... Patapoutian, A. (2015). Chemical activation of the mechanotransduction channel Piezo1. *eLife*, 4(MAY). <https://doi.org/10.7554/eLife.07369>
- Vogel, V., & Sheetz, M. (2006). Local force and geometry sensing regulate cell functions. *Nature Reviews Molecular Cell Biology*, 7(4), 265–275. <https://doi.org/10.1038/nrm1890>
- Volkers, L., Mechoukhi, Y., & Coste, B. (2014). Piezo channels: from structure to function. *Pflugers Archiv European Journal of Physiology*, 467(1), 95–99. <https://doi.org/10.1007/s00424-014-1578-z>
- Wheeler, M. A., Smith, C. J., Ottolini, M., Barker, B. S., Purohit, A. M., Grippo, R. M., ... Güler, A. D. (2016). Genetically targeted magnetic control of the nervous system. *Nature Neuroscience*, 19(5), 756–761. <https://doi.org/10.1038/nn.4265>
- Woo, S.-H., Lukacs, V., de Nooij, J. C., Zaytseva, D., Criddle, C. R., Francisco, A., ... Patapoutian, A. (2015). Piezo2 is the principal mechanotransduction channel for proprioception. *Nature Neuroscience*, 18(12), 1756–1762. <https://doi.org/10.1038/nn.4162>
- Woo, S.-H., Ranade, S., Weyer, A. D., Dubin, A. E., Baba, Y., Qiu, Z., ... Patapoutian, A. (2014). Piezo2 is required for Merkel-cell mechanotransduction. *Nature*, 509(7502), 622–626. <https://doi.org/10.1038/nature13251>

- Wu, J., Goyal, R., & Grandl, J. (2016). Localized force application reveals mechanically sensitive domains of Piezo1. *Nature Communications*, 7. <https://doi.org/10.1038/ncomms12939>
- Wu, J., Lewis, A. H., & Grandl, J. (2017). Touch, Tension, and Transduction – The Function and Regulation of Piezo Ion Channels. *Trends in Biochemical Sciences*, 42(1), 57–71. <https://doi.org/10.1016/j.tibs.2016.09.004>
- Wu, Z., Grillet, N., Zhao, B., Cunningham, C., Harkins-Perry, S., Coste, B., ... Müller, U. (2017). Mechanosensory hair cells express two molecularly distinct mechanotransduction channels. *Nature Neuroscience*, 20(1), 24–33. <https://doi.org/10.1038/nn.4449>
- Zarychanski, R., Schulz, V. P., Houston, B. L., Maksimova, Y., Houston, D. S., Smith, B., ... Gallagher, P. G. (2012). Mutations in the mechanotransduction protein PIEZO1 are associated with hereditary xerocytosis. *Blood*, 120(9), 1908–1915. <https://doi.org/10.1182/blood-2012-04-422253>
- Zhang, W., Cheng, L. E., Kittelmann, M., Li, J., Petkovic, M., Cheng, T., ... Jan, Y. N. (2015). Ankyrin Repeats Convey Force to Gate the NOMPC Mechanotransduction Channel. *Cell*, 162(6), 1391–1403. <https://doi.org/10.1016/j.cell.2015.08.024>

## Biography

My name is Jason Wu. I was born on February 4, 1987 in St. Louis, Missouri. I received a Bachelors of Arts in Architecture from Rice University in May, 2009 where I was awarded membership in the Tau Sigma Delta Honor Society. I received the professional degree of Bachelors of Architecture from Rice University in May, 2011. I attended the University of North Carolina in Chapel Hill as a continuing student from 2011-2012 while working in a laboratory in the Department of Biomedical Engineering. In the fall of 2012, I joined the Department of Neurobiology at Duke University to obtain a PhD in Neurobiology. I have published the following articles as first author, titled "Localized force application reveals mechanically sensitive domains of Piezo1," and "Inactivation of mechanically activated Piezo1 ion channels is determined by the C-terminal extracellular domain and the inner pore helix," and as co-first author, the review article "Touch, Tension, and Transduction - The Function and Regulation of Piezo Ion Channels." I have published the following articles as a secondary author, titled "Synergy between Piezo1 and Piezo2 channels confers high-strain mechanosensitivity to articular cartilage," "Directionality of temperature activation in mouse TRPA1 ion channel can be inverted by single-point mutations in ankyrin repeat six," and "Axonal translation of  $\beta$ -catenin regulates synaptic vesicle dynamics." Since obtaining my bachelor's degree, I have been awarded the Ruth L. Kirschstein National Research Service Award Predoctoral Fellowship.